Old Dominion University
ODU Digital Commons

Chemistry & Biochemistry Theses & Dissertations | Chemistry & Biochemistry

Winter 2014

Spectroscopic Characterization of Dissolved Organic Matter: Insights Into the Linkage Between Sources and Chemical Composition

Xiaoyan Cao
Old Dominion University

Follow this and additional works at: https://digitalcommons.odu.edu/chemistry_etds

 Part of the Biogeochemistry Commons, Geochemistry Commons, Hydrology Commons, and the Organic Chemistry Commons

Recommended Citation
Cao, Xiaoyan. "Spectroscopic Characterization of Dissolved Organic Matter: Insights Into the Linkage Between Sources and Chemical Composition" (2014). Doctor of Philosophy (PhD), dissertation, Chemistry and Biochemistry, Old Dominion University, DOI: 10.25777/2td6-2f08
https://digitalcommons.odu.edu/chemistry_etds/26

This Dissertation is brought to you for free and open access by the Chemistry & Biochemistry at ODU Digital Commons. It has been accepted for inclusion in Chemistry & Biochemistry Theses & Dissertations by an authorized administrator of ODU Digital Commons. For more information, please contact digitalcommons@odu.edu.

SPECTROSCOPIC CHARACTERIZATION OF DISSOLVED ORGANIC MATTER: INSIGHTS INTO THE LINKAGE BETWEEN SOURCES AND CHEMICAL COMPOSITION

By

Xiaoyan Cao
B.S. June 2008, Nanjing Agricultural University, China

A Doctoral Dissertation Submitted to the Faculty of
Old Dominion University in Partial Fulfillment of the
Requirements for the Degree of

DOCTOR OF PHILOSOPHY

CHEMISTRY

OLD DOMINION UNIVERSITY
December 2014

Approved by:

Jingdong Mao (Director)

John R. Donat (Member)

Tom Isenhour (Member)

Margaret R. Mulholland (Member)

ABSTRACT

SPECTROSCOPIC CHARACTERIZATION OF DISSOLVED ORGANIC MATTER: INSIGHTS INTO THE LINKAGE BETWEEN SOURCES AND CHEMICAL COMPOSITION

Xiaoyan Cao
Old Dominion University, 2014
Director: Dr. Jingdong Mao

This dissertation investigated the chemical structure of DOM by advanced solid-state nuclear magnetic resonance (NMR) spectroscopy and Fourier transform ion cyclotron resonance mass spectrometry (FT-ICR MS) techniques, as well as isotopic measurements and UV-visible spectroscopy, to shed light on the linkages between DOM sources and DOM composition. Unique and extensive sets of DOM samples studied here were isolated from various aquatic systems, covering end-member environments in which DOM is considered either microbially derived or terrestrially derived, and areas in which DOM has characteristics intermediate between the two end members. Important insights into specific site-related questions were also gained such as the fate of terrestrial DOM in the marine system, the seasonal variability in chemical structure of DOM in the Yukon River, and the chemical structure of DOM in lakes driven by hydrology.

First, the presence of CRAM as the major structural units in DOM samples from the Penobscot River to Gulf of Maine transect and the Pacific Ocean implied that CRAM may cycle on time scales long enough to be transported into the ocean. Second, whereas spring DOM from the Yukon River was more enriched in lignin residues and carbohydrates than summer-fall and winter DOM, DOM samples across seasons shared relatively more refractory components such as CRAM, and nonprotonated OC and OCO pool. Third, CRAM occurred as the major component in three different lakes, though

there was a selective loss of terrestrially derived DOM such as aromatics with increasing lake water residence time. Lastly, the ubiquity of CRAM in DOM from microbially and terrestrially derived end members and understudied environments like groundwaters was further confirmed by NMR spectroscopy coupled with FT-ICR mass spectrometry.

The research in my dissertation clearly revealed the ubiquity of CRAM in DOM from vastly different environments with different source strengths. This implicates the chemical homogenization of DOM relative to source material in aquatic environments under the influence of diagenetical degradation processes.

This thesis is dedicated to my family.

To my parents, Liangqin Cao and Zuoying Zhu;
To my brother, Xiaogang Cao and his family;
And to my husband, Xiaojin Li.

ACKNOWLEDGMENTS

This dissertation is not only a summation of my research, but a testament to all of the help and encouragement I have received during my Ph.D. journey. I most fervently thank my advisor, Dr. Jingdong Mao, for his guidance, mentorship, and support at all stages of my doctoral research; he always sees my potential and inspires me to achieve success. I would also like to thank my dissertation committee members, Dr. John R. Donat, Dr. Thomas Isenhour, and Dr. Margaret R. Mulholland; their comments and suggestions have added to the quality of this dissertation.

I must thank Dr. George R. Aiken and Dr. Kenna D. Butler at the U.S. Geologic Survey for providing all samples studied in this dissertation, as well as elemental, isotopic, UV-visible absorbance and fluorescence analyses. I also thank Dr. George R. Aiken for discussing experimental results, editing manuscripts, and helping with my conference presentation. My sincere thanks go out to Dr. Klaus Schmidt-Rohr at Iowa State University (ISU), for providing access to his NMR lab and NMR training, and helping with data interpretation and manuscript editing. I have benefited from the supervision of such a well-established expert in the NMR field. Thanks also go to Dr. Mei Hong at ISU for her teaching on NMR theory and insightful discussions during group meetings, and Schmidt-Rohr and Hong group members for their assistance in lab. The mass spectra included in this dissertation were obtained at the FT-ICR MS Facility of National High Magnetic Field Laboratory in Tallahassee, Florida. I particularly thank Dr. Amy McKenna and Logan Krajewski for performing the FT-ICR MS analyses, and their help in data processing and visualization.

Many thanks to the collaborators I have interacted with over the years as they have taught me so much about science and greatly expanded my research interests and background. They are Drs. Pignatello J. Joseph, Jerry A. Leenheer, Daniel Olk, Kyoung S. Ro, Arndt Schimmelmann, Maria Mastalerz, Charisma Lattao, Justin E. Birdwell, Mark Chappell, and Zhigao Zhou.

I am grateful to many friends I have met at ODU and at ISU: Yuan Li, Na Chen, Hongmei Chen, Luni Sun, Wenying Chu, Wenlu Zhang, Stephen Herman, Sangbum Han, Shibin Lin, Kimberly Leister, Robert Johnson, and Jinfang Cui for all the good times, help, support and encouragement. I am indebted to Debbie Younkin for our "Monday one-on-one English conversation". I would also like to thank the ODU Chemistry Department faculty and staff; each has played a role in my graduate education.

Finally to my family: your love and support have carried me throughout the last five and a half years. I am especially grateful for my amazing husband Xiaojin Li who is my best friend and the one always there for me every day despite the distance.

TABLE OF CONTENTS

Page

LIST OF TABLES

LIST OF FIGURES

CHAPTER I

INTRODUCTION

SOURCE, BIOGEOCHEMICAL PROCESSING, AND CHEMICAL COMPOSITION OF DISSOLVED ORGANIC MATTER

Dissolved organic matter (DOM), operationally defined as the portion of organic matter that passes through a filter with a pore size of 0.2-0.7 μm, comprises a complex and heterogeneous continuum of low to high molecular weight organic molecules exhibiting different solubilities and reactivities (Aiken, 2014a; Dittmar and Stubbins, 2014; Mopper et al., 2007). DOM is a quantitatively and functionally important component in aquatic ecosystems. The oceanic DOM pool holds more carbon (~700 Pg C) than land plants (~610 Pg C), and is of similar magnitude as the atmospheric load of CO_2 (~750 Pg C) (Bauer and Bianchi, 2011; Hedges, 1992). Dissolved organic carbon (DOC) typically accounts for ~60% and >95% of the total organic carbon (OC) load in rivers and oceans, respectively (Benner, 2003). In addition to being the largest pool of organic matter in aquatic systems, DOM is central to many ecological and geochemical processes (Aiken, 2014a; Dittmar and Stubbins, 2014; Findlay and Sinsabaugh, 2003; Mopper et al., 2007). Namely, DOM serves as a source of carbon and energy for microbial food webs, affects light penetration, and plays significant roles in metal chelation, as well as retention of hydrophobic organic contaminants (Findlay and Sinsabaugh, 2003). Moreover, DOM can interact with disinfectants to form disinfection by-products during the treatment of drinking water supplies (Ahuja, 2013). These aspects of DOM imply the need for a more fundamental understanding of its chemistry.

The chemical composition of DOM is shaped by its source materials and biogeochemical processing (Aiken, 2014a). DOM in aquatic systems can originate, in a broad sense, from two distinct sources. Autochthonous DOM is produced within the aquatic environments, and essentially derived from algae and macrophytes via several different mechanisms: predatory grazing, cell death and senescence, viral lysis, and extracellular release (Bertilsson and Jones, 2003). Allochthonous DOM is imported from outside the aquatic environments by processes such as riverine inflow and atmospheric deposition, and is of mostly terrestrial (or terrigenous) origin (Aitkenhead-Peterson et al., 2003). Structural studies of DOM derived from different source materials reveal distinctive chemical characteristics associated with those source materials (Aiken, 2014a). For instance, autochthonous DOM is more enriched in aliphatic structures (proteins and lipids) and has relatively high nitrogen content, while allochthonous DOM features high aromaticity associated with the presence of tannin/lignin-like substances derived from higher plants and has low nitrogen contents (McCallister et al., 2006; McKnight and Aiken, 1998; McKnight et al., 1997; Opsahl and Benner, 1998).

Biogeochemical processes such as microbial degradation and photochemical oxidation also alter the physicochemical characteristics of DOM (Aiken, 2014a; Amon and Benner, 1996; Hernes and Benner, 2003; Jaffé et al., 2004; Obernosterer and Benner, 2004; Osburn et al., 2001; Zhang et al., 2009). Studies have shown that microbial uptake results in the progressive decrease in the larger molecular weight fractions of the ultrafilterable DOM and accumulation of smaller molecular weight DOM material, as well as loss of carbohydrate moieties (McKnight et al., 2003). Evidence suggests that photolysis of DOM may release nutrients (N and P), and lead to changes in DOM

chemistry, such as decreases in average molecular weight and lignin phenol concentrations (Cory et al., 2007; Dittmar et al., 2007; Helms, 2012; Helms et al., 2008; McKnight et al., 2003; Opsahl and Benner, 1998; Osburn et al., 2001; Osburn and Morris, 2003; Spencer et al., 2009b; Strome and Miller, 1978), and changing molecular signatures as identified by Fourier transform ion cyclotron resonance (FT-ICR) mass spectrometry (MS) (Gonsior et al., 2009; Kujawinski et al., 2004; Stubbins et al., 2010). Alternatively, the photochemical and biological reactivity of DOM also depends on its source and hence its chemical composition (Shank and Evans, 2011; Sulzberger and Durisch-Kaiser, 2009). For instance, algal-derived DOM with more aliphatic compounds and peptides tends to be biologically more labile than terrigenous DOM, while allochthonous DOM with high aromaticity is known to be very photoreactive (Stubbins et al., 2010). However, allochthonous DOM has also proven to be an important substrate for bacterial growth, and photochemical transformations can enhance the bioavailability of previously recalcitrant DOM but decrease the bioavailability of initially more labile DOM such as algal exudates (Catalán et al., 2013).

The disparity in the sources of DOM, and in the biogeochemical processes controlling its transport and alteration, is expected to lead to structural differences in DOM from different environments. For instance, numerous studies have highlighted the differences in DOM composition, as mentioned previously, between marine and non-marine, microbially- and terrestrially-derived environments (Aiken, 2014a; Hedges et al., 1992; Malcolm, 1990). However, recently evidence has appeared which implies chemical homogenization of DOM relative to source materials in soil (Sanderman and Kramer, 2013). This was attributed to two microbially mediated processes: (1) similar

extracellular enzymatic oxidation conferring solubility to a subset of degradation products, and (2) rapid selective consumption of the more labile organic compounds in soil solution (Ågren and Bosatta, 1996; Sanderman and Kramer, 2013; Wickland et al., 2007). It is worth noting that the authors focused on DOM extracted at different sites across a soil chronosequence in Hawaii (Sanderman and Kramer, 2013), where the associated biogeochemical processes are different from those involved in aquatic environments. For instance, aquatic environments are generally more sensitive to photochemically mediated processes than terrestrial environments. Furthermore, photochemical degradation is effective at eliminating and modifying the unique terrestrial signatures of lignin phenols (Benner and Kaiser, 2011; Hernes and Benner, 2003; Spencer et al., 2009b) and δ^{13}C-DOC (Opsahl and Zepp, 2001; Spencer et al., 2009b; Vahatalo and Wetzel, 2008), and similarity between photodegraded land-derived DOM and open-ocean DOM has also been observed (Dittmar et al., 2007; Helms, 2012).

The overarching research goal of this dissertation is to apply advanced solid-state NMR spectroscopy and FT-ICR mass spectrometry techniques to investigate the chemical structure of DOM, shedding light on the linkages between DOM sources and DOM composition. This dissertation study intends to evaluate the hypothesis of the chemical homogenization of DOM relative to source materials in aquatic environments. There has been some evidence for the structural similarity of marine and freshwater DOM (Hertkorn et al., 2006; Lam et al., 2007; Leenheer, 1994; McCaul et al., 2011; Repeta et al., 2002). Repeta et al. (2002) observed a high degree of similarity of NMR spectra of ultrafiltered DOM from freshwater (rivers and lakes) and marine systems. Ultrafiltered DOM from six major streams across North America also revealed

remarkably similar ^{13}C NMR patterns (Jaffé et al., 2012). In particular, Hertkorn et al. (2006) using a range of modern solution NMR approaches coupled with FT-ICR MS, identified carboxyl-rich alicyclic molecules (CRAM) as a major component in the marine ultrafiltered DOM (Figure 1). These CRAM contribute to 8% of the DOM pool, have core structures similar to sterols and hopanoids, and are likely derived from the membranes of marine microbes (Hertkorn et al., 2006; Hertkorn et al., 2013). Subsequently, Lam et al. (2007) and McCaul et al. (2011) extended their findings to show that CRAM, along with heteropolysaccharides and aromatic compounds, were also major structural components in freshwater DOM. Indeed, as early as 1994, Leenheer (1994) proposed molecular models of freshwater DOM from allochthonous and autochthonous sources that contain short-chain, branched, and alicyclic structures terminated by carboxyl or methyl groups, and concluded that "as degradation proceeds in the aquatic environment, carbohydrates and lignin degradation products disappear within days to a few years. Only the carboxylated aliphatic alicyclic component persists for thousands of years in the marine environment or in isolated lake environments". This is probably the first documentation of CRAM-like structures in DOM. The alicyclic structures of CRAM are resistant to biological oxidation, while the absence of chromophoric structures in CRAM confers resistance to degradation by UV radiation (Leenheer, 1994). According to Leenheer (1994), the precursors of CRAM likely arise from terpenoid hydrocarbon lipids, or polyunsaturated lipid precursors that are oxidatively coupled and cyclized by free-radical mechanisms (Harvey et al., 1983). In this dissertation, I also intend to investigate the presence of CRAM in DOM from across different biomes, ecosystem types, and with a large range of autochthonous, allochthonous, and anthropogenic influences.

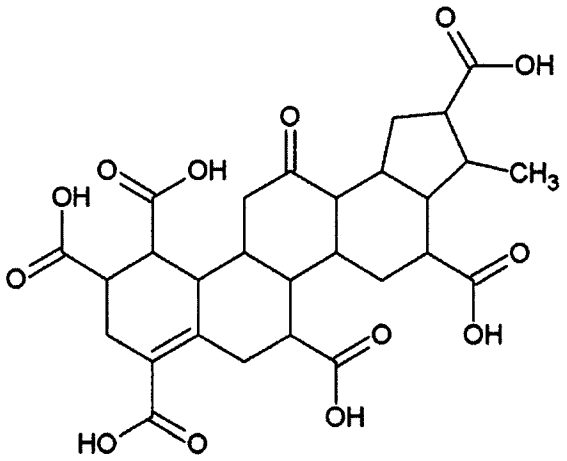

Figure 1. Carboxyl-rich alicyclic molecules (CRAM; Hertkorn et al. (2006)).

ISOLATION OF DISSOLVED ORGANIC MATTER FROM NATURAL WATERS

DOM isolation techniques can be generally divided into (1) membrane-based approaches such as ultrafiltration (Benner et al., 1997) and reverse osmosis coupled with electrodialysis (RO/ED) (Gurtler et al., 2008; Koprivnjak et al., 2009; Vetter et al., 2007), and (2) retention-based solid phase extraction (SPE) methods using hydrophobic sorbents such as XAD resins (Aiken et al., 1992; Leenheer, 2009), C_{18} silica (Green and Blough, 1994), and PPL resins (Dittmar et al., 2008). These various isolation protocols differ in their underlying principles of operation and therefore isolate operationally defined DOM fractions, which may not be chemically equivalent (Aiken, 2014a; Dittmar and Stubbins, 2014; Green et al., 2014; Kaiser et al., 2003; Koprivnjak et al., 2009; Minor et al., 2014; Mopper et al., 2007). For instance, ultrafiltration collects only the high molecular weight fraction of DOM, typically > 1000 Dalton (Da), denoted as ultrafitered DOM (UDOM) or high molecular weight DOM (HMW DOM). SPE methods are generally selective for

hydrophobic DOM molecules. Among those, SPE using XAD (XAD-8 and XAD-4 resins in tandem) selectively collects biogeochemically relevant "humic" fractions of DOM. The fractions recovered from XAD-8 and XAD-4 are referred to as hydrophobic acids (HPOA) and transphilic acids (TPIA), respectively. The fulvic acid (FA, soluble in water under all pH conditions) isolate generally accounts for 90–95% of the HPOA fraction, with the remainder of HPOA being humic acid (HA, insoluble in water below pH 2). RO/ED process is capable of isolating more representative DOM that contains both hydrophobic moieties preferentially isolated by SPE and more polar, carbohydrate-like moieties selectively isolated by ultrafiltration (Koprivnjak et al., 2009; Mao et al., 2012b). However, significant retention of inorganic components associated with RO/ED DOM may pose interferences with analytical methods like NMR spectroscopy (inducing differential NMR relaxation from metal coordination) and FT-ICR mass spectrometry (extensive formation of cluster ions) (Hertkorn et al., 2013; Mao et al., 2012b).

CHEMICAL CHARACTERIZATION OF DISSOLVED ORGANIC MATTER

The highly heterogeneous complexity, and dynamic nature of DOM pose severe difficulties to understanding its composition and reactivity, making it among the least characterized natural organic matter fractions known (Hedges et al., 2000). Despite extensive research on DOM characterization, a comprehensive understanding of DOM structures and their variations in different aquatic systems remains elusive (Minor et al., 2014). Recent advances in DOM analytical techniques from the bulk to molecular level, however, have greatly enhanced our capability to characterize DOM (Aiken, 2014a; Dittmar and Stubbins, 2014; Leenheer, 2009; Mopper et al., 2007). In particular, high-

performance, non-target, and high-resolution analytical approaches such as NMR spectroscopy and FT-ICR mass spectrometry are leading to exciting advances related to DOM chemistry (Hertkorn et al., 2006; Hertkorn et al., 2013; Mao et al., 2012b; Mopper et al., 2007; Sleighter and Hatcher, 2008; Stenson et al., 2003; Thorn and Cox, 2009).

Carbon Isotopes. Measurements of stable carbon isotopes (^{12}C and ^{13}C) and radiocarbon (^{14}C) have proven useful tracers of sources and turnover times of the average DOC pool (Bauer, 2002; McNichol and Aluwihare, 2007; Raymond and Bauer, 2001b). Carbon isotope fractionation is associated with photosynthesis, which favors the lighter isotope ^{12}C over heavier ^{13}C. This effect is more pronounced with C_3 class of land plants than with C_4 plants, leading to lower $^{13}C/^{12}C$ ratios (i.e., more negative $\delta^{13}C$ values) of C_3 plants. The photosynthetic source contributions result in distinctive carbon isotopic signatures of DOM isolated from freshwater and seawater. Riverine DOM has $\delta^{13}C$ values ranging from approximately −30‰ to −25‰, while marine DOM $\delta^{13}C$ values generally fall in the range of −23‰ to −18‰ (Bauer, 2002).

Radiocarbon values are usually reported as $\Delta^{14}C$, which has a greater dynamic range (−1000 to ~ +200‰) compared to $\delta^{13}C$ (−32‰ to −12‰) (McNichol and Aluwihare, 2007; Raymond and Bauer, 2001b). The radiocarbon-based equivalent age of DOM can then be estimated directly from $\Delta^{14}C$, and expressed in years before present (ybp), where present refers to 1950. The use of paired ^{14}C and ^{13}C measurements in DOC ensures a more robust interpretation of sources, ages, and transformations of DOC (Bauer, 2002; Raymond and Bauer, 2001b).

Optical Properties. The ultraviolet and visible (UV-visible) absorbance and fluorescence measurements of DOM are straightforward, readily adapted to field settings, and provide average data about the chromophoric DOM (CDOM) and fluorescent DOM (FDOM), respectively (Aiken, 2014a; Aiken, 2014b). The UV-visible spectra for DOM samples are typically featureless with absorptivity increasing exponentially toward shorter wavelengths. Useful parameters such as specific UV absorbance (SUVA), absorbance ratios, spectral slope, and spectral slope ratios (Blough and Del Vecchio, 2002; Helms et al., 2008; Weishaar et al., 2003), can be obtained and related to aromatic C content and the molecular weight of DOM. DOM fluorescence data are usually presented as three-dimensional excitation–emission matrices (EEMs), produced from sequential fluorescence emission scans at successively increasing excitation wavelengths. EEMs spectra of DOM are generally comprised of a number of fluorophore peaks and contain information about composition, origin and processing of DOM on the basis that individual excitation-emission pairs or peaks are characteristic to specific molecular structures (Aiken, 2014b; Coble et al., 1990; Fellman et al., 2010; McKnight et al., 2001). Two distinct types of DOM fluorescence groups contribute to these peaks: the humic-like and amino acid-like fluorophores (Coble, 2007; Jørgensen et al., 2011). Parallel factor (PARAFAC) analysis is further applied to decompose the fluorescence signature of DOM into individual components and provide estimates of the relative contribution of each component to total DOM fluorescence (Stedmon and Bro, 2008; Stedmon and Markager, 2005; Stedmon et al., 2007). However, caution must be taken in the assignment of the fluorophores to particular classes of compounds without additional compound specific

analyses, because numerous types of compounds with different fluorophores may share similar fluorescence properties (Aiken, 2014b).

Ultrahigh-Resolution Mass Spectrometry. Mass spectrometry has been used to characterize DOM for the past three to four decades, previously mostly coupled with a chromatographic separation technique to improve the resolution and selectivity (Mopper et al., 2007). The advent of ultrahigh-resolution FT-ICR MS eliminates the need for prior separation by chromatographic or other methods (Dittmar and Stubbins, 2014; Marshall et al., 1998; Mopper et al., 2007). With its ultrahigh mass resolving power, FT-ICR MS is unparalleled in its capability to resolve the incredible molecular complexity within the bulk of marine and terrigenous DOM (Dittmar and Stubbins, 2014; Mopper et al., 2007; Stenson et al., 2002). Its ultrahigh mass accuracy enables the calculation of molecular formulas for detected DOM molecules. FT-ICR MS analyses have revealed within DOM more than 10, 000 elemental formulas of intact compounds; with numerous structural isomers behind each molecular formula (Dittmar and Stubbins, 2014). DOM molecules are also shown to occupy a small mass range from mainly 250 to 550 Da (Dittmar and Stubbins, 2014), consistent with previously proposed small size of DOM molecules (Aiken and Malcolm, 1987; Simpson, 2002).

Even with information of the exact masses and empirical formulas, structural details remain speculative due to the possibilities of many structural isomers per molecular formula. Kim et al. (2003a) developed the use of van Krevelen (vK) diagrams (van Krevelen, 1950) to visualize large and complicated MS datasets of DOM. The vK diagram is a plot of H/C molar ratio on the y-axis versus the O/C molar ratio on the x-

axis and serves to cluster molecules based on their functional group compositions. Major chemical classes (lignin, condensed hydrocarbons, and polysaccharides, etc.) commonly found in DOM have characteristic H/C and O/C ratios and therefore tend to cluster within specific regions of the diagram (Gonsior et al., 2009; Kim et al., 2003a). The patterns in vK diagrams of DOM reflect not only source material, but also identify similarities/differences in the molecular composition among samples by overlaying their plots. Additionally, a 3D vK diagram can be constructed by incorporating relative peak intensities on a z-axis or using a contour plot (Kim et al., 2003a), which allows for a comparison of the relative abundance of each class of compounds among samples.

The FT-ICR MS coupled with electrospray ionization (ESI) currently stands apart as the most frequent option for MS analysis of DOM (Dittmar and Koch, 2006; Hertkorn et al., 2006; Hertkorn et al., 2013; Kellerman et al., 2014; Kim et al., 2006; Koch et al., 2008; Kujawinski et al., 2009; Sleighter and Hatcher, 2008; Sleighter et al., 2009; Tremblay et al., 2007). However, the quantitative use of ESI MS data is significantly constrained because of its considerable selectivity; with polar compounds containing functional groups such as amines ($-NH_2$) and carboxylic acids ($-COOH$) being preferentially ionized (Gaskell, 1997). ESI also shows a decreasing sensitivity with increasing molecular size of the molecules in DOM (These and Reemtsma, 2003). Different classes of compounds are not equally well observed, and therefore the ion relative abundances in mass spectra do not accurately represent the relative abundances of the corresponding parent neutrals, indicating that specific use of intensities is at best a relative approach. However, the ESI FT-ICR technique can be a powerful tool for comparative studies of DOM at the molecular level of detail as long as the

presence/absence of particular peaks instead of changes in peak height is used as indicators of structural differences in DOM as a function of sources and biogeochemical processes (Kujawinski et al., 2004).

NMR Spectroscopy. NMR spectroscopy has gained immense popularity as a powerful spectroscopic tool for quantitative and comprehensive characterization of DOM since the pioneering work of Stuermer and Payne (1976) and introduction of newer and advanced NMR approaches (Leenheer, 2009; Mitchell et al., 2013; Mopper et al., 2007). NMR spectroscopy yields highly complementary information to the molecular-level information obtained from FT-ICR MS.

Both solid-state and solution-state NMR techniques have been employed in DOM research. One may have the intuition that solution-state NMR would be a better choice because DOM is soluble and readily amenable to modern solution-state NMR techniques. Yet this aspect does not offer a huge benefit because it remains challenging or even impractical to analyze DOM directly in natural waters due to the low NMR signal obtained at natural concentrations of DOM and the interference of water itself. The Simpson group (Lam and Simpson, 2008; Mitchell et al., 2013) recently demonstrated the use of a novel water suppression technique for direct ^{1}H NMR analysis of bulk DOM from river, lake, and ocean waters without isolation or preconcentration. This advance only provides coarse-level structural information about the whole DOM pool. Nevertheless the majority of NMR-based DOM research requires sample isolation or concentration prior to analysis because NMR spectroscopy is inherently an insensitive technique. The signal intensity in solution-state NMR depends on the amount of DOM

that can be dissolved into approximately 1 mL of solvent. However, when present at high concentrations in solution-state, DOM constituents aggregate, leading to lower signal-to-noise ratios and spectral resolution associated with altered spin dynamics and spin-spin interactions (Kim et al., 2003b; Mopper et al., 2007). Solid-state NMR instead analyzes a sample at its highest concentration, i.e., as a solid. This represents an important advantage of solid-state NMR over solution-state NMR. Second, solid-state NMR requires less sample handling, is non-destructive and free from solvent effects that may alter chemical shifts, introduce new peaks (i.e., solvent peaks), or eliminate peaks (e.g., loss of peaks from exchangeable ^{1}H) (Mopper et al., 2007). Lastly, solid-state NMR can also characterize nonprotonated/quaternary C, not detected in modern and advanced solution NMR experiments that rely on ^{1}H detection. Applications of different solid-state and solution-state NMR techniques in DOM characterization have been well summarized in two recent reviews (Mitchell et al., 2013; Mopper et al., 2007). The rest of this section presents main NMR findings in chemical-structural information of DOM extracted by different isolation methods, because they very likely recover different suites of compounds within the bulk DOM pool. Many studies cited below have used NMR spectroscopy in conjunction with other analytical techniques such as mass spectrometry; however, it is primarily the contribution of NMR that is highlighted here.

Ultrafiltered DOM (UDOM) has been widely studied in the literature. ^{13}C and ^{1}H NMR spectral analysis of UDOM in surface waters shows that more than 50% of the carbon in UDOM is carbohydrate (Aluwihare et al., 1997; Benner et al., 1992), consisting of compositionally well-defined acylpolysaccharides according to Repeta and his group (Aluwihare et al., 1997; Eglinton and Repeta, 2004; Repeta et al., 2002). There is a

discrepancy between NMR-defined carbohydrate fraction and wet chemical measurements of hydrolysable carbohydrates, which recover only 10-20% of UDOM carbon as simple neutral sugars. Using modified acid hydrolysis coupled with NMR spectroscopy, the Repeta group (Aluwihare et al., 2005; Panagiotopoulos et al., 2007; Quan and Repeta, 2007) further demonstrated the presence of methyl sugars, 6-deoxy sugars, and methyl deoxy sugars as well as significant N-acetyl amino sugars (e.g., chitin and peptidoglycan) in UDOM. Nevertheless, most UDOM carbohydrate remains uncharacterized at the molecular level. In addition, a new class of carboxyl-rich alicyclic molecules (CRAM) has been identified in marine UDOM based on two-dimensional (2D) NMR and FT-ICR MS (Hertkorn et al., 2006; Hertkorn et al., 2013), as previously mentioned.

RO/ED isolated DOM is the least characterized among other DOM isolates by advanced spectroscopic methods. The NMR spectra of RO/ED DOM contain a relatively higher percentage of alkyl carbon but lower proportion of carbohydrate carbon than those of UDOM, and RO/ED DOM likely represents an intermediate of UDOM and SPE-DOM (Koprivnjak et al., 2009). Mao et al. (2012b) compared RO/ED DOM from coastal and marine environments, which shared major structural units of carbohydrate-like moieties, peptides or amino sugars, COO-bonded alkyls, and nonpolar alkyl groups. Coastal RO/ED DOM also showed additional contribution from lignin residues. Helms (2012) studied five oceanic RO/ED isolates collected at different depths by solid-state NMR, which identified a previously unknown and uncharacterized fraction of carbohydrates containing quaternary anomeric carbons. The enrichment of carboxylic carbons in bio-

refractory DOM also supported the presence and refractory nature of CRAM (Helms, 2012).

The SPE method via XAD resins has been used by International Humic Sciences Society (IHSS) as a standard procedure for isolating dissolved humic substances from natural waters. The IHSS standard Suwannee River (SR) FA has been extensively characterized. Leenheer and Rostad (2004) further fractionated SR FA and identified sub-fractions derived from terpenoids and condensed tannins respectively. The ^{13}C NMR analyses of hydrophobic DOM fractions from surface water and groundwater also revealed the presence of branched methyl groups and quaternary aliphatic carbon structures, suggesting terpenoid hydrocarbon precursors (Leenheer et al., 2003; Leenheer et al., 2004). Though carbohydrates have been recognized as a significant component in RO/ED-DOM, and especially in UDOM, carbohydrate structures represent only a very minor fraction of SPE-DOM isolates. Studies of other SPE-DOM isolates via diethylaminoethylcellulose resin from freshwater (Lam et al., 2007; McCaul et al., 2011) also indicated CRAM as a major component.

SYSTEMATIC SOLID-STATE NMR APPROACH FOR NON-DESTRUCTIVE CHARACTERIZATION OF DOM

Because this dissertation heavily relies on the use of solid-state NMR spectroscopy to elucidate DOM structure, a synthesis of our systematic protocol (Figure 2) for nondestructively characterizing complex natural organic matter such as DOM (Mao et al., 2011) is presented here. Such a protocol includes identification and quantification of specific functional groups, detection of connectivities of specific functional groups, and

investigations of domains and heterogeneities. Results extracted from various solid-state NMR techniques offer greater and more detailed structural information, as illustrated below, than general distribution of functional groups in DOM by simply integrating the broad and overlapping resonances.

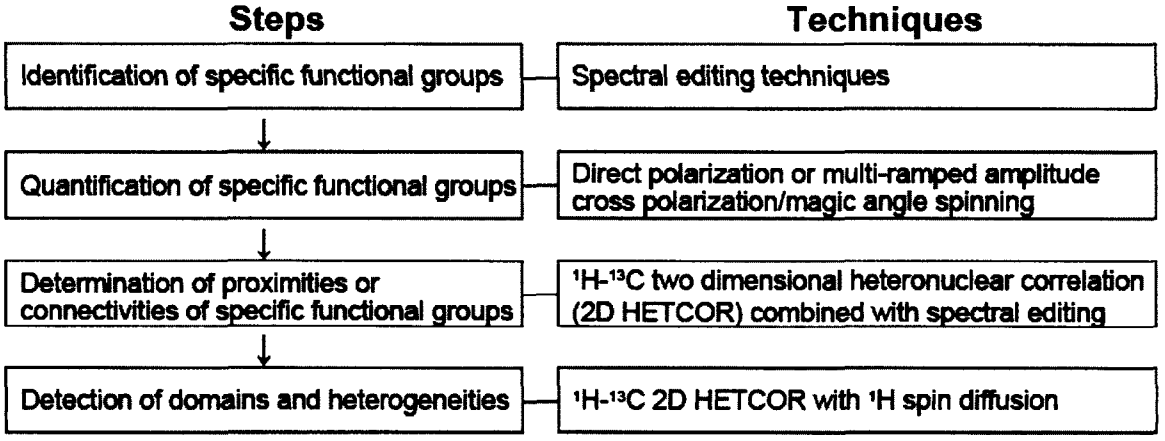

Figure 2. Systematic solid-state NMR approach for non-destructive characterization.

Identification of Specific Functional Groups. Routine ^{13}C cross polarization/magic angle spinning (CP/MAS), the most-widely used technique for DOM characterization, yields broad spectra in which only a few specific functional groups can be clearly assigned due to the overlap of potentially thousands of individual molecules. Spectral editing techniques can improve the identification of specific bands within the CP/MAS spectrum. Figure 3 shows the application of various spectral editing techniques to a DOM sample. Signals routinely exist between 0 and 220 ppm in ^{13}C NMR spectra of

DOM samples. Figure 3(a) is the cross polarization/total sideband suppression (CP/TOSS) spectrum which shows the semi-quantitative structural information as a reference. Similar to most CP/MAS spectra of DOM (SPE-DOM in particular), it is characterized by five major overlapping resonance regions at 0-60 ppm (alkyl C, with some NCH/OCH_3 in 45-60 ppm), 60-100 ppm (O-alkyl C), 100-120 ppm (anomeric C and some aromatic and olefinic C), 120-162 ppm (aromatic and aromatic C-O), 162-190 ppm (carboxylate and amide C), and 190-220 ppm (aldehyde and ketone C). Figure 3(b) shows the CP/TOSS spectrum obtained after dipolar dephasing, which selects the signals from nonprotonated C, and mobile C groups such as rotating CH_3/OCH_3 groups. Figure 3(c) exhibits CP/TOSS spectrum after the insertion of the ^{13}C chemical shift anisotropy (CSA) filter, which selects the resonances of sp^3-hybridized C. In particular, this technique separates signals of anomeric C (O–C–O) from those of aromatic C in 100-120 ppm region. The di-oxygenated anomeric carbon signals resonating near 103 ppm now become obviously visible. The combination of this CSA filter technique with dipolar dephasing (Figure 3(d)) shows the signals of nonprotonated or mobile sp^3-hydridized C, which in particular identifies nonprotonated anomeric C. The CH-only spectrum (Figure 3(e)) shows the signals from CH groups, such as aromatic C-H around 120 ppm, OCH at 72 ppm, and NCH/CCH at 53 ppm. The CH_2-only spectrum (Figure 3(f)) displays two bands: a small OCH_2 signal around 62 ppm and a major broad band attributed to CCH_2 around 30 ppm. Figure 3 shows that the spectral editing techniques, CH and CH_2 selection in particular, have successfully resolved overlapping peaks and identified specific functional groups such as CH_3, OCH_2, OCH, OCO, CCH_2 and NCH/CCH.

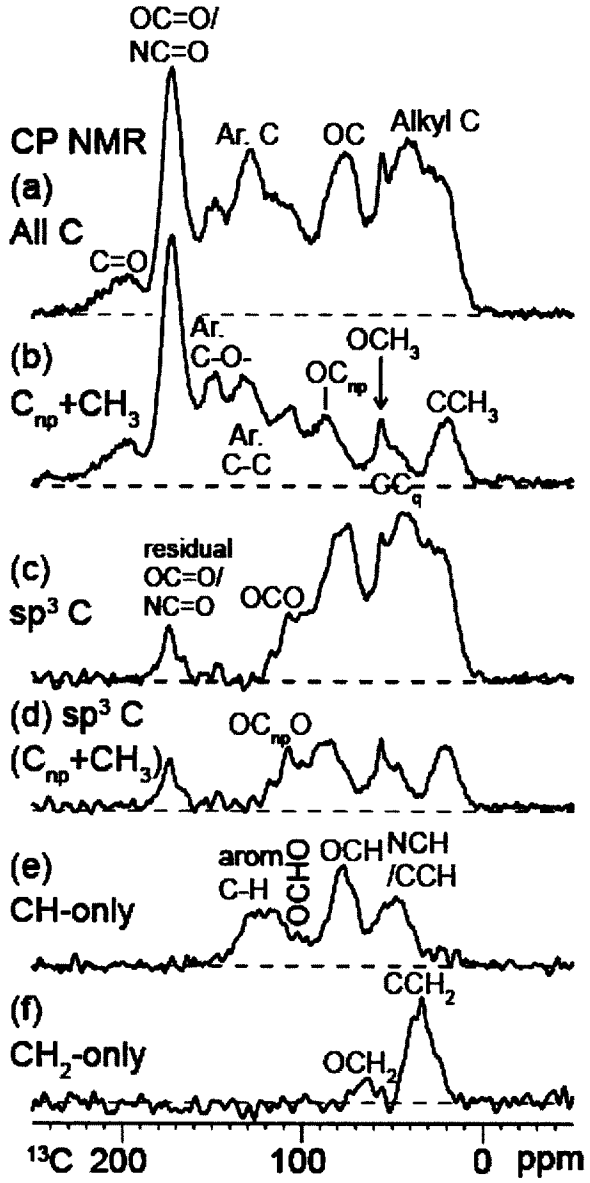

Figure 3. Identification of specific functionalities in DOM isolated with the XAD-8 resin from Penobscot River, Maine by spectral editing techniques. (a) CP/TOSS (cross polarization/total sideband suppression) spectrum. (b) dipolar-dephased CP/TOSS. (c) sp^3-hybridized C selected by a ^{13}C CSA (chemical shift anisotropy) filter. (d) nonprotonated or mobile sp^3-hybridized C by a ^{13}C CSA filter and dipolar dephasing. (e) CH-only. (f) CH_2-only.

Quantification of Specific Functional Groups. The ^{13}C CP/MAS spectra are usually not quantitative, since the magnetization transfer from ^{1}H is more efficient for carbons bonded to ^{1}H than for nonprotonated C or mobile segments with their weaker H–C dipolar couplings. The most reliable method for obtaining quantitative NMR spectra is magic-angle spinning with direct polarization (DP) and sufficient recycle delays that permit essentially complete longitudinal (T_1) relaxation of the magnetization of the observed nuclei. However, this approach is time-consuming when T_1 is long. Acquiring a quantitative DP/MAS spectrum of ^{13}C in natural abundance with acceptable signal-to-noise ratio usually takes overnight for DOM. The high spinning speed multi-ramped amplitude cross polarization/magic angle spinning (multiCP) technique, recently developed by Johnson and Schmidt-Rohr (2014), provides a simple, robust way to obtain quantitative solid-state ^{13}C NMR spectra of organic materials, with good signal-to-noise ratio. It achieves long (>10 ms) CP from ^{1}H without significant magnetization losses due to relaxation and with a moderate duty cycle of the radio-frequency irradiation, by multiple 1-ms CP periods alternating with ^{1}H spin-lattice relaxation periods that repolarize the protons. To evaluate the suitability of multiCP technique for quantitative characterization of DOM, the DP/MAS and multiCP techniques will be applied to some samples. Once consistent spectra are obtained, this new multiCP pulse sequence will be employed for all other samples to obtain quantitative ^{13}C NMR spectra. Based on quantitative ^{13}C and spectral-editing techniques, specific functional groups can be quantified.

Connectivities and Proximities Investigated by Short Range ^{1}H-^{13}C 2D Hetronuclear Correlation (HETCOR) NMR. ^{1}H-^{13}C 2D NMR can provide structural information beyond the individual functional groups because ^{1}H-^{13}C dipolar couplings can be employed to reveal structural information about inter-nuclear distances on a 6-Å scale. The junctions between different groups (e.g., aromatic and aliphatic) can be identified, primarily by 2D ^{1}H-^{13}C HETCOR experiments. In addition, 2D ^{1}H-^{13}C HETCOR NMR is capable of characterizing the environment of nonprotonted carbon sites such as COO/N-C=O.

Heterogeneities and Domains. There could be chemical and physical domains in DOM. In polymer science, the domains of crystalline and amorphous poly (methylene) are examples of physical domains. Chemical domains indicate the same kinds of chemical compounds associated together such as lipid, lignin and polysaccharide domains. Usually, the terminology "domain" is used if its diameter is more than 5 nm while "heterogeneity" is adopted if its diameter is below 5 nm (Schmidt-Rohr and Spiess, 1994). In order to build chemical models of DOM, it is of fundamental importance to establish whether large-scale heterogeneities or domains exist. If they do, a small structural model cannot approximate the structure; instead, a separate model must be provided for each distinct component. ^{1}H-^{13}C 2D HETCOR with ^{1}H spin diffusion can be used to identify domains or heterogeneities.

THESIS ORGANIZATION AND CHAPTER SYNOPSES

This dissertation study intends to evaluate the hypotheses of the chemical

homogenization of DOM relative to source material and the ubiquity of CRAM in DOM in aquatic environments. This dissertation presents results from four research projects. The first three projects study three suites of DOM samples with each set of samples designed to address site-related questions. Chapter II explores the chemical-structural changes of DOM along a salinity gradient from Penobscot River, Penobscot Bay to the Gulf of Maine, and from Pacific Ocean to provide insights into the fate of terrestrial DOM in the marine system. Chapter III investigates the seasonal variability in chemical structure of DOM in a large northern high-latitude river system (Yukon River, Alaska, USA). Chapter IV studies the chemical structure of DOM in three hydrologically distinct lakes (Minnesota, USA). These chapters (II, III, and IV) also serve to address the CRAM hypothesis. Lastly, the ubiquity of CRAM in DOM from microbially and terrestrially derived end members and understudied environments like groundwaters is addressed in Chapter V by the use of solid-state NMR spectroscopy and FT-ICR mass spectrometry.

CHAPTER II

STRUCTURAL CHARACTERIZATION OF DISSOLVED ORGANIC MATTER FROM RIVER TO COASTAL MARINE WATERS INVESTIGATED BY SOLID-STATE NMR

INTRODUCTION

Dissolved organic matter (DOM) is a quantitatively and functionally important component in aquatic ecosystems (Hedges et al., 1992). Comprising the majority (>90%) of marine organic carbon (Benner, 2002), oceanic dissolved organic carbon (DOC) pool is comparable in magnitude to all of the C in terrestrial plants, or to all the CO_2 in the atmosphere (Hedges and Oades, 1997). In addition to affecting light penetration and fueling the microbial loop, DOM also plays important roles in metal chelation and retention of hydrophobic organic contaminants, among many other biogeochemical processes.

Considerable progress has been made toward understanding the origin, composition and cycling of marine DOM thanks to increasingly sophisticated DOM isolation (XAD resins and C_{18} extractions, ultrafiltration, reverse osmosis, and reverse osmosis coupled with electrodialysis) and analytical techniques (lignin-derived phenols as biomarkers, fluorescence spectroscopy, size-exclusion chromatography, high-resolution mass spectrometry, and NMR spectroscopy). Nevertheless, a large fraction of DOM remains uncharacterized at the molecular level (Hedges et al., 2000). This is primarily due to exceptionally high degree of complexity in DOM structure in addition to its dilute nature. The structural complexity of DOM arises from the diversity of

allochthonous (terrestrial vegetation and soil leachates) and autochthonous (algae, macrophytes, and heterotrophs) sources, as well as diagenetic alterations from geo-, photo-, and biochemical reactions (Kim et al., 2006). As a result, certain key questions such as the fate of terrigenous DOM in the ocean, and reasons and mechanisms behind the refractory nature of DOM remain unclarified (Dittmar and Paeng, 2009; Hansell et al., 2004; Hedges et al., 1997; Ogawa et al., 2001; Yamashita and Tanoue, 2008).

The world's rivers transport approximately 0.25 Pg of DOC (< 0.5 μm) from continents to the ocean each year (Hedges et al., 1997). The input of riverine DOC is sufficient alone to sustain the turnover of the entire marine DOC pool. However, the fate of this important contribution to the global C cycle has remained enigmatic. Previous estimates based on lignin-derived molecular markers concluded that only a small percentage of oceanic DOM was derived from terrestrial sources (Benner et al., 2005; Hedges et al., 1997; Hernes and Benner, 2006; Meyers-Schulte and Hedges, 1986; Moran et al., 1991; Opsahl and Benner, 1997; Opsahl et al., 1999). Yet, by assuming that lignin is a reliable marker of all terrigenous organic matter entering the oceans, the lignin-biomarker technique intrinsically underestimates the contribution of terrigenous DOM. Evidence from photochemical studies of DOM has shown that lignin phenol components are efficiently removed or modified upon photodegradation (Benner and Kaiser, 2011; Dalzell et al., 2009; Dittmar et al., 2007; Hernes and Benner, 2003; Opsahl and Benner, 1998). It remains unclear whether other photochemically and microbially stable structures exist in terrigenous DOM which can survive the transit from the river to the coastal ocean and can accumulate there because of their refractory nature.

More recent studies have traced the structural changes that occur during DOM transformation from terrestrial to marine end members with the goal of deciphering the role of terrestrial OM in the marine system (Abdulla et al., 2010a; Abdulla et al., 2010b; Esteves et al., 2009; Liu et al., 2011; Mannino and Harvey, 2000; Sleighter and Hatcher, 2008). Sleighter and Hatcher (2008) observed a considerable amount of molecular formula overlap between samples from sites along a river to estuary to ocean transect, which could be due to the presence of refractory material that persists throughout the transect, or materials with the same molecular formulas but different chemical structures. Liu et al. (2011) further compared DOM samples from similar locations (Great Dismal Swamp, Town Point and Coastal marine sites) with a water extract from degraded wood. They noted the presence of lignin-derived compounds in all samples from the river to the coastal ocean. Abdulla et al. (2010b) studied high molecular weight dissolved organic matter (HMW-DOM) isolated along an Elizabeth River/Chesapeake Bay salinity transect. Their results showed that the contribution of heteropolysaccharide increased, carboxyl-rich compounds decreased, and amide/amino sugar percentages stayed almost constant along the salinity transect. Overall, our understanding of DOM transformation from terrestrial sources to the ocean is still limited, due to our inability to unravel the "molecular messages" in DOM.

Solid-state NMR is capable of seeing both the molecularly characterized and the molecularly uncharacterized fractions, with NMR observabilities not affected by DOM degradation, and the additional benefit of being non-destructive. Solid-state NMR can also provide information about nonprotonated C, not detected in advanced solution NMR experiments that rely on ^{1}H detection or inverse detection. While it is a useful, non-

destructive approach to investigating functional group distributions, many published solid-state ^{13}C NMR spectra of DOM show only broad peaks due to the presence of many different compounds containing similar functional groups in DOM. Recent breakthroughs in advanced NMR spectroscopy involving spectral editing (such as CH-, CH_2-selection, and ^{13}C chemical-shift-anisotropy filtering) and multidimensional techniques can potentially bring a major fraction of DOM within our analytical window and greatly facilitate the deciphering of DOM's molecular messages. The present study applied advanced NMR techniques to investigate the chemical composition and structural changes of DOM samples collected from the Penobscot River, Penobscot Bay and Scotian Shelf waters of the Gulf of Maine with the intended goal of understanding the fate of terrestrial OM in the Gulf of Maine. For comparison with a 'purer' marine sample, one DOM sample from a site in the Pacific Ocean minimally influenced by terrestrial inputs is also included.

MATERIALS AND METHODS

Sample Collection and XAD Isolation. Whole water samples were collected from the Penobscot River (PR), Maine – an organic rich river and the second largest river system in New England, an estuarine site (Penobscot Bay, Maine; PB) and a marine site in the Gulf of Maine (GoM; Table 1). Large volume (27–230 L) water samples were filtered in the field with capsule filters (0.45 μm; Geotech Dispos-a-filter) and pre-rinsed with at least 2 L of sample water. Samples were kept in the dark and shipped on ice to the USGS laboratory in Boulder, CO.

Table 1

Elemental analyses and stable carbon and radiocarbon isotope compositions of hydrophobic acids isolated from the Penobscot River, Penobscot Bay, Gulf of Maine and Pacific Ocean.

Site Name	Key	Sampling Date	C	H	O	N	S	C/N	$\delta^{13}C$	$\Delta^{14}C$	^{14}C age
			(wt %)					mole	(‰)		(years BP)
Penobscot River at Eddington	PR	06/2008	52.96	4.80	40.81	0.95	0.48	65.0	-27.6	72.8 ± 3.2	> Modern
Penobscot Bay at Buoy F	PB	06/2008	50.74	5.40	40.52	1.92	1.42	30.8	-25.3	-65.9 ± 2.7	490 ± 25
Gulf of Maine	GoM	05/2008	53.82	5.71	38.03	1.66	0.79	37.8	-24.3	-215.6 ± 3.4	1890 ± 35
Pacific Ocean - 800 ft depth	PO	02/1986	57.49	6.10	34.53	1.48	0.39	45.3	-23.0	-401.1 ± 1.9	4060 ± 30

XAD isolation and concentration were performed as described by Aiken et al. (1992). Briefly, samples were acidified to pH 2 with hydrochloric acid (HCl) and passed through an XAD-8 resin column. The hydrophobic organic acid (HPOA) fraction was retained on the XAD-8 resin and then eluted with 0.1 M sodium hydroxide (NaOH). The eluate was immediately desalted using H^+ saturated AG-MP 50 cation exchange resin (Bio-Rad), lyophilized, and stored in a desiccator.

The Pacific Ocean (PO) sample was extracted from water collected in the eastern equatorial Pacific Ocean near Hawaii from a depth of about 200 m (Malcolm, 1990). The sample was processed in the same manner by XAD-8 resin method as noted above. The fulvic acid (FA) fraction analyzed in the present study was obtained by acidifying the XAD-8 eluate to pH < 1 using HCl. The supernatant containing FA was then desalted, hydrogen saturated, lyophilized, and stored in a desiccator. The FA fraction generally accounts for 90–95% of the HPOA fraction.

Elemental Analyses and Carbon Isotopic Measurements. Elemental analyses (C, H, O, N, S and ash) of isolates were performed by Huffman Laboratories (Golden, Colorado) by the method of Huffman and Stuber (1985). Stable carbon isotope ratios ($\delta^{13}C$) were determined by isotope ratio mass spectrometry on dried samples following vapor phase acidification, and are expressed relative to the PDB standard. The radiocarbon ratios were measured by accelerator mass spectrometry at the Center for Accelerator Mass Spectrometry at Lawrence Livermore National Laboratory (California, USA). ^{14}C data (in ‰) were corrected for isotopic fractionation using measured $\delta^{13}C$ values and radiocarbon ages were determined from percent modern carbon using the year

of sample analysis according to Stuiver and Polach (1977). Ages are presented as Modern when the fraction modern exceeded 1. The results of elemental analyses and carbon isotopic data are given in Table 1.

NMR Analysis. ^{13}C NMR experiments were performed using a Bruker DSX400 spectrometer at 100 MHz (400 MHz ^{1}H frequency). All the 1D experiments were run with a 4-mm double-resonance probehead, while 2D experiments were performed using a 7-mm double-resonance probehead. The ^{13}C chemical shifts were referenced to tetramethylsilane, using the COO resonance of glycine in the α-modification at 176.46 ppm as a secondary reference.

Quantitative ^{13}C DP/MAS and DP/MAS with Recoupled Dipolar Dephasing (DP/MAS/DD) NMR. Quantitative ^{13}C DP/MAS NMR experiments were performed at a spinning speed of 14 kHz. A Hahn spin echo was generated before detection to avoid baseline distortions associated with detection directly after the 90° excitation pulse (Mao and Schmidt-Rohr, 2004a). ^{1}H decoupling of sufficiently high-power at $|\gamma B_1|/2\pi = 72$ kHz with two-pulse phase-modulated (TPPM) (Bennett et al., 1995) was applied during detection. Recycle delays (20-150 s) were determined by the cross polarization/spin-lattice relaxation time/total sideband suppression technique to ensure that all carbon sites were > 95% relaxed (Mao et al., 2000). To obtain quantitative information on the nonprotonated and mobile carbon fractions, ^{13}C DP/MAS NMR with recoupled dipolar dephasing was used (Mao and Schmidt-Rohr, 2004a). The dipolar dephasing time was 68 μs. The recycle delay was 130 s and the number of transients averaged was 320 scans for PB HPOA and GoM HPOA, and 150 s and 192 scans for PO FA, respectively. Recycle

delays of 20 s and 130 s were tested for PR HPOA, and the spectra obtained were very similar and thus added up. The number of scans averaged was 1920. The total time for DP/MAS and DP/MAS/DD experiments was 14-23 h per sample.

^{13}C Cross Polarization and Total Suppression of Sidebands (CP/TOSS) and ^{13}C CP/TOSS Plus Dipolar Dephasing (CP/TOSS/DD). Semi-quantitative compositional information was obtained with good sensitivity using a ^{13}C CP/TOSS NMR technique at a spinning speed of 7 kHz, a CP time of 1 ms, and a ^{1}H 90° pulse-length 4.1 μs, and a recycle delay of 0.5 s. Four-pulse TOSS (Dixon, 1982) was employed before detection, with the TPPM decoupling applied for optimum resolution. Sub-spectra for nonprotonated and mobile carbon groups were obtained by combining the ^{13}C CP/TOSS sequence with a 48-μs dipolar dephasing. For ^{13}C CP/TOSS experiments, 6144 scans were collected for PR and GoM HPOA isolates, 8192 scans for PB HPOA, and 4096 scans for PO FA. The number of scans was doubled in corresponding ^{13}C CP/TOSS/DD experiments for each sample.

^{13}C Chemical-Shift-Anisotropy (CSA) Filtering. Both anomeric (O-C-O) and aromatic carbons resonate between 120 and 90 ppm. To resolve the overlapping resonances, the aromatic carbon signals were selectively suppressed using a three-pulse ^{13}C CSA filter with a CSA-filter time of 68 μs (Mao and Schmidt-Rohr, 2004b). The number of scans averaged was 3072 for PR and GoM HPOA isolates, 4096 for PB HPOA, and 2048 for PO FA, respectively. In order to detect nonprotonated anomeric carbons, the CSA filter was combined with a dipolar dephasing time of 48 μs. The number of scans averaged for the spectrum of CSA filter coupled with dipolar dephasing was twice that of the corresponding CSA-filtered spectrum for each sample.

CH Spectral Editing. The signals of CH groups were selected by dipolar distortionless enhancement by polarization transfer (Schmidt-Rohr and Mao, 2002) at a spinning speed of 5.787 kHz. CH group multiple quantum coherence was not dephased by the spin-pair CH dipolar coupling while CH_2 coherence was dephased by dipolar coupling of the carbons to the two protons. The first of a pair of recorded spectra contains signals of CH, as well as residual quaternary carbon and CH_3 peaks that were removed by taking the difference with a second spectrum acquired with the same pulse sequence except for additional 40 μs dipolar dephasing before detection. Each spectrum of PR HPOA was based on 61,440 scans, and that of GoM HPOA was based on 49,152 scans.

CH_2 Spectral Editing. Spectral editing of CH_2 signals was achieved by selection of the three-spin coherence of CH_2 groups, using a ^{13}C 90° pulse and ^{1}H 0°/180° pulses applied after the first quarter of one rotation period with MREV-8 decoupling (Mao and Schmidt-Rohr, 2005). A total of 174,080 scans for PR HPOA and 176,128 scans for GoM HPOA were collected with a 0.5 s recycle delay and the spinning speed was 5.787 kHz.

Two Dimensional (2D) ^{1}H-^{13}C Heteronuclear Correlation (HETCOR) NMR. 2D HETCOR NMR experiments (Mao and Schmidt-Rohr, 2006) were performed at a spinning speed of 6.5 kHz. The scale on which ^{1}H-^{13}C proximities were probed was chosen by the cross polarization method and by ^{1}H spin diffusion before cross polarization. Two kinds of CP were employed. Lee-Goldburg cross polarization (LG-CP) of 0.5 ms was used to suppress ^{1}H-^{1}H spin diffusion during polarization transfer, and the spectra show three- or less bond ^{1}H-^{13}C connectivities. Standard Hartmann-Hahn CP (HH-CP) with 80 μs CP time reveals primarily one-bond ^{1}H-^{13}C connectivities. HH-CP of 0.5 ms allows for some ^{1}H spin diffusion and so correlates the carbons with protons

within a ~ 4 Å radius. In addition, a 40-μs dipolar dephasing delay was inserted in the LG-CP and HH-CP HETCOR to reveal ^{1}H-^{13}C proximities for nonprotonated carbons (multi-bond) and mobile groups like CH_3. The recycle delays were 0.7 s for PR HPOA, and 2 s for PO FA.

The sizes of aromatic and aliphatic domains were probed by ^{1}H spin diffusion during a mixing time using 2D HETCOR at a spinning speed of 6.5 kHz and HH-CP of 0.5 ms. The mixing times ranged from 10 μs to 10 ms. The recycle delays were 0.7 s for PR HPOA, and 2 s for PO FA. Each 2D HETCOR spectrum took 5-27 h.

RESULTS

Stable Carbon and Radiocarbon Isotopic Compositions. The $\delta^{13}C$ value was -27.6‰ for PR (Table 1), falling within the range of $\delta^{13}C$ values reported for DOM from riverine waters (McCallister et al., 2004) and indicative of terrigenous sources. The $\delta^{13}C$ values became less negative for samples obtained from PB (-25.3‰), GoM (-24.3‰), and PO (-23.0‰); i.e., these samples became increasingly ^{13}C enriched. The $\Delta^{14}C$ values were 72.8 ± 3.2‰ for PR, -65.9 ± 2.7‰ for PB, -215.6 ± 3.4‰ for GoM, and -401.1 ± 1.9‰ for PO. These values translated to ^{14}C ages of modern, 490 ± 25, 1890 ± 35, and 4060 ± 30 years before present (ybp), respectively. The modern ^{14}C age of PR HPOA pointed to a predominant source from fresh or recent plant litter and surface soil organic matter (modern terrestrial primary production). The ^{14}C ages increased in PB and further in GoM and the open ocean PO FA.

Quantitative DP NMR and Detailed NMR Analyses Based on Spectral-Editing Techniques. Quantitative ^{13}C NMR analyses were performed for all the samples, with their spectra of all C (DP/MAS, thin lines) and of nonprotonated and mobile C (DP/MAS/DD, bold lines) shown in Figure 4. The assignments of the following peaks were relatively straightforward: 220-190 ppm, ketone, quinone, or aldehyde; 190-162 ppm, COO and N-C=O; 162-145 ppm, aromatic C-O; 145-100 ppm, aromatic C; 120-100 ppm, anomeric C (O-C-O); and 100-64 ppm, O-alkyl C. Signals in the 64-0 ppm region, however, included contributions from various alkyl C groups (i.e., OCH_3, quaternary C, OCH_2, CCH_2, NCH, CCH, CCH_2 and CCH_3). Specific assignments were difficult because the alkyl band was broad and overlapping; however, the interpretation was assisted by spectral editing as described below.

Figure 5 shows the spectra from ^{13}C CP/TOSS and spectral editing techniques of samples isolated along the salinity transect as well as from the Pacific Ocean. The ^{13}C CP/TOSS spectrum of each sample (Figure 5(a-d)) was dominated by resonances of nonpolar alkyl C (0-64 ppm), O-alkyl C (64-100 ppm), aromatic or olefinic C (100-160 ppm, also containing anomeric C), and carboxyl/amide C (160-190 ppm). The C=O peak around 200 ppm (assigned to ketone/aldehyde C) was weak yet evident in spectrum of PR, was weaker in PB and GoM, and essentially absent in PO.

Figure 5(a1-d1, bold lines) shows the CP/TOSS spectra obtained after dipolar dephasing, which selected the signals from nonprotonated C and mobile C groups. These spectra were characterized by resonances from COO/NCO, aromatic C-C, CCH_3, nonprotonated OC (OC_{np}), nonprotonated anomeric C ($OC_{np}O$), quaternary C (CC_q), and

ketone C. The signals arising from OCH_3 and aromatic C-O were distinct in the spectrum of PR, much less obvious in that of PB, and absent in spectra of GoM and PO.

Figure 5(a2-d2) exhibits CP/TOSS spectra after the insertion of the CSA filter, which selected the resonances of sp^3-hybridized C. The signal from anomeric C (OCO) was now unambiguously identified in all samples as a shoulder that appeared around 100-120 ppm. The combination of this CSA filter technique with dipolar dephasing (Figure 5(a3-d3)) showed the signals of nonprotonated sp^3-hydridized C, further indicating that nonprotonated anomeric C ($OC_{np}O$) was present in significant amounts and that protonated anomeric C (OCHO) was a more minor component in all samples.

Due to the large degree of signal overlap in the aliphatic region, the spectral editing techniques of CH and CH_2 selection were further applied to PR and GoM HPOA isolates and the resulting spectra were shown in Figure 6(c, d, h, and i). The full spectra and sub-spectra of nonprotonated C and mobile C from DP experiments were also shown for reference (Figure 6(a, b, f and g)). The CH-only spectra of both PR and GoM showed the resonances of aromatic/olefinic CH (110-140 ppm), OCH (62-90 ppm), NCH/CCH (30-62 ppm), as well as minor resonances arising from OCHO as a shoulder at ~100 ppm. The CH_2-only spectra of both samples showed a major peak from CCH_2 (20-50 ppm), with the remaining minor signals assigned to OCH_2, whose relative intensities were higher in PR than in GoM HPOA.

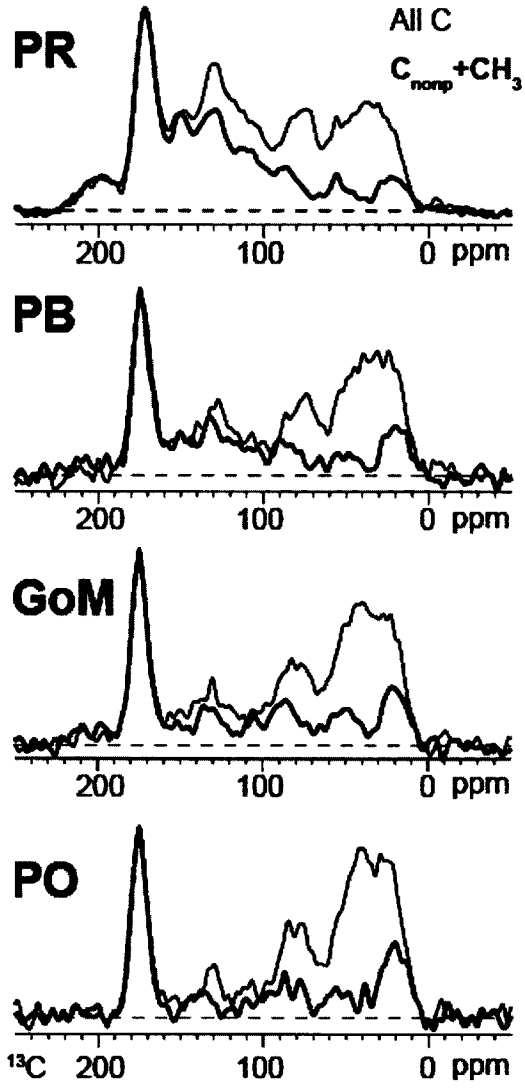

Figure 4. Quantitative ^{13}C NMR spectra, obtained with direct polarization at 14 kHz MAS of (a) PR HPOA, (b) PB HPOA, (c) GoM HPOA, and (d) PO FA. Thin line: spectrum of all C; bold line: corresponding spectrum of nonprotonated C and CH_3, obtained after 68 μs of dipolar dephasing.

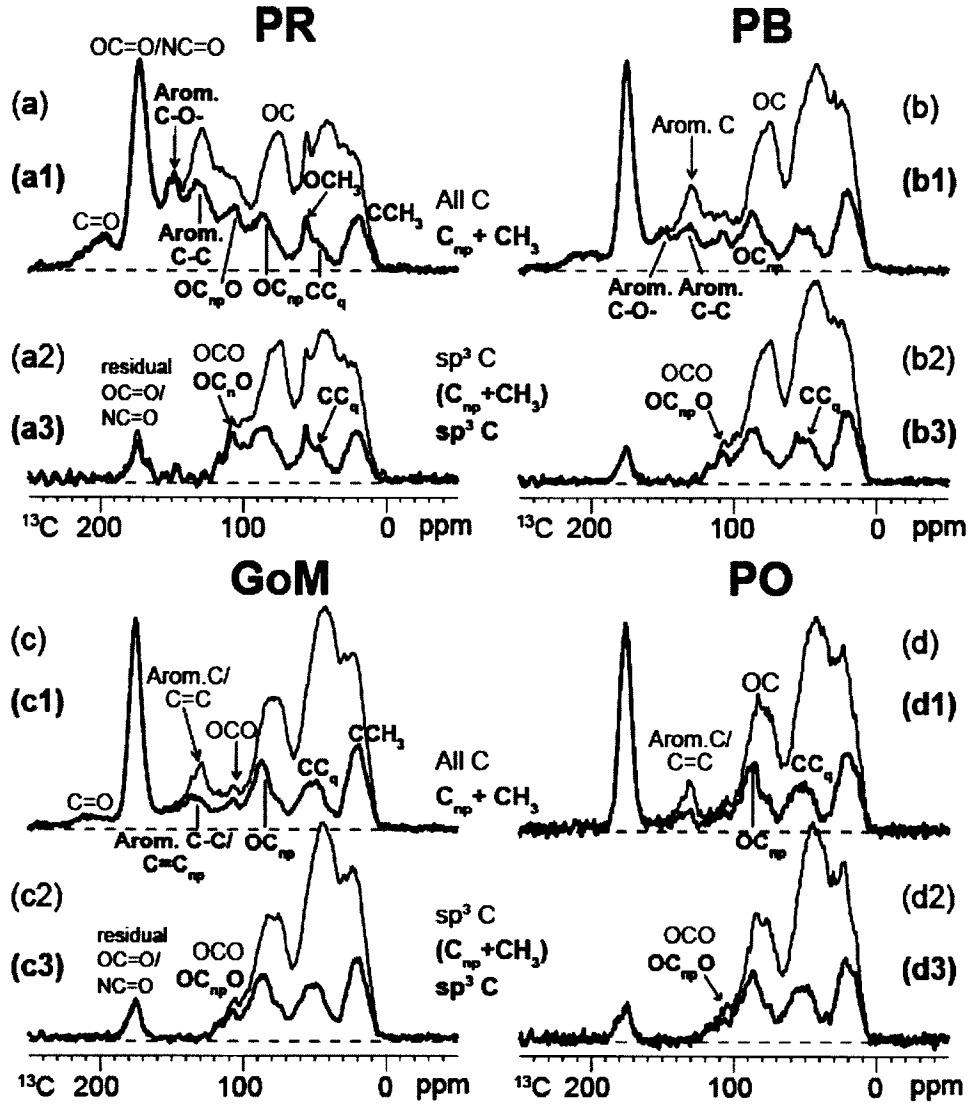

Figure 5. Spectral editing for identification of functional groups in river and marine HPOA/FA samples. (a-d) ^{13}C CP/TOSS spectra in thin lines for reference. (a1-d1) CP/TOSS spectra with 40-μs dipolar dephasing showing nonprotonated carbons and mobile segments such as CH_3 in bold lines. (a2-d2) Selection of sp^3-hybridized carbon signals by a ^{13}C CSA filter (thin lines). (a3-d3) Selection of nonprotonated sp^3-hybridized carbon signals and mobile segments such as CH_3 (bold lines). All CP/TOSS spectra are scaled to match the intensity of the COO/NCO band.

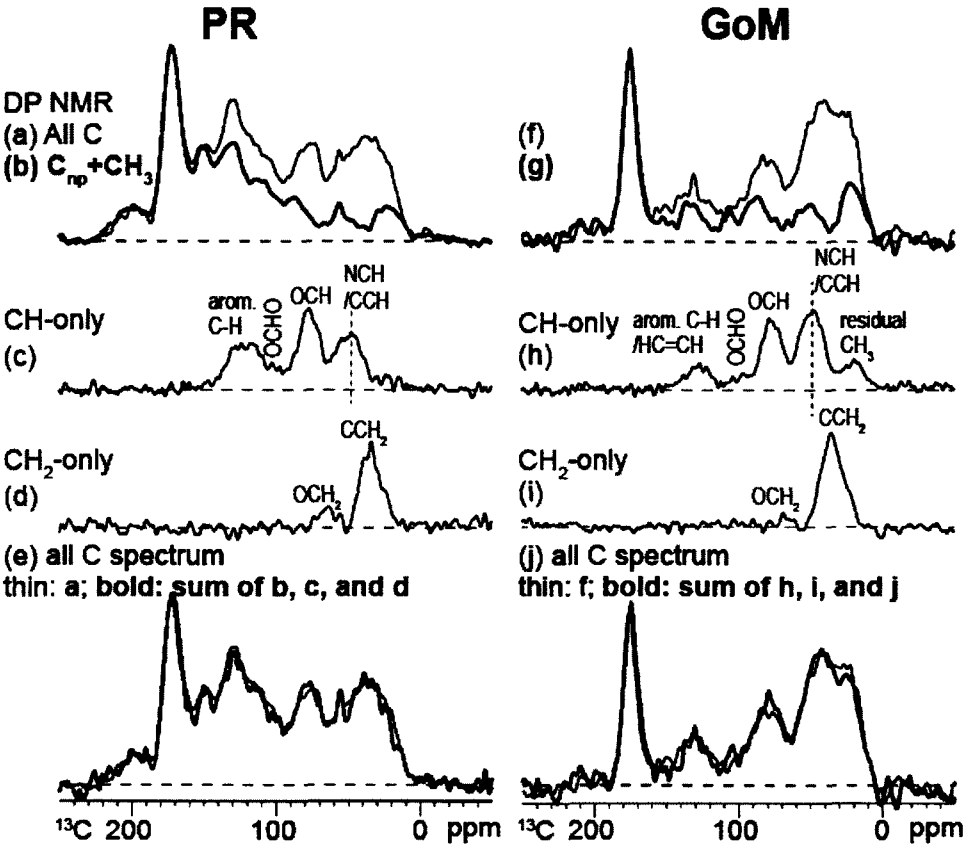

Figure 6. ^{13}C NMR with spectral editing of PR HPOA and GoM HPOA. (a, f) ^{13}C DP/MAS NMR spectra. (b, g) DP/MAS with recoupled dipolar dephasing. (c, h) CH-only spectra. (d, i) CH_2-only spectra. (e) Estimated all C spectrum (bold line) by adding up signals of properly scaled (b), (c), and (d). (j) Estimated all C spectrum (bold line) by adding up signals of properly scaled (g), (h), and (i). Thin lines are experimental ^{13}C DP/MAS spectra shown for reference.

The composite all C spectra (Figure 6(e, j), bold lines) produced by adding up signals of respective dipolar dephased spectra (Figure 6(b, g)), CH- and CH_2-only spectra (Figure 6(c, d, h, and i)), closely resembled the experimental all C spectra (Figure 6(e, j), thin lines; i.e., Figure 6(a, f)). Figure 6 demonstrates that the spectral editing techniques, CH and CH_2 selection in particular, have successfully resolved overlapping peaks, and identified specific functional groups such as CH_3, OCH_2, OCH, OCO, CCH_2 and NCH/CCH.

Distribution of Functional Groups Based on Quantitative DP NMR and Spectral-Editing Techniques. The abundances (in %) of different functional groups from DP and spectral-editing spectra were compiled in Table 2. For PR, the dominant component was aromatic C (34%), followed by alkyl C (26%). By contrast, the dominant component in the other three samples was alkyl C, accounting for 40-53%. Aromatic C was much less abundant in PB (21%) than in PR, and further depleted in GoM (15%) and PO (9%). The abundances of O-alkyl and anomeric C (18-21%), and COO/NC=O (18-19%) were rather constant in four samples. Ketone C, which comprised 2-4% in other samples, was absent in PO. It is worth noting that all samples contained significant amounts of nonprotonated O-alkyl C (OC_{np}, 8-10%), quaternary C (CC_q, 3-6%), and CH_3 (6-16%). Though aromatic C-O still comprised a considerable fraction of all C (9% and 5%, respectively) in PR and PB HPOA, OCH_3 was a very minor component (< 1%). The GoM and PO samples contained less aromatic C-O (4% and 2%, respectively) and no contribution from OCH_3.

Structural Information from Short-Range ^{1}H-^{13}C HETCOR NMR and HETCOR NMR with Spin Diffusion. Figures 7, 8 and 9 show 2D HETCOR spectra of PO FA and PR HPOA acquired under various conditions. The ^{1}H slices at different ^{13}C chemical shifts were extracted to observe the correlations more clearly. Proton chemical shifts were assigned as follows: 0.8-3 ppm, nonpolar alkyl protons; 3-5.5 ppm, protons associated with O/N-alkyl groups; 5.5-9 ppm, aromatic/amide protons; and above 9 ppm, COOH protons.

Figure 7(a) shows the 2D HETCOR spectrum of PO FA with HH-CP of 80 μs (effective spin diffusion time, $t_{m,e}$ = 20 μs), in which primarily one-bond connectivities were observed. ^{1}H slices (Figure 7(b)) extracted at the alkyl ^{13}C chemical shifts of 24 (CH_3), 30 (CH_2), and 40 ppm (CH) showed correlations primarily with their own alkyl protons resonating at 1-3 ppm. The ^{1}H spectrum associated with the 130 ppm resonance showed contributions from aromatic protons around 7 ppm. ^{1}H slices extracted at 76 ppm of O-alkyl carbons indicated that the dominant contributions were from the directly bonded O-alkyl protons (~ 4 ppm). With a longer 0.5-ms HH-CP contact time ($t_{m,e}$ = 0.125 ms), the major band in ^{1}H spectra associated with O-alkyl C (76 ppm) shifted to 2.5 ppm (Figure 7(c)), indicating that O-alkyl C sites were in close proximity to alkyl protons.

In order to observe nontrivial correlations between nonprotonated carbons and their nearby protons, which are separated by at least two bonds, a 2D HETCOR spectrum with 0.5-ms LG-CP and 40-μs dipolar dephasing (Figure 7(d)) was recorded and proton slices were extracted (Figure 7(e)). The use of LG-CP suppressed ^{1}H-^{1}H spin diffusion during polarization transfer. Interestingly, the ^{1}H slice extracted at nonprotonated OC (86 ppm) showed major contributions from CH/CH_2 resonating near 2 ppm, indicating that

nonprotonated OC was found predominantly near alkyl protons, rather than, near O-alkyl protons. Similarly, the ^{1}H slices extracted at 108 ppm (nonprotonated anomeric C, $OC_{np}O$), and 48 ppm (quaternary C, C_q), showed primarily correlations with alkyl CH/CH_2 (~2.5 ppm). The ^{1}H spectrum associated with the nonprotonated aromatic ^{13}C chemical shifts of 130 ppm indicated contributions from aromatic protons, as well as correlations with alkyl protons (~2.5 ppm). The dominant ^{1}H signal at the COO resonance is near 2.8 ppm, indicating that COO groups were in close proximity with CH protons. The broad band extending beyond 12 ppm indicated contributions from COOH protons.

Table 2

Assignments and integrated areas (in %) of the ^{13}C NMR signals of all samples.

Samples	ppm												
	220-190	190-162	162-145	145-107		123-100 (OCO)		100-64 (OC)		64-0 (Alkyl C)			
	Ketone C	COO/ NC=O	Arom. C-O	Arom. C-C[a]	Arom. C-H	$OC_{np}O$[b]	OCHO[b]	OC_{np}[a]	OCH_n	C_q[a]	OCH_3[a]	$CH_2/CH/NCH$	CH_3[a]
PR HPOA	3.6	17.5	8.8	15.1	10.1	3.1	0.1	6.4	9.7	2.9	0.9	15.4	6.4
PB HPOA	2.1	18.3	5.2	9.9	6.1	2.0	0.3	6.2	9.4	3.4	0.3	25.6	11.2
GoM HPOA	1.9	18.9	3.8	6.1	4.8	2.1	0.5	7.8	9.5	5.8	0.0	26.3	12.4
PO FA	0.0	18.1	1.8	2.9	4.0	2.0	0.4	6.5	11.6	4.8	0.0	32.0	15.8

[a] Based on DP and DP spectra with 68-μs dipolar dephasing.

[b] Based on CSA-filtered CP/TOSS spectrum and CSA-filtered CP/TOSS spectrum with dipolar dephasing.

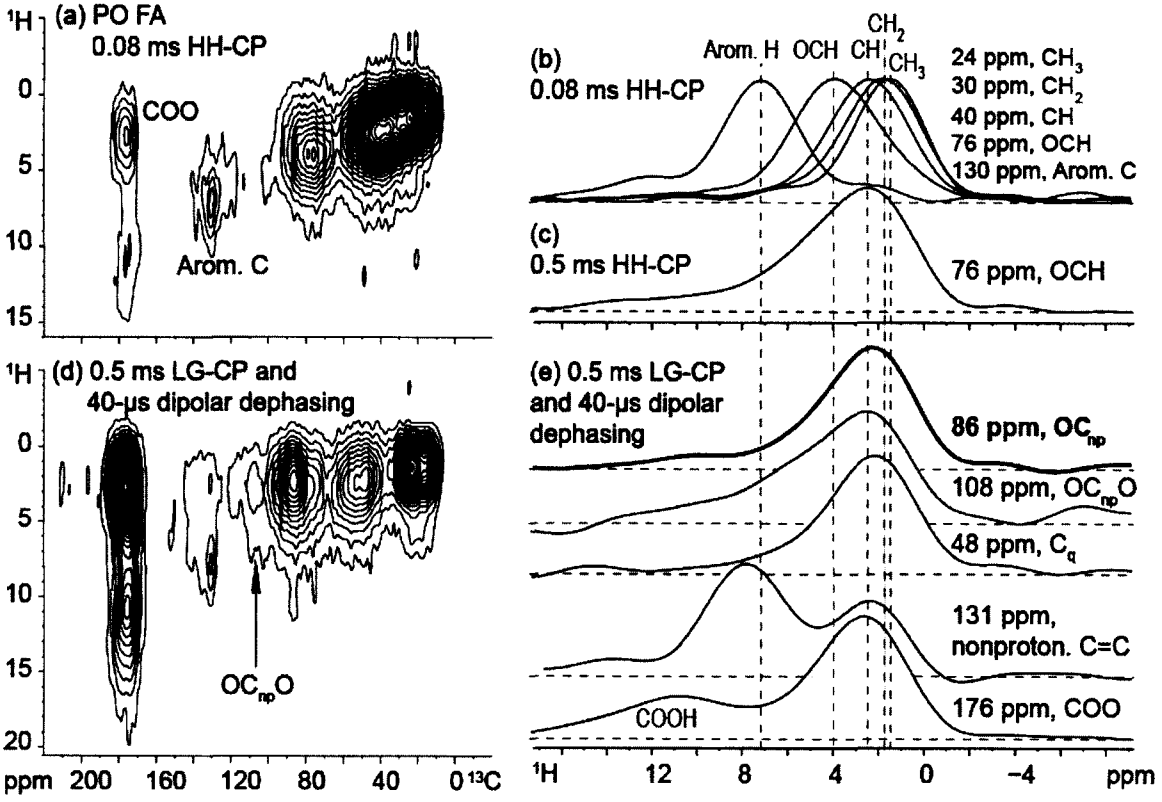

Figure 7. 2D ^{1}H-^{13}C HETCOR NMR spectra of PO FA. (a) Contour plot of the 2D spectrum with 80-μs HH-CP. (b) Cross sections of spectrum in (a), at the ^{13}C chemical shifts indicated: 24 ppm, 30 ppm, 40 ppm, 76 ppm, and 130 ppm. (c) Cross section from 0.5-ms HH-CP 2D spectrum at 76 ppm. (d) Contour plot of the 2D spectrum with 0.5-ms LG-CP and 40-μs dipolar dephasing. (e) Cross sections of spectrum in (d), at the ^{13}C chemical shifts indicated: 86 ppm, 108 ppm, 48 ppm, 131 ppm, and 176 ppm.

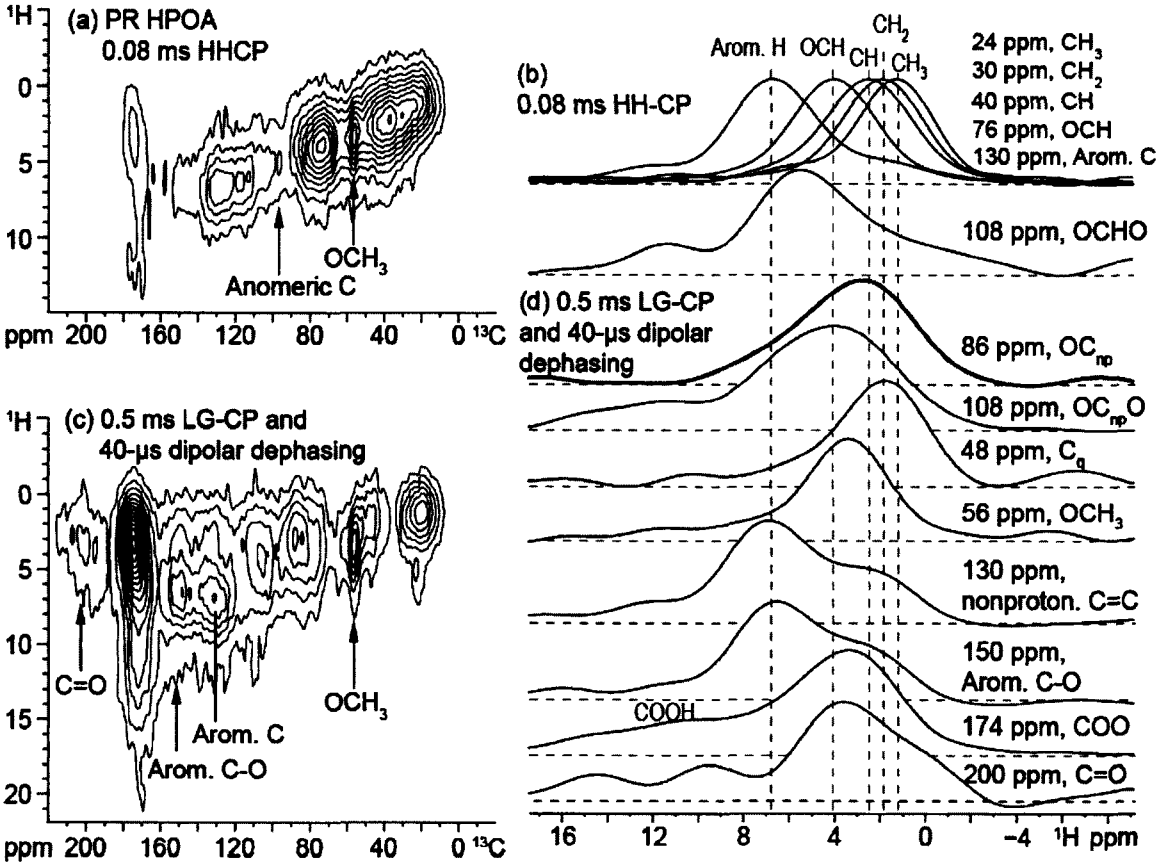

Figure 8. 2D ^{1}H-^{13}C HETCOR NMR spectra of PR HPOA. (a) Contour plot of the 2D spectrum with 80-μs HH-CP. (b) Cross sections of spectrum in (a), at the ^{13}C chemical shifts indicated: 24 ppm, 30 ppm, 40 ppm, 76 ppm, 130 ppm, and 108 ppm. (c) Contour plot of the 2D spectrum with 0.5-ms LG-CP and 40-μs dipolar dephasing. (d) Cross sections of spectrum in (c), at the ^{13}C chemical shifts indicated: 86 ppm, 108 ppm, 48 ppm, 56 ppm, 130 ppm, 150 ppm, 174 ppm, and 200 ppm.

The 2D HETCOR spectrum of PR HPOA with HH-CP of 80 μs (Figure 8(a), $t_{m,e}$ = 20 μs) showed similar cross peaks as observed in corresponding spectrum of PO FA. In addition, 2D HETCOR spectrum of PR showed cross peaks of OCH_3 and of protonated anomeric C (OCHO). Proton slices were extracted at the ^{13}C chemical shifts of 24 (CH_3), 30 (CH_2), 40 ppm (CH), 76 ppm (OCH), and 130 ppm (aromatic C), served as the reference for ^1H chemical shifts (Figure 8(b)). Anomeric carbons (108 ppm) showed correlations with their directly bonded protons (5-6 ppm) as well as OCH protons. With 0.5-ms LG-CP and 40-μs dipolar dephasing (Figure 8(c)), correlations between nonprotonated carbons and their nearby protons (e.g. aromatic C and non-aromatic H) can be detected. The ^1H slices extracted at nonprotonated OC (86 ppm) and at quaternary C (48 ppm) showed major contributions from CH/CH_2 resonating near 2 ppm (Figure 8(d)), similar to those of PO. The ^1H slice extracted at 108 ppm ($OC_{np}O$), however, showed primarily correlations with OCH (4 ppm). The ^1H slice extracted at 56 ppm due to OCH_3 demonstrated that these carbons were mainly associated with their directly bonded protons (~3.6 ppm). The ^1H slices from 130 ppm (nonprotonated aromatic C) and 150 ppm (aromatic C-O) showed correlations predominantly with aromatic protons but also contributions from O-alkyl and alkyl protons. The ^1H slice associated with COO resonances (174 ppm) showed contributions primarily from alkyl, O-alkyl protons, as well as COOH protons. The dominant ^1H signal at the ketone resonances (200 ppm) was near 3 ppm, indicating that ketones were in close proximity with alkyl and O-alkyl protons.

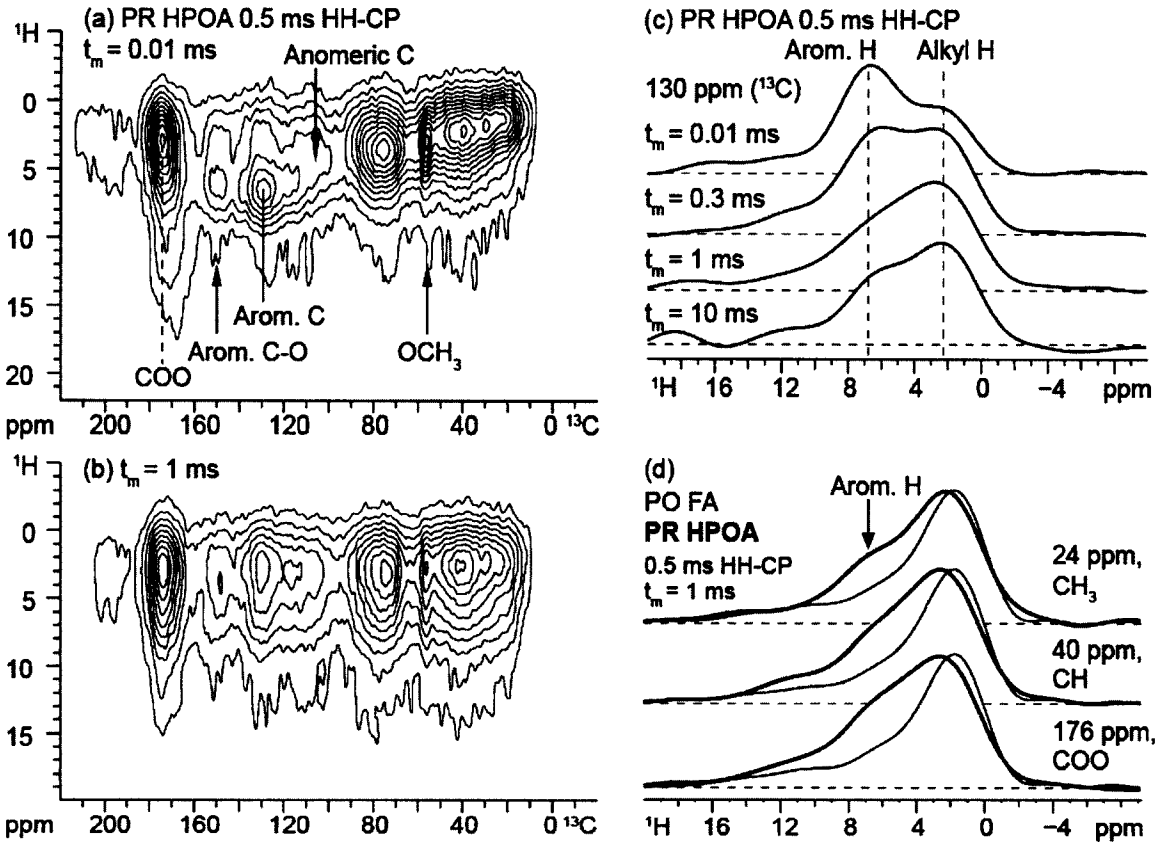

Figure 9. Spatial proximity of functional groups in PR HPOA probed using ^{1}H-^{13}C HETCOR with ^{1}H spin diffusion during 0.5 ms of HH-CP and (a) nominal t_m = 0.01 ms, (b) t_m = 1 ms. (c) Cross sections taken at ^{13}C chemical shift of 130 ppm, from 2D spectra collected at different spin-diffusion times (0.01 ms, 0.3 ms, 1 ms, and 10 ms). (d) ^{1}H slices extracted from 0.5-ms HH-CP HETCOR spectra of PR HPOA (bold lines) and PO FA (thin lines) with spin-diffusion time of 1 ms, at the ^{13}C chemical shifts indicated: 24 ppm, 40 ppm, and 176 ppm.

The 2D HETCOR NMR spectra of PR HPOA were also collected with 0.5-ms HH-CP at several different spin-diffusion times (0.01 ms, 0.3 ms, 1 ms, and 10 ms) to probe the proximities of different components at the nanometer scale. Figure 9(a, b) shows HETCOR spectra with 0.01-ms and 1-ms spin diffusion. After 1 ms ($t_{m,e}$ = 1.125 ms), cross peaks of aromatic C-alkyl H were clearly visible. Figure 9(c) shows the ^{1}H slices extracted at ^{13}C chemical shift of 130 ppm (aromatic C) for the four different mixing times. As mixing time increased the relative intensity of aromatic ^{1}H peak decreased while that of the alkyl H increased, indicating magnetization transfer from alkyl to aromatic residues. Figure 9(d) displays ^{1}H slices extracted from 0.5-ms HH-CP HETCOR spectra of PR (bold lines) and PO (thin lines) with spin-diffusion time of 1 ms. The ^{1}H spectra associated with ^{13}C chemical shifts of 24 ppm (CH_3), 40 ppm (CH), and 176 ppm (COO) of PR clearly showed contributions from aromatic H, indicating the proximities of these carbon sites to aromatic protons. For PO shown for comparison, the dominant ^{1}H signals at these resonances were from alkyl H.

Synopsis-Major Structural Units Based on 1D and 2D NMR Spectra. Combining the information extracted from all the 1D and 2D spectra, we probed the chemical environments of functional groups present in all samples from right to left in the ^{13}C spectrum.

CH_3 groups. Most of the signals in the 0-35 ppm range were due to CH_3 groups bonded to C; this is proven by the survival of the signal in the dipolar-dephased spectra (Figures 4 and 5) and by their ^{1}H chemical shifts (Figure 7(b) and Figure 8(b)). The CH_3 peak of all samples (Figure 8), centered at 21 ppm, was broad and indicated a variety of

structural environments. In order to shed more light on the degree of branching near the CH_3 groups, Figure 10(a) shows a diagram of chemical shifts of CH_3 (C-substituted only), computed via ACD CNMR predictor software, versus the number of its β-carbons, which has the strongest influence on CH_3 chemical shifts (Bovey, 1987). The chemical shifts of CH_3 with one β-carbon (e.g., CH_3 bonded to CH_2 at the end of aliphatic chains) were restricted to < 16 ppm. From the experimental CH_3 chemical shifts of PR and GoM samples, the majority of CH_3 groups in our samples seemed to have two to three β-carbons, and could be attached to an aryl ring, or tertiary aliphatic carbons, consistent with previous assignments (Wilson et al., 1983; Wu and Zilm, 1993). In Figure 9(d), the ^1H slices extracted at 24 ppm (CH_3) showed that while some CH_3 groups in PR were attached to aromatic rings, CH_3 groups in PO seemed to be primarily attached to aliphatic and O-alkyl groups.

CH_2 groups. Mobile $(CH_2)_n$ chains were absent in our samples; otherwise, a peak would appear at ~30 ppm in their dipolar-dephased spectra (Hu et al., 2000). In the CH_2-only spectra (Figure 6(d, i)), CH_2 chemical shifts, centered at 35 ppm, spanned a range from 20 to 50 ppm. 2D spectra showed that CH_2 structures were mostly present in aliphatic environments.

OCH_3 groups. The sharp peak at 56 ppm was apparent in ^{13}C dipolar-dephased spectra of PR and PB samples (Figure 8(a1, b1)). In Figure 8(c), strong cross peak was observed between OCH_3 carbons and their own protons. With longer spin diffusion time (t_m = 1 ms, Figure 9(b)), cross peaks between OCH_3 carbons and aromatic protons became more prominent, showing that the OCH_3 were in a lignin-like structure: $C_{arom}H–C_{arom}–O–CH_3$.

O-alkyl groups. The signals in the 64-100 ppm range could be due to CHO, CH_2O, or $C_{np}O$. The CH_2-only spectra (Figure 6(d, i)) and quantitative data (~1% in PR and < 1% in GoM) showed that contributions of $-CH_2-O-$ were almost negligible. The 2D spectra of PO (Figure 7(c, e)) indicated that both protonated and nonprotonated O-alkyl carbon sites were in close proximity to alkyl protons, suggesting an $O-C(H)-CH_n$ structure. Hence they were not in carbohydrate-like environments. The 2D spectra of PR HPOA (Figure 8) indicated that nonprotonated O-alkyl carbon sites were in close proximity both to alkyl protons and O-alkyl protons; hence a fraction of these could be in carbohydrate-like environments.

Anomeric C groups. Signals in the 100-120 ppm region (Figure 8) could arise from anomeric C (acetal, O–CHR–O; ketal, $O-C_{np}RR'-O$), or aromatic C (Leenheer et al., 1987; Wilson and Hatcher, 1988; Wilson et al., 1983). Based on the CSA-filtered CP/TOSS spectra, whereas signals in this region in the other samples include contributions from aromatic C, those in PO arose exclusively from anomeric C. Our 2D HETCOR data also confirmed the assignment to anomeric C (Figures 7 and 8). For the protonated C near 108 ppm, its proton slice showed a major band near 5.5 ppm (Figure 8(b)), consistent with anomeric proton assignment. For the nonprotonated C near 108 ppm, its proton slices were mainly associated with alkyl protons (Figure 7(e)) and O-alkyl protons (Figure 8(d)). Furthermore, the proton slices of $OC_{np}O$ revealed a CH_n-O-C_{np}-O structure in PO, but OCH-O-C_{np}-O structure in PR. This indicated that anomeric C in PR HPOA could be in carbohydrate-like environments.

Aromatic C groups. Nonprotonated aromatic C groups were found near the aromatic protons as expected, but also showed proximity to alkyl protons, and OCH

protons in the case of PR. Aromatic C-O groups in PR, also showed correlations with OCH_3 protons (Figure 8(d)), consistent with lignin-like aromatic C–O–CH_3 structures.

COO groups. The COO groups were found predominantly near CH_n and OCH_n protons. The OCH_n might be due to CO–O–CH_n ester linkages, but these have a three-bond C– – –H distance, which would not favor the rapid H-to-C cross polarization observed in the experiments. In contrast, O–CH_n–CO–O– groups have a fixed and generally shorter two-bond C– –H distance, consistent with the structures derived by Leenheer et al. (1995) for a fulvic acid.

Ketones. The 1D spectra of PR HPOA showed clear peaks of carbonyl groups near 200 ppm, the majority of which were nonprotonated ketones or quinones. The cross peaks of carbonyls were only visible in the HETCOR spectrum of PR HPOA (Figure 8). According to Figure 8(d), most of the carbonyls were close to OCH_n and CH_n protons, indicating O=C–CH_n– or O=C–OCH_n-like structure.

DISCUSSION

Evidence for Carboxyl-Rich Alicyclic Molecules (CRAM). As early as 1994, Leenheer (1994) proposed molecular models of freshwater DOM from allochthonous and autochthonous sources that contain short-chain, branched, and alicyclic structures terminated by carboxyl or methyl groups. Indeed, this is the first documentation of CRAM-like structures in DOM. Hertkorn et al. (2006) using a range of modern 1D and 2D solution NMR approaches coupled with FT-ICR MS, identified similar structures in marine ultrafiltered DOM (UDOM) and named them CRAM. Subsequently, CRAM have been shown to be present as major structural components in freshwater DOM (Lam et al.,

2007; McCaul et al., 2011; Woods et al., 2011). We show evidence for the presence of CRAM as the major structural units of these HPOA samples from the Penobscot River to Gulf of Maine transect and from the Pacific Ocean, based on advanced spectral editing and quantitative peak analysis.

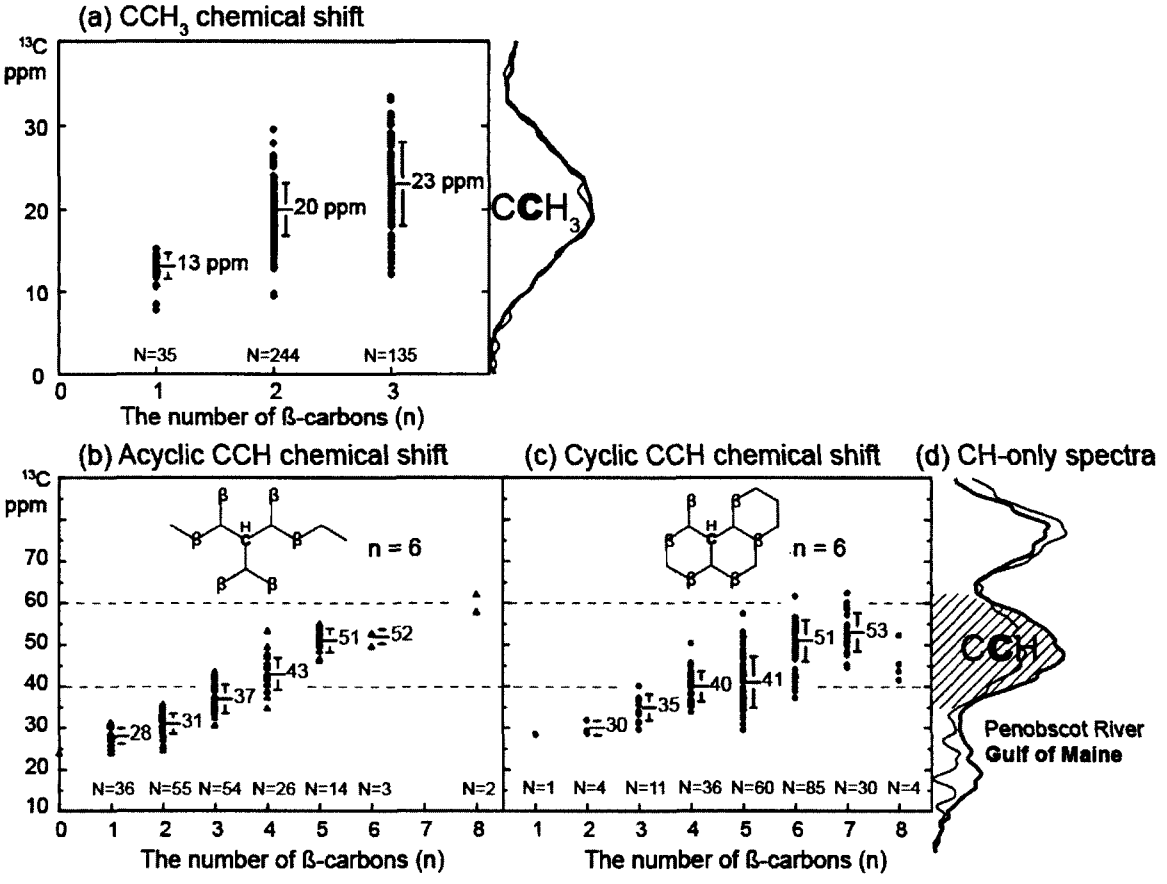

Figure 10. Diagram of chemical shifts of (a) CCH_3, (b) acyclic CCH, and (c) cyclic CCH, computed via ACD CNMR predictor software, versus the number of their β-carbons. (d) The CH-only spectra of PR HPOA (thin line) and GoM HPOA (bold line).

Abundant carboxyl groups are an essential element of CRAM. The COO/NCO band at ~176 ppm could include contributions from carboxyls, amides and aliphatic esters, accounting for ~18% of C in all HPOA samples. The C:N atomic ratios were 65, 31, 38, and 45, respectively for PR, PB, GoM, and PO samples, consistent with the values reported for marine and freshwater DOM isolated using XAD-8 resins (Aiken et al., 1992; Druffel et al., 1992; Hedges et al., 1992). Assuming all N is in amide form, 2-3%, at most, of the total ^{13}C NMR integral could be amide C. The content of ester linkages was also expected to be insignificant based on our analysis of 2D data. In addition, mobile poly(methylene) C typical of lipid was absent in dipolar dephased spectra of all samples. In summary, at least 14% of all C in HPOA samples was in COO groups: the structure was carboxyl-rich.

The discrimination between alicyclic and open chain aliphatic environments is more challenging. As pointed out earlier, all the samples studied were enriched in quaternary alkyl C, nonprotonated O-alkyl and anomeric C, which necessitate a highly branched structure. In the case of PR HPOA and GoM HPOA, CH-selection spectra estimated the contribution from CCH and NCH to be 7% and 12%, respectively. Due to the low abundance of N in the HPOA samples, NCH percentage was at most 2-3%; i.e., CCH accounted for most of these signals. Other interesting observations included the considerable ranges of CCH (34-62 ppm) and the shift of the OCH peak maximum from 72 ppm (typically observed in sugar rings) to ~78 ppm. Aliphatic branching imparts predictable chemical shifts in ^{13}C NMR spectra, for example, β carbon added to methine C could induce a downfield C NMR chemical shift of ~5 ppm each on average (Bovey, 1987). Figure 10(b, c) shows the diagrams of chemical shifts of methine C (C-substituted

only) in acyclic and cyclic environments, computed via ACD CNMR predictor software, versus the number of its β-carbons. Increasing the number of β-carbons of methine C clearly led to higher chemical shift values of methine C. Combined with experimental methine C chemical shifts in CH-only spectra (Figure 10(d)), our results showed that methine C with 6 β-carbons was most abundant in PR HPOA and GoM HPOA. Whereas methine C with 6 β-carbons is common in fused cyclic systems, the presence of such methine C necessitates a highly branched aliphatic chains and such system is much less common.

Changes in DOM Composition along the Salinity Gradient. Overall, aromatic components were lost, alkyl structures became more enriched, and contributions from COO/NC=O, O-alkyl and anomeric C stayed relatively constant in HPOA samples from the Penobscot River, through Penobscot Bay to Gulf of Maine and the Pacific Ocean. The contribution of ketone C decreased in the same order and was absent in Pacific Ocean FA.

Potential sources of aromatics in freshwater DOM could be lignin or tannin from terrestrial materials. Leenheer and Rostad (2004) identified tannins as one of the major precursors of Suwannee River fulvic acid, while lignin precursors were shown to be minor components. Our 2D analysis excluded tannin derivatives as a significant contributor to aromatics, in agreement with Mao et al. (2012b). It is possible, though, that tannin-like products which are relatively hydrophilic, were not recovered in HPOA/FA samples examined in this study (Liu et al., 2011; Sleighter and Hatcher, 2008). The peaks of aromatic C-O (~150 ppm) and OCH_3 (~57 ppm) associated with lignin, instead, were distinct in Penobscot River HPOA, suggesting the presence of lignin structural units,

which were further reduced in abundances in Penobscot Bay HPOA. Quantitative results (Table 2) showed 5-9% of aromatic C-O but <1% of OCH_3, suggesting demethylation or the transformation of -OCH_3 to -OH. The Gulf of Maine and Pacific Ocean samples contained less aromatic C-O (2-4%) and no contribution from OCH_3, indicating that lignin-like products were present at most in trace amounts, or were more severely modified. Liu et al. (2011) who studied C_{18} extracted bulk DOM and hydrophobic HPLC fractions using FT-ICR MS, however, suggested that lignin-derived compounds may survive the transit from the river to the coastal ocean. They reasoned that lignin-derived molecules could become structurally altered such that it escaped the analytical window of lignin phenol analysis. Nonetheless, with the low abundance of aromatic C-O (2-4%) detected by NMR in oceanic samples, our results imply that influence of local riverine inputs in terms of lignin may extend offshore in the coastal area, but may be efficiently removed from the ocean. Photooxidation is the major process in removing lignin compounds in aquatic systems (Benner and Kaiser, 2011; Dalzell et al., 2009; Dittmar et al., 2007; Hernes and Benner, 2003; Opsahl and Benner, 1998). The rate of photodegradation of lignin phenols has been shown to correlate positively with the number of OCH_3 on the aryl ring; syringyl (two -OCH_3) showed the highest photochemical decay constants, followed by vanillyl (one -OCH_3), and p-hydroxy phenols with no OCH_3 (Benner and Kaiser, 2011). This explained the paucity of OCH_3 even in Penobscot River HPOA. The Gulf of Maine HPOA contained relatively more aromatic/olefinic C, likely derived from modified lignin or aromatic amino acids of algal origin (phenylalanine and tyrosine), than Pacific Ocean FA.

The enrichment of aliphatic C in HPOA samples from oceanic sources relative to their freshwater or coastal counterparts has been well documented, indicative of their predominantly autochthonous sources, or likely due to the removal of lignin-like structure from terrestrial sources (Esteves et al., 2009; Hedges et al., 1992). Esteves et al. (2009) further pointed out that fulvic acids from ocean tend to be more branched than their terrestrial counterparts, based on the presence of a sharp peak at 18 ppm assigned to terminal methyl C in the CP/MAS spectra of open ocean fulvic acids. Highly branched aliphatic structures have been reported to be present in HPOA samples from both riverine and marine sources, primarily based on the identification of quaternary C and terminal methyl C in dipolar-dephased NMR spectra (Berwick et al., 2010; Esteves et al., 2009; Hedges et al., 1992; Leenheer et al., 2003; Leenheer and Rostad, 2004; McIntyre et al., 2005). Our quantitative analysis confirmed that, abundances of methyl C increased from 6% in PR HPOA, to ~12% in PB HPOA and GoM HPOA, and ~16% in PO FA. The contribution from quaternary C (6% and 5%, respectively) was slightly higher in GoM and PO samples, as compared to ~3% in PR HPOA and PB HPOA. It is very likely that HPOA samples from riverine sources have similar branched aliphatic structures as their oceanic counterparts, though abundances of these structures are diluted to a certain extent due to the presence of lignin in riverine HPOA.

Changes in Stable Carbon and Radiocarbon Isotopic Compositions. Results showed an enrichment of ^{13}C with salinity in the samples obtained from Penobscot River to Penobscot Bay, Gulf of Maine, and Pacific Ocean. This is typically interpreted as the significant dilution of land-derived material by marine inputs as marine DOC becomes

more important with distance from shore. However, the shifts in $\delta^{13}C$ of DOC observed during the mixing of river and marine waters could also be due to the removal of isotopically "light" DOC (depleted in ^{13}C) relative to bulk DOC, leaving a residual fraction of isotopically "heavy" DOC (Opsahl and Zepp, 2001). Our results combined with others provide evidence, as illustrated below, that lignin can be considered a good candidate for such isotopically "light" DOC fraction.

First, lignin decreased in abundance from Penobscot River to Gulf of Maine, and Pacific Ocean. NMR results showed the presence of lignin residues in Penobscot River, Penobscot Bay in much less abundance, and almost absent in Gulf of Maine and Pacific Ocean samples. In addition, dissolved lignin phenols of HPOA samples from similar sites were analyzed by Spencer et al. (2010), and their carbon-normalized yields (Λ_6, mg (100 mg OC)$^{-1}$) were found to decrease dramatically from 0.358 in Penobscot River to 0.124 and 0.023 in Penobscot Bay and Gulf of Maine, respectively. Secondly, it is well documented that lignin (from C_3 plants) is depleted in ^{13}C relative to bulk DOC. Lignin phenols have $\delta^{13}C$ values of -34‰–-26‰ for C_3 plants and -20‰–-12‰ for C_4 plants (Feng et al., 2013; Goñi and Eglinton, 1996; Leenheer et al., 2003). Given that the Penobscot River HPOA has $\delta^{13}C$ value of -27.6‰, C_4 plant sources are expected to be only a minor component. Furthermore, lignin is susceptible to photodegradation (Benner and Kaiser, 2011; Dalzell et al., 2009; Dittmar et al., 2007; Hernes and Benner, 2003; Opsahl and Benner, 1998; Stubbins et al., 2010). Moreover, previous studies (Opsahl and Zepp, 2001; Vahatalo and Wetzel, 2008) observed that the $\delta^{13}C$ values of DOC became progressively more positive after exposure of riverine waters or vascular wetland plant leachate to natural sunlight. They suggested that photochemically-induced fractionation

of $\delta^{13}C$ result from the selective degradation of certain biochemical constituents including lignin phenols. In another study, the enrichment of $\delta^{13}C$-DOC and loss of carbon-normalized lignin phenol yields (Λ_8) during irradiation was found to be strongly correlated ($r = 0.99$) (Spencer et al., 2009b). Such tight coupling between these biomarkers provides supporting evidence that selective photodegradation of lignin moieties depleted in ^{13}C shifts the $\delta^{13}C$-DOC signature of terrestrial DOC toward typical marine values.

The observation that the ^{14}C ages of DOC increased with salinity could be similarly due to the mixing of river and marine waters. However, it is worth noting that young (^{14}C enriched) riverine DOC can be selectively degraded over the residence times of river and coastal waters, leaving an older fraction for oceanic export (Raymond and Bauer, 2001a). Pacific Ocean sample studied here was collected at a depth of 244 m whereas other samples were collected at a depth of 2 m. Pacific Ocean sample therefore will not be considered here because unlike $\delta^{13}C$ values, ^{14}C ages have been shown to increase significantly with water depth (Loh et al., 2004). The possibility of microbially- and photocheically-induced diagenetic effects on riverine DOC is not routinely incorporated into simple mixing models.

Comparison with DOM Isolated by Different Methods. The 1D NMR spectra of river and marine HPOA/FA samples (Figure 8(a-d)) were typical of aquatic humic substances isolated using XAD resins, i.e., they contained a major broad band of alkyl C, a narrow band of COO/NCO, an O-alkyl C band, and/or an aromatic/olefinic C band with its intensities depending on the source of DOM (Aiken et al., 1992; Hedges et al., 1992;

Leenheer et al., 2003; Leenheer et al., 2004; Malcolm, 1990; McIntyre et al., 2005; Perdue and Ritchie, 2003; Templier et al., 2005). Similar spectral features were observed for C_{18} isolated DOM because both chromatographic methods preferentially isolate the more nonpolar components. The C_{18} method seems to preferentially isolate hydrophobic aliphatic groups, resulting in its higher aliphatic abundance (Schwede-Thomas et al., 2005). As carbohydrates are considerably more polar than other DOM moieties, they are less likely retained in XAD or C_{18} isolated DOM, than in DOM samples isolated by ultrafiltration (UDOM) or reverse osmosis-electrodialysis (RO/ED) (Benner et al., 1992; Koprivnjak et al., 2009; Mao et al., 2012b; Sannigrahi et al., 2005). Koprivnjak et al. (2009) compiled the C distributions from ^{13}C NMR spectroscopy in marine and freshwater DOM isolated by different methods. The HPOA samples generally contain much more alkyl C and much less alkoxy C than UDOM samples from similar sources, with RO/ED samples being intermediate between the peak intensities for the HPOA and UDOM samples (Table 5 and Figure 5 in Koprivnjak et al. (2009); Table 2). Though carbohydrates have been recognized as a significant component in RO/ED, and especially in UDOM, carbohydrate structures are only a minor fraction of our HPOA samples. Specifically, 2D HETCOR data suggested the presence in Penobscot River HPOA of carbohydrate-like structures, which were absent in Pacific Ocean FA.

Fate of Terrestrial Inputs in the Ocean. The question of the fate of terrestrial OM in the ocean has intrigued scientists for decades. Before attempting to address this question, it is necessary to define the term "terrestrial organic carbon". The term "terrestrial/terrigenous DOC" used in literature implies either DOC that is "fixed" or

biosynthesized in the terrestrial environment, or all OC discharged from rivers to the coastal ocean. The latter connotation was considered and applied in the present paper. However, DOC in marine environments is often considered to be of terrestrial origin only if it has characteristic chemical or isotopic signatures that are indicative of vascular plant origin (Benner, 2004).

Previous studies of dissolved humic substances have emphasized the difference in DOM composition between marine and non-marine environments (Hedges et al., 1992), and led to the assumption that riverine humic substances comprised a small fraction of seawater humic substances and must be efficiently and rapidly removed from the ocean. Our data showed that CRAM represented a significant fraction of HPOA samples from riverine, coastal, and marine environments. CRAM may be a ubiquitous component of DOM in all aquatic systems, whether freshwater or marine. The alicyclic structures of CRAM are resistant to biological oxidation, while the absence of chromophoric structures in CRAM confers resistance to degradation by UV radiation (Leenheer, 1994). Therefore, structures of CRAM may cycle on time scales long enough to be transported into the ocean. The origins of CRAM remain unresolved, but they likely arise from terpenoid hydrocarbon lipids (Leenheer, 1994), or polyunsaturated lipid precursors that are oxidatively coupled and cyclized by free-radical mechanisms (Harvey et al., 1983).

CHAPTER III

SEASONAL CHANGES IN COMPOSITION OF DISSOLVED ORGANIC MATTER EXPORTED TO THE BERING SEA BY THE YUKON RIVER

INTRODUCTION

Arctic biomes contain up to 1672 Petagrams (Pg) organic carbon (OC), which represents an estimated 50% of OC stored globally in soils, and more than twice the size of the atmospheric C pool (Dittmar and Kattner, 2003; Schuur et al., 2008; Tarnocai et al., 2009). The majority of this pool (88%) is estimated to be locked in perennially frozen soils and deposits (Tarnocai et al., 2009), one of the so-called vulnerable C pools as a result of global warming (Gruber et al., 2004). There has been growing concerns that permafrost thaw due to global warming may cause mobilization of this huge terrestrial OC pool to the atmosphere, and to aquatic systems as dissolved and particulate C (Frey and McClelland, 2009; Grosse et al., 2011; McGuire et al., 2009).

Dissolved organic matter (DOM) is a fundamental link between terrestrial and aquatic systems, and dissolved organic carbon (DOC) export from land to aquatic ecosystems is a significant mover of C through continents and local landscapes (Roulet and Moore, 2006). Arctic rivers export large quantities of DOM, approximately 10% of the global river discharge, to the Arctic Ocean. Because of the large size, and potential environmental sensitivity of DOM fluxes from Arctic rivers due to global warming, they have received increased attention over the past decade (Dittmar and Kattner, 2003; Guo et al., 2013; Holmes et al., 2013; Holmes et al., 2012; Opsahl et al., 1999; Wickland et al., 2012). Growing evidence indicates that Arctic rivers exhibit striking seasonal patterns in

water discharge, DOC concentration (Holmes et al., 2012; Striegl et al., 2005; Striegl et al., 2007), chemical composition, and age (Aiken et al., 2014; Guo et al., 2013; Neff et al., 2006; Raymond et al., 2007; Spencer et al., 2009a; Spencer et al., 2008). DOM exported during the spring freshet (May 1–June 30) has relatively high lignin phenol content and is typically ^{14}C-enriched (Aiken et al., 2014; Amon et al., 2012; Neff et al., 2006; Raymond et al., 2007; Spencer et al., 2009a; Spencer et al., 2008). Under winter base flow conditions (November 1–April 30), DOM has a greater aged component (Aiken et al., 2014; Neff et al., 2006; Raymond et al., 2007), and shows low lignin phenol content and aromaticity (Spencer et al., 2009a; Spencer et al., 2008). During the summer-autumn period (July 1–October 31), DOM generally shows characteristics intermediate between peak flow and winter base flow DOM (Neff et al., 2006; Raymond et al., 2007; Spencer et al., 2009a; Spencer et al., 2008).

The significance of Arctic river DOM for the biogeochemistry of the Arctic Ocean is not currently resolved and largely depends on its susceptibility to microbial and photochemical degradation processes (Cory et al., 2007). Arctic riverine DOM was historically considered refractory, based on the observations of apparent conservative mixing behavior across the continental shelf (Amon, 2004; Amon and Meon, 2004; Cauwet and Sidorov, 1996; Dittmar and Kattner, 2003) and extremely low consumption of Arctic river DOM during extended incubation experiments (Amon, 2004; Lobbes et al., 2000). This view, however, is developed mainly through the analysis of samples collected during mid to late summer after sea ice retreat. Recent incubation studies with better seasonal sampling resolution indicate that spring freshet DOM (Holmes et al., 2008; Mann et al., 2012) or winter DOM (Wickland et al., 2012) is highly biodegradable.

Photochemical transformation of Arctic river DOM has been considered of less importance due to the prevailing low solar angle and sea ice cover at high latitudes (Amon and Meon, 2004; Benner et al., 2004; Osburn et al., 2009). Future losses of sea ice or reductions in ozone levels may point to an enhanced role for photochemistry in cycling of DOM within Arctic regions (Cory et al., 2007).

Chemical composition of DOM underlies its susceptibility to bacterial and photochemical degradation processes, and in turn, the fate of Arctic river DOM in the Arctic Ocean (Del Giorgio and Davis, 2003). Currently, detailed structural information of DOM in these rivers is lacking. Furthermore, most detailed measurements of Arctic river DOM are made during the late-summer season and have missed the bulk of DOM discharge from these environments which occur during spring floods when both flow and concentrations are high. In this study, we aim to capture detailed seasonal variability in chemical structure of DOM by sampling across the three distinct seasons in a large northern high-latitude river system (Yukon River, Alaska, United States, and Canada). The Yukon River represents one of a few remaining great rivers that are uncontrolled, thereby facilitating an unconfounded examination of the response of C cycles to environmental changes in the basin (Guo et al., 2013). Distinct from most other major Arctic rivers which flow from south to north, the Yukon River drains from east to west and has a uniformly high latitude (59-69 °N), making it particularly sensitive to ongoing climate change (Guo et al., 2013). In the present work we applied advanced solid-state NMR spectroscopy, coupled with isotopic measurements and UV-visible spectroscopy to investigate the chemical structure and source of DOM samples collected from distinct phases of the Yukon River hydrograph (spring freshet, summer-autumn, and winter).

MATERIALS AND METHODS

Study Area, Water Sampling and Processing. The Yukon River (YR) with an annual water discharge of ~208 km^3, is the largest river in Alaska and the fifth largest river draining to the Arctic Ocean, contributing ~8% of the total freshwater input to the Arctic Ocean via the Bering Strait (Aagaard and Carmack, 1989). The YR basin encompasses 854,700-km^2 of northwestern Canada and Alaska, and covers diverse terrain including high mountainous regions, forested uplands, and wide expanses of low-lands rich in wetlands and lakes. The YR basin is predominantly subarctic or boreal, and much of it is underlain by continuous and discontinuous permafrost, which is actively warming and thawing (Brabets et al., 2000; Striegl et al., 2007).

Sampling was conducted at various times of the year 2008-2009 at Pilot Station, Alaska to obtain a representative data set reflecting the changing seasonal hydrograph, including sampling under ice cover during winter (Table 3). Pilot Station is located close to the river mouth, just above the influence of seawater from the Bering Sea, and therefore best represents the DOM characteristics which are products of the entire basin and its biogeochemical processes (Guo et al., 2012).

Large volume (40–95 L) water samples were filtered in the field with prerinsed Gelman AquaPrep 600 capsule filters (0.45 μm). Early spring samples were collected through the ice before breakup, and late spring samples were collected when most ice had passed. After transport to the USGS laboratory in Boulder (Colorado, United States), water samples were processed by XAD isolation and concentration as described by Aiken et al. (1992). Briefly, samples were acidified to pH 2 with hydrochloric acid (HCl) and passed first through a column of XAD-8 resin, followed by a column of XAD-4 resin.

Each column was then eluted with 0.1 N sodium hydroxide (NaOH) to obtain the XAD-8 (referred to as the hydrophobic organic acids, HPOA) and XAD-4 (referred to as the transphilic organic acids, TPIA) fractions, respectively. The eluates were desalted and hydrogen saturated using cation exchange resin, lyophilized, and stored in a desiccator.

Elemental Analyses and Carbon Isotopic Measurements. Elemental analyses (C, H, O, N, S and ash) of DOM isolates were performed by Huffman Laboratories (Golden, Colorado) by the method described in Huffman and Stuber (1985). Isolate samples were combusted and converted to graphite targets at the USGS' Radiocarbon Laboratory in Reston, Virginia. Radiocarbon abundance determinations were made at the Center for Accelerator Mass Spectrometry at Lawrence Livermore National Laboratory in Livermore, California. Samples were combusted at 900 °C for 6 hours with cupric oxide (CuO) and silver (Ag) in sealed quartz test tubes to form CO_2 gas. The CO_2 was then reduced to graphite through heating at 575 °C in the presence of hydrogen (H_2) gas and an iron (Fe) catalyst (Vogel et al., 1987). Graphite targets were then analyzed for carbon isotopes ($\delta^{13}C$ in ‰ and ^{14}C as fraction modern carbon) (Davis et al., 1990). $\Delta^{14}C$ data (in ‰) were corrected for isotopic fractionation using measured $\delta^{13}C$ values and radiocarbon ages were determined from percent modern carbon using the year of sample analysis according to Stuiver and Polach (1977). Ages are presented as Modern when the fraction modern exceeded 1. Results of elemental analyses and carbon isotopic data of selected samples are given in Table 3.

Table 3

Seasonal variations in DOC concentrations, $SUVA_{254}$, and major chemical fractions of DOM, ash-free elemental contents and isotopic data of HPOA fractions, Yukon River at Pilot Station (2008-2009).

Sampling Date	Sample	DOC (mg C L^{-1})	Fraction	% of DOC	$SUVA_{254}$ (L mg C^{-1} m^{-1})	Ash-free elemental contents (%) and C isotopic data (‰)							
						C	H	O	N	S	$\delta^{13}C$	$\Delta^{14}C$	Age (ybp)
07/01/2008	Summer07	5.9	HPOA	54	3.8	ND	ND	ND	ND	ND	-27.81	19.6	>Modern
			TPIA	16	2.9	ND	ND	ND	ND	ND	ND	ND	ND
08/12/2008	Summer08	7.0	HPOA	56	3.7	52.84	4.81	41.05	0.87	0.43	-27.67	26.7	>Modern
			TPIA	18	2.8	ND	ND	ND	ND	ND	ND	ND	ND
09/24/2008	Summer09	5.4	HPOA	49	3.4	ND	ND	ND	ND	ND	-27.57	6.2	>Modern
			TPIA	18	2.4	ND	ND	ND	ND	ND	ND	ND	ND
01/21/2009	Winter01	3.3	HPOA	51	2.8	ND	ND	ND	ND	ND	-27.46	-71.1	530
			TPIA	18	2.1	ND	ND	ND	ND	ND	ND	ND	ND
03/26/2009	Winter03	2.7	HPOA	47	2.8	52.65	5.12	40.85	0.93	0.44	-27.1	-111.5	890
			TPIA	17	2.1	ND	ND	ND	ND	ND	ND	ND	ND
05/12/2009	Spring0512	5.7	HPOA	51	3.9	51.77	4.91	42.06	0.87	0.39	-28.32	6.1	>Modern
			TPIA	17	2.6	ND	ND	ND	ND	ND	ND	ND	ND
05/22/2009	Spring0522	17.3	HPOA	57	3.9	52.08	5.01	41.73	0.87	0.32	-28.1	92.2	>Modern
			TPIA	16	2.8	ND	ND	ND	ND	ND	ND	ND	ND
05/29/2009	Spring0529	14.9	HPOA	52	4.1	52.74	4.64	41.38	0.91	0.32	-28.12	82.1	>Modern
			TPIA	15	2.9	ND	ND	ND	ND	ND	ND	ND	ND

DOC is dissolved organic carbon, and $SUVA_{254}$ is specific UV absorbance determined at 254 nm. HPOA is hydrophobic acid, and TPIA is transphilic acid. ND, not determined. ybp, years before present.

NMR Analysis. All ^{13}C NMR experiments were performed at 100 MHz using a Bruker Avance 400 spectrometer equipped with a 4-mm double-resonance probe head. Samples filled the radio-frequency coil from end to end; a cylindrical glass plug of 2-mm height at the bottom of the rotor prevented sample materials from being placed outside the coil. The ^{13}C chemical shifts were referenced to tetramethylsilane, using the COO resonance of glycine in the α-modification at 176.46 ppm as a secondary reference.

The multiple-cross polarization (multiCP) technique recently developed by Johnson and Schmidt-Rohr (2014) provides a simple and robust approach to obtain quantitative solid-state ^{13}C NMR spectra of organic materials, with good signal-to-noise ratios. This new multiCP pulse sequence was employed for all samples to obtain quantitative ^{13}C NMR spectra. The spectra were measured at a spinning speed of 14 kHz, where spinning sidebands are fairly small (< 3%) and have little overlap with centerbands. The 90° pulse lengths were 4.3 μs for ^{1}H and 4 μs for ^{13}C. To achieve dead-time-free detection, which is indispensable for spectra with broad lines, all spectra were recorded with a Hahn echo generated by an 180° pulse with EXORCYCLE phase cycling (Bodenhausen et al., 1977) applied one rotation period (t_r) after the end of cross polarization. The ^{1}H decoupling field strength was $|\gamma B_1|/2\pi = 65$ kHz during the period of $2\ t_r = 0.14$ ms duration before the Hahn echo, and about 55 kHz during signal detection. The ramp for cross polarization was implemented with 11 steps of 0.1 ms duration and a 1% amplitude increment (90 to 100%). The recycle delays were 0.35 s. The duration of the repolarization period t_z in multiCP was 0.3 s. Corresponding multiCP spectra of nonprotonated C and mobile groups like rotating CH_3 were obtained by combining multiCP sequence with a 68-μs recoupled dipolar dephasing (multiCP/DD). Between

1536 and 4608 scans were collected per spectrum. The total time for multiCP and multiCP/DD experiments was 2-6 h per sample.

To evaluate the suitability of the multiCP technique for quantitative characterization of DOM, quantitative ^{13}C direct polarization/magic angle spinning (DP/MAS) was also employed. The ^{13}C DP/MAS NMR experiments were performed at a spinning speed of 14 kHz. A Hahn spin echo was generated before detection to avoid baseline distortions associated with detection directly after the 90° excitation pulse (Mao and Schmidt-Rohr, 2004a). ^{1}H decoupling of sufficiently high-power at $|\gamma B_1|/2\pi = 72$ kHz with two-pulse phase-modulated (TPPM) (Bennett et al., 1995) was applied during detection. Recycle delays (20-84 s) were determined by the cross polarization/spin-lattice relaxation time/total sideband suppression technique to make sure that all carbon sites were > 95% relaxed (Mao et al., 2000). ^{13}C DP/MAS NMR with recoupled dipolar dephasing (DP/MAS/DD) was used to determine the fractions of nonprotonated and mobile carbons (Mao and Schmidt-Rohr, 2004a). The dipolar dephasing time was 68 μs. The recycle delays and the number of scans averaged were 80 s and 800 for Summer08 HPOA, 84 s and 512 for Winter03 HPOA, 20 s and 2048 for Spring0512 HPOA, 40 s and 1024 for Spring0522 HPOA, 80 s and 640 for Summer08 TPIA, 80 s and 512 for Winter03 TPIA, 20 s and 1536 for Spring0512 TPIA, 40 s and 768 for Spring0522 TPIA, respectively. The total time for DP/MAS and DP/MAS/DD experiments was 17-29 h per sample.

The ^{13}C cross polarization and total suppression of sidebands (CP/TOSS) NMR experiments were conducted at a spinning speed of 7 kHz, a CP time of 1 ms, a ^{1}H 90° pulse-length 4.1 μs, and a recycle delay of 0.5 s. Four-pulse TOSS (Dixon, 1982) was

employed before detection, with the TPPM decoupling applied for optimum resolution. Sub-spectra showing signals from nonprotonated and mobile groups were obtained by combining the ^{13}C CP/TOSS sequence with a 48-μs dipolar dephasing (CP/TOSS/DD). For ^{13}C CP/TOSS experiments, 5120-7168 scans were collected for each sample. The number of scans was doubled in corresponding ^{13}C CP/TOSS/DD experiments.

To resolve the overlapping resonances of anomeric (O-C-O) and aromatic carbons between 120 and 90 ppm, the aromatic carbon signals were selectively suppressed using a three-pulse ^{13}C chemical-shift-anisotropy (CSA) filter with a CSA-filter time of 68 μs (Mao and Schmidt-Rohr, 2004b). The number of scans averaged was 2560-3584 for each spectrum. The CSA filter was also combined with 48-μs dipolar dephasing to isolate signals from nonprotonated anomeric carbons. The number of scans averaged for the spectrum of CSA filter coupled with dipolar dephasing was twice that of the corresponding CSA-filtered spectrum for each sample.

^{1}H-^{13}C two dimensional heteronuclear correlation (2D HETCOR) NMR experiments (Mao and Schmidt-Rohr, 2006) were performed at a spinning speed of 7.5 kHz. Standard Hartmann-Hahn CP (HH-CP) with 80-μs CP time reveals primarily one-bond ^{1}H-^{13}C connectivities. HH-CP of 0.5 ms allows for some ^{1}H spin diffusion and so correlates the carbons with protons within ~ 0.5 nm radius. In addition, a 40-μs dipolar dephasing delay was inserted in the HH-CP HETCOR to reveal ^{1}H-^{13}C proximities for nonprotonated carbons (multi-bond) and mobile groups like CH_3. The recycle delay was 0.5 s. More long-range proximities were probed by ^{1}H spin diffusion during a mixing time of 1 ms and 10 ms, correlating the carbons with protons within ~ 1.6 and 5 nm radius, respectively. Each 2D HETCOR spectrum took 5-27 h.

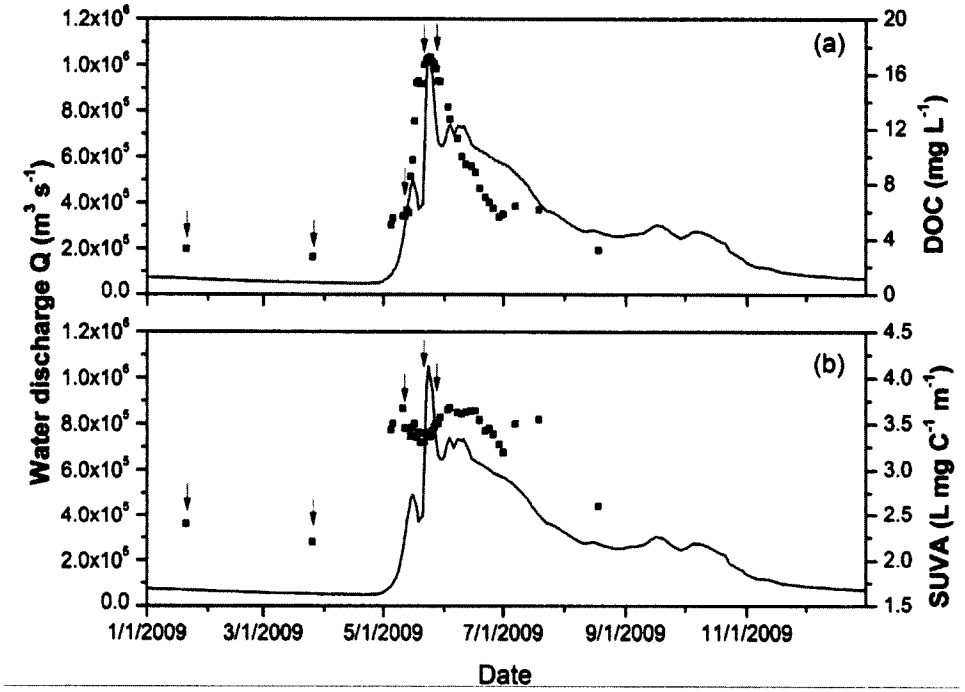

Figure 11. Water discharge (Q) hydrograph for the Yukon River at Pilot Station (near the river mouth) for the year 2009 versus (a) dissolved organic carbon (DOC) concentration, and (b) specific UV absorbance determined at 254 nm ($SUVA_{254}$). The arrows indicate sampling dates of samples in the present study.

RESULTS

Seasonal Patterns of DOC Concentration, $SUVA_{254}$, and Major Chemical Fractions. DOC concentrations varied with sampling dates and water discharge Q (Table 3 and Figure 11(a)). DOC concentrations peaked during the spring flush (Spring0522 and Spring0529) at peak Q, were lowest at low Q during winter base flow (Winter01 and Winter03), and intermediate in values before the spring flush event (Spring0512) and during summer base flow (Summer07, Summer08, and Summer09). The hydrophobic acids (HPOA) were the dominant DOC fraction (ca. 47-57% of DOC) in all the samples, but were less abundant in winter than in spring and summer months (Table 3). The transphilic acids (TPIA) accounted for 15-18% of DOC and did not show a clear trend across seasons. The values of specific UV absorbance at 254 nm ($SUVA_{254}$, an indicator of aromaticity) generally followed the same trend as DOC concentrations but their seasonal changes were less prominent (Table 3 and Figure 11). The $SUVA_{254}$ values associated with HPOA and TPIA fractions were elevated during spring at high Q, slightly declining during the summer months, and lowest during the winter at low Q. Similar relationships between Q and DOC (concentrations and $SUVA_{254}$) have been reported in earlier Yukon River basin studies (O'Donnell et al., 2012; Spencer et al., 2008; Wickland et al., 2012).

Elemental compositions for HPOA across seasons showed that spring HPOA isolates contained slightly less C but more O than summer and winter samples, leading to relatively higher atomic O/C ratios of spring HPOA (~0.60 vs. 0.58). The H content ranged from 4.64 to 5.12%, yielding atomic H/C values of 1.06-1.17 for all HPOA samples. The N contents were low (< 1%) in all HPOA samples, resulting in high atomic

C/N values (66.0-70.9). Sulfur was an even minor component (< 0.5%) and relatively more abundant in summer and winter HPOA than in spring HPOA. The $\delta^{13}C$ values of all HPOA fell into a rather narrow range (-28.32‰ – -27.1‰), and generally became less negative from spring HPOA to summer HPOA and to winter HPOA. The winter HPOA isolates had the most depleted $\Delta^{14}C$ values (-71.1‰ and -111.5‰), corresponding to oldest ages (530 ybp and 890 ybp). Spring HPOA isolates had relatively more enriched $\Delta^{14}C$ values than summer HPOA samples, but all contained modern DOC.

Suitability of MultiCP Technique for Quantitative Characterization of DOM.

Figure 12 shows the ^{13}C spectra of Summer08, Winter03, Spring0512, Spring0522 obtained with three different techniques: multiCP (bold lines), DP/MAS (solid thin lines), and CP/TOSS (dashed thin lines). The three spectra of each sample were scaled to match the height of the COO/NC=O band. For nearly all samples, CP/TOSS spectra showed considerable enhancement of alkyl and O-alkyl signals but relative underestimation of aromatic signals. The agreement between multiCP and DP spectra was quite well, with the former showing slight signal enhancement of alkyl and O-alkyl C in the spectra of Summer08 HPOA/TPIA, Spring0512 HPOA, and Spring0522 HPOA, which can be tackled by further optimization of the NMR parameters. Because a quantitative DP/MAS spectrum of DOM with acceptable signal-to-noise ratio typically takes overnight while multiCP technique yields a near-quantitative spectrum with good signal-to-noise within 2 hours, the multiCP technique offers an advantage in saving expensive NMR machine time without losing quantitative information. The multiCP and multiCP with recoupled

dipolar dephasing were applied replacing more time-consuming DP experiments to all samples.

Seasonal Changes in Functional Group Composition of DOM. The solid-state ^{13}C multiCP spectra for HPOA and TPIA samples from the Yukon River at Pilot Station across different seasons are given in Figure 13. The ^{13}C all C spectra of both HPOA and TPIA samples (bold black line) were composed of five relatively well-resolved peaks assigned to signals from nonpolar alkyl C (0-64 ppm), O-alkyl C (64-100 ppm), aromatic or olefinic C (100-160 ppm, also containing anomeric C), COO/NC=O (160-190 ppm), and ketone/aldehyde C (190-220 ppm). In addition, the resonances due to anomeric C (OCO) were better resolved in the spectra of TPIA isolates (spring TPIA in particular, see Figure 13(k, l)) than in the spectra of HPOA isolates. MultiCP/DD spectra (thin black line) further identified nonprotonated and mobile C components such as CCH_3, quaternary C (CC_q), nonprotonated OC (OC_{np}), nonprotonated anomeric C ($OC_{np}O$), nonprotonated aromatic C-C, and aromatic C-O in phenolic groups and aromatic ethers (143-160 ppm). The intensities of ketone/aldehyde signal remained the same after dipolar dephasing, indicating that these carbonyls were present in the nonprotonated form, i.e., ketone C, in all HPOA and TPIA isolates. The CP/TOSS spectra after the insertion of the CSA filter (gray line), only shown in Figure 13(f, l)) to avoid overlapping spectra, identified unambiguously anomeric C (OCO, shaded area). The combination of CSA filter technique with dipolar dephasing (spectra not shown) further selected nonprotonated anomeric C ($OC_{np}O$). Several observations were noted based on visual comparison of spectra of HPOA/TPIA samples across different seasons. First, signals

from OCH_3 and aromatic C (including aromatic C-O) characteristic of lignin residues were more discernible in summer than in winter HPOA, and became prominent in the spectra of spring HPOA (Spring0512 and Spring0522). Second, the OC peak maximum shifted from 77 ppm in summer and winter HPOA to 74 ppm in spring HPOA, suggestive of different environments of these O-alkyls. Third, spectra of spring TPIA (Spring0512 and Spring0522) were markedly different from those of summer and winter TPIA samples, with the former showing a very sharp OC peak at 72 ppm and a relatively well-resolved OCO peak at 102 ppm. Quantitative distributions of specific C functional groups, compiled in Table 4, provided more detailed comparisons among samples across different seasons. The HPOA/TPIA isolates within the same seasons were compositionally very similar (data not shown), consistent with their similar spectral features. Differences do exist between the two spring TPIA samples: Spring0512 was more enriched in O-alkyl and OCO but depleted in aromatic C and COO/NC=O than Spring0522.

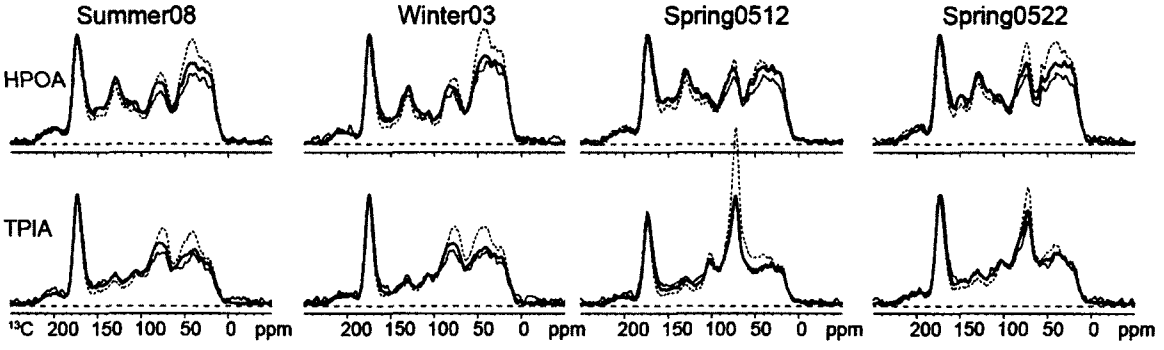

Figure 12. The ^{13}C NMR spectra obtained with three different techniques: multiple-cross polarization (multiCP, bold line), direct polarization/magic angle spinning (DP/MAS, solid thin line), and cross polarization and total suppression of sidebands (CP/TOSS, dashed thin line).

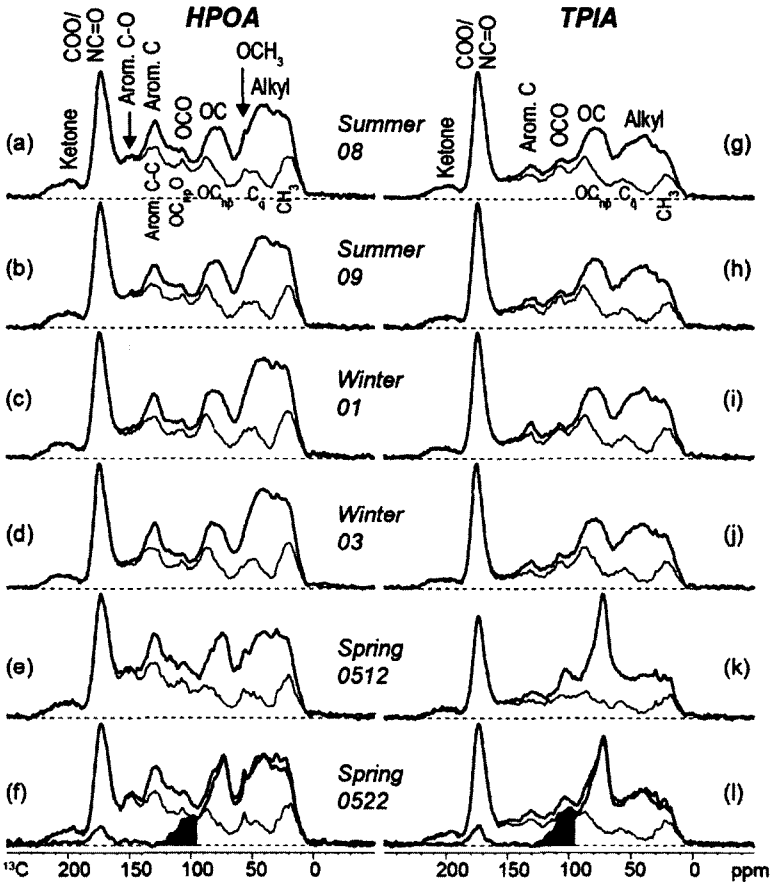

Figure 13. Solid-state ^{13}C multiCP NMR spectra (bold black line) and multiCP with dipolar dephasing (thin black line) obtained for HPOA and TPIA samples across different seasons. Dipolar dephasing shows primarily nonprotonated and highly mobile carbons. Solid-state ^{13}C CP/TOSS NMR spectra with CSA-filter (gray line, see (f, l)) are shown as examples, for demonstrating the separation of anomeric C (shaded area) from aromatic C. All multiCP spectra are scaled to match the intensity of the highest band.

Table 4

Integrated areas (in %) from ^{13}C multiCP NMR spectra for HPOA and TPIA samples across different seasons, and the assigned structural moieties associated with the spectral region.

Samples		ppm											
		220-190	190-160	160-143	143-100		123-100		100-64		64-0		
		Ketone C	COO/ NC=O	Arom. C-O	Arom. C-C[a]	Arom. C-H	$OC_{np}O$[b]	OCHO[b]	OC_{np}[a]	OCH_n	C_q[a]	CH_2/CH	CH_3[a]
HPOA	Summer08	3.1	17.3	6.0	11.3	6.0	3.0	0.3	8.0	9.3	5.1	20.3	10.2
	Winter03	2.7	17.1	4.4	9.3	5.4	2.5	0.1	8.4	8.6	5.9	23.8	11.8
	Spring0512	2.9	16.5	6.9	11.9	7.7	4.0	1.3	5.3	10.9	4.7	18.5	9.6
	Spring0522	2.8	16.1	6.8	12.2	7.2	3.5	1.2	5.3	11.2	4.7	19.6	9.4
TPIA	Summer08	3.1	20.7	4.1	7.6	3.8	3.9	0.3	11.4	13.2	4.2	20.0	7.7
	Winter03	2.8	20.2	2.8	5.8	3.5	3.5	0.4	11.9	13.3	4.7	21.3	9.9
	Spring0512	2.1	17.6	3.7	7.1	3.1	4.3	4.7	7.0	21.8	3.7	16.5	8.4
	Spring0522	2.7	20.0	4.6	8.2	3.9	5.3	2.6	7.1	17.1	3.2	17.6	7.5

[a] Based on multiCP spectrum with 68-μs dipolar dephasing.

[b] Based on CSA-filtered CP/TOSS spectrum and CSA-filtered CP/TOSS spectrum with dipolar dephasing.

Seasonal variations of HPOA structures. The HPOA isolates were all considerably more aliphatic than aromatic in composition. The alkyl C (0-64 ppm) accounted for 33-42% of the C in HPOA isolates, and its relative abundance increased in the order: Spring0512/0522, Summer08, and Winter03. The aromatic C fraction (including protonated aromatic C-H, nonprotonated aromatic C-C, and oxygen substituted aromatic C-O) ranged from 19-26% and decreased as alkyl C increased. The relative abundances of O-alkyl C (including OC and OCO), were generally constant across seasons, accounting for 20-21% of total C. The anomeric C (OCO) was slightly more enriched in spring HPOA (~5%) than in summer and winter HPOA samples (~3%). The COO/NC=O constituted 16-17% of the C in all HPOA, with NC=O contributing at most 1-2% to all C based on the high atomic C/N values (66.0-70.9) associated with HPOA isolates. The relative fraction of ketone C was small and constant (~3%) in HPOA isolates across all seasons.

Consistent with spectral observation, the spring and summer HPOA samples contained more aromatic C-O (and aromatic C-C and aromatic C-H) than the winter HPOA (6-7% vs. 4%). Though the OCH_3 peak was evident in spectra of spring HPOA, its contribution was <1% of all C for all HPOA isolates. Whereas the ratio of the relative fraction of protonated to nonprotonated OC (OCH_n/OC_{np}) is approximately 1 in summer and winter HPOAs, this ratio doubled in the two spring HPOA samples. This explained the shift of OC peak maximum from 77 to 74 ppm in spring HPOA because OCH_n appeared to resonate at lower chemical shift than OC_{np} (Figure 13). The spring HPOA isolates were also relatively more enriched in protonated anomeric C (OCHO) than summer and winter HPOA. In addition, the summer and winter HPOA isolates contained

relatively more nonprotonated aliphatic C (C_q + OC_{np} + $OC_{np}O$) than spring HPOA (16% vs. 13%).

Seasonal variations of TPIA structures. The alkyl C (0-64 ppm) was the dominant component in winter and summer TPIA isolates, and its relative abundance decreased in the order: winter (36%) > summer (32%) > spring (~28%). The dominant component in spring TPIA samples was O-alkyl C (OC + OCO), which accounted for 38% and 32% of total C in Spring0512 and Spring0522, respectively. Hence Spring0512 TPIA contained more O-alkyl C than Spring0522 TPIA, which was sampled only 10 days later. The contribution of O-alkyl C decreased in summer and winter TPIA isolates (~29%). Consistent with the intense COO/NC=O peak, it contributed to 20-21% of C in all TPIA except about 18% in Spring0512 TPIA. The aromatic C (including aromatic C-H, aromatic C-C, and aromatic C-O) comprised 12-17%, and increased in the order: Winter03 < Spring0512 < Summer08 < Spring0522. The ketone C constituted only a small portion (2-3%) in all TPIA isolates.

The ratio of the relative fraction of protonated to nonprotonated OC (OCH_n/OC_{np}) was about 1 in summer and winter TPIA, but increased to 3 in Spring0512 and 2.4 in Spring0522, in agreement with the shift of OC peak maximum in spectra of spring TPIA isolates (Figure 13). The spring TPIA contained more protonated anomeric C (OCHO, Spring0512 ~5%, Spring0522 ~3%) than summer and winter TPIA (< 1%). Similarly, nonprotonated aliphatic C (C_q + OC_{np} + $OC_{np}O$) was relatively more abundant in summer and winter TPIA than spring TPIA isolates (19-20% vs. 15%).

Proximities of Functional Groups in DOM Across Different Seasons. Though quantitative ^{13}C NMR spectra showed definitive differences in functional group distributions among HPOA/TPIA isolates across different seasons, the assignment of structural components associated with these functional groups remained ambiguous. For instance, the ^{13}C NMR signal intensity in the 60-110 ppm region is most often assigned to carbohydrate components. This assignment is reasonable when it comes to DOM isolated from ultrafiltration, but tends to be problematic when it comes to DOM isolated by XAD-8 resin, which is known not to retain large carbohydrates. Here more accurate assignment or evaluation of structural components associated with different functional groups can be aided with ^{1}H-^{13}C heteronuclear correlation (HETCOR) NMR, which provides through-space ^{1}H-^{13}C correlations and information on proximities of functional groups.

HPOA structures. Figure 14 shows the 2D HETCOR spectra of Spring0522 HPOA (Figure 14(a)) and Winter03 HPOA (Figure 14(b)) with HH-CP of 0.5 ms, showing ^{1}H-^{13}C correlations within ~ 0.5 nm radius, i.e., within the size of a sugar ring or aromatic ring (~ 0.6 nm in diameter). Both spectra shared common cross peaks of CH_3, CH_2/CH, and aromatic C with their directly attached protons, and those of COO and ketone C with their neighboring protons. The spectrum of Spring0522 also showed the cross peak of OCH_3, which was absent in the spectrum of Winter03, consistent with their ^{13}C multiCP spectra. In addition, the cross peaks of OC and OCO had different patterns in spectra of Spring0522 and Winter03, which were more clearly demonstrated in their corresponding proton slices (Figure 14(c, d)). For Spring0522 HPOA, the ^{1}H spectra associated with OC (72 ppm) and OCO (102 ppm) showed primarily contributions from

O-alkyl protons, but signals from alkyl protons were also seen (Figure 14(c). In the case of Winter03 HPOA, the ^{1}H spectrum associated with OC (77 ppm) contained equal contributions from alkyl and O-alkyl protons. The major band in ^{1}H spectra associated with OCO (108 ppm) appeared at 2 ppm (Figure 14(d)), indicating that OCO sites were in close proximity to alkyl protons. This suggests that in Winter03 HPOA, OC and OCO carbons were not primarily associated with carbohydrates; otherwise these C sites would correlate predominantly with O-alkyl protons. For both Spring0522 and Winter03 HPOA (Figure 14(c, d)), the ^{1}H slices extracted at the chemical shifts of aromatic C and aromatic C-O indicated contributions from aromatic protons, as well as correlations with alkyl and O-alkyl protons, indicating close association of aromatic and alkyl components. The COO and ketone C showed correlations primarily with alkyl protons, with additional contribution from O-alkyl protons, indicating that they were attached mostly to alkyl and O-alkyl carbons. Therefore, linkages between COO and O-alkyl groups can be either $\underline{C}(=O)-O-C\underline{H}_n$ or $O-C\underline{H}_n-\underline{C}(=O)-O-$. The latter carboxyl linkage involved a shorter C–H distance (two-bond C– –H) than the former ester linkage (three-bond C– – –H), and therefore favored the rapid H-to-C cross polarization observed in the experiments. In addition, the 2D HETCOR spectra of both Spring0522 and Winter03 (Figure 14(a, b)) clearly showed the cross peaks of COO carbons with the acidic COOH protons which resonated near 12 ppm (Figure 14(c, d)), proving the presence of carboxylic acids.

With a mixing time of 1 ms, the through-space ^{1}H-^{13}C correlations probed can be extended to a length scale of ~ 1.6 nm radius, within the size of 2-3 sugar/aromatic rings. The 2D HETCOR spectra of Spring0522 HPOA and Winter03 HPOA (Figure 15(a, b)) became more similar, with the major band in ^{1}H spectra associated with all types of C

centered near 2 ppm (Figure 15(c, d)), indicating that all C sites were in close proximity to alkyl protons. For Spring0522, the ^{1}H slices associated with OC and OCO also showed nearly equal contributions from O-alkyl protons. The presence of isolated sugar ring unit in Spring0522 HPOA is likely, but there are no carbohydrates moieties composed of more than 3 sugar rings.

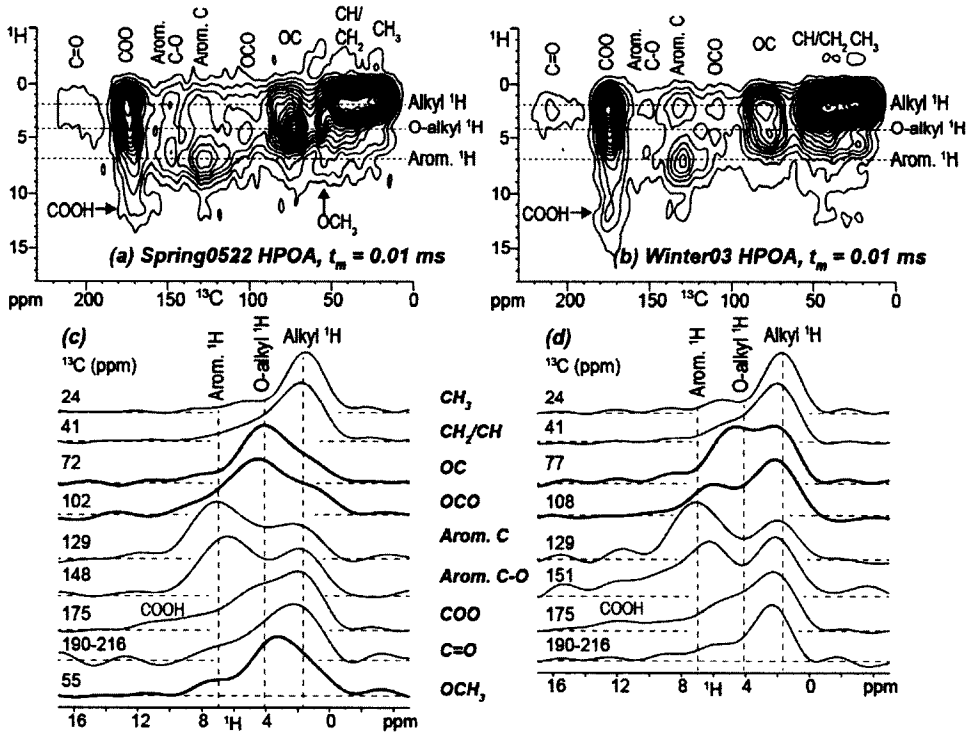

Figure 14. 2D ^{1}H-^{13}C HETCOR spectra with 0.5-ms HH-CP of (a) Spring0522 HPOA and (b) Winter03 HPOA. ^{1}H slices extracted from the 2D spectra: (c) refers to ^{1}H slices of spectrum (a), and (d) to spectrum (b).

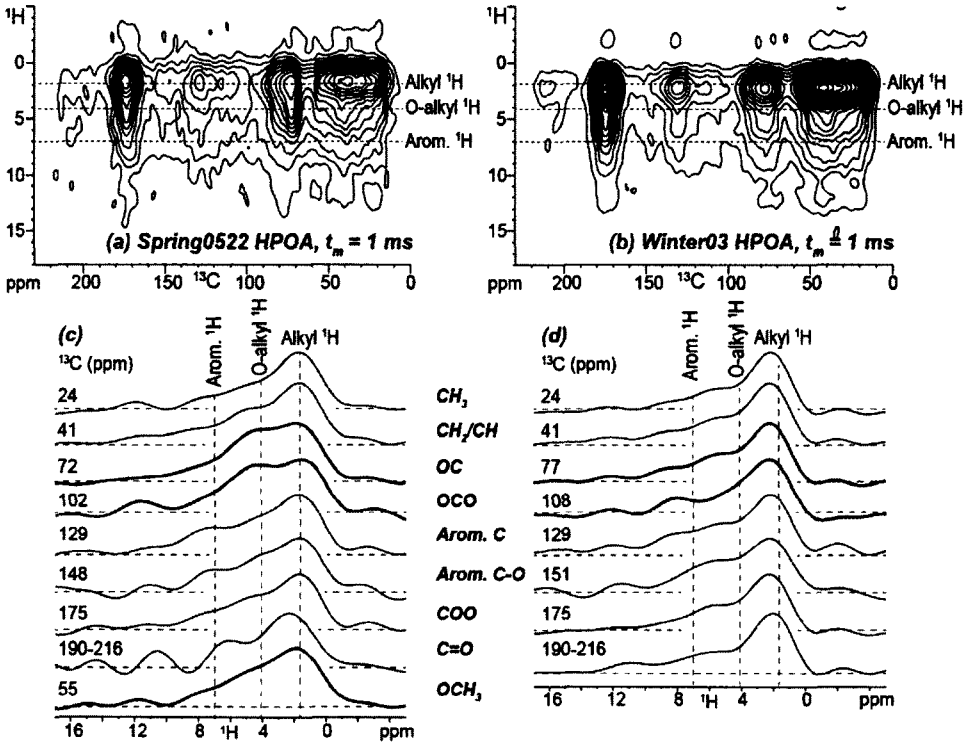

Figure 15. 2D ^{1}H-^{13}C HETCOR spectra with 0.5-ms HH-CP and 1-ms mixing time of (a) Spring0522 HPOA and (b) Winter03 HPOA. ^{1}H slices extracted from the 2D spectra: (c) refers to ^{1}H slices of spectrum (a), and (d) to spectrum (b).

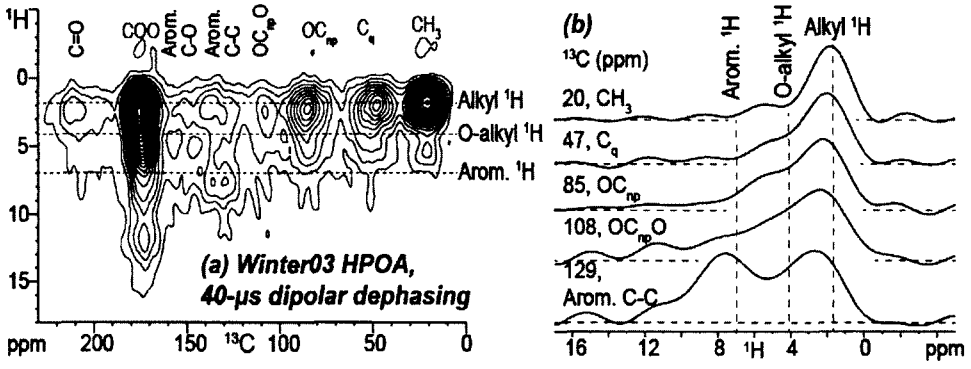

Figure 16. 2D ^{1}H-^{13}C HETCOR spectrum with 0.5-ms HH-CP and 40-μs dipolar dephasing (a) and extracted ^{1}H slices (b) of Winter03 HPOA.

Quantitative data have shown the presence of abundant nonprotonated aliphatic C (C_q + OC_{np} + $OC_{np}O$, 13-16% of all C). The nontrivial correlations between these nonprotonated carbons and their nearby protons, which are separated by at least two bonds, can be observed with a 2D HETCOR spectrum with 0.5-ms HH-CP and 40-μs dipolar dephasing (Figure 16(a)) and corresponding proton slices (Figure 16(b)) for Winter03 HPOA. The ^1H slice extracted at 47 ppm (C_q) showed primarily correlations with alkyl protons (~2.5 ppm). The ^1H spectra associated with OC_{np} (86 ppm) and $OC_{np}O$ (108 ppm) contained major contributions from alkyl protons resonating near 2 ppm, indicating that OC_{np} and $OC_{np}O$ were found predominantly near alkyl protons, rather than, near O-alkyl protons. This provided evidence that these nonprotonated OC and OCO fractions were not in carbohydrate environments. The ^1H spectrum associated with the nonprotonated aromatic C (arom. C-C) showed nearly equal contributions from aromatic protons and alkyl protons (~2.5 ppm).

TPIA structures. The 2D HETCOR spectra of Spring0522 TPIA and Winter03 TPIA are presented in Figure 17(a, b), with their corresponding protons slices extracted at different ^{13}C chemical shifts shown in Figure 17(c, d). The alkyl carbons (CH_3, CH_2, and CH) were mainly associated with their directly attached protons, but also showed correlations with O-alkyl protons, suggesting that alkyl and O-alkyl components were in close proximity. The cross peaks of OC and OCO carbons with their directly attached protons were more pronounced in spectrum of Spring0522 than that of Winter03. Alkyl protons also contributed to the proton spectra associated with the OC and OCO carbons in Spring0522, and in Winter03 to a greater extent. The cross peaks of aromatic C were

generally weak in both spectra, and their associated proton spectra showed major contributions from aromatic protons in addition to minor contributions from non-aromatic protons. The ^{1}H spectrum associated with COO (175 ppm) in Spring0522 TPIA had a major band centered at 4 ppm, suggesting that COO groups were mostly attached to OC carbons. The alkyl and O-alkyl protons contributed almost equally to the ^{1}H spectrum associated with COO in Winter03 TPIA, suggesting that COO groups were connected to both OC and alkyl carbons. The ketone C showed extremely weak cross peaks.

After introducing a mixing time of 1 ms which allowed proton magnetization transfer from more distant sites, the 2D HETCOR spectra of Spring0522 TPIA and Winter03 TPIA (Figure 18(a, b)) showed even greater differences. Overall, the major band in ^{1}H spectra associated with all types of C centered near 4 ppm for Spring0522 but near 2 ppm for Winter03 (Figure 18(c, d)). Specifically, compared to ^{1}H spectra obtained without mixing time (Figure 17(c, d)), increasing contributions from O-alkyl protons to the ^{1}H spectra associated with alkyl C were observed for Winter03, and Spring0522 to a much greater extent (Figure 18(c, d)). The ^{1}H spectra associated with OC and OCO carbons instead showed increasing contributions from alkyl protons for both Spring0522 and Winter03. This indicated the proximity of alkyl and O-alkyl components. Though we cannot exclude the presence of isolated sugar rings, these sugar-ring like structure did not seem to associate together to form carbohydrate moieties of more than 3 sugar rings in both Spring0522 and Winter03 TPIA. The non-aromatic resonances dominated the proton spectra associated with aromatic C for both Spring0522 and Winter03. The proton slices extracted at COO/NC=O carbons also showed increased contribution from alkyl protons

(Figure 18(c, d)) as compared to ^{1}H spectra obtained without mixing time (Figure 17(c, d)).

Spring0512 TPIA contained significantly more OC and OCO than those of all other TPIA isolates (Table 4), and its CP/MAS spectrum (data not shown) closely resembled those of DOM isolated by ultrafiltration. To examine whether these OC and OCO carbons were present in large carbohydrate domains, 2D HECTOR spectra with additional mixing times (t_m = 0.01 ms, 1 ms, and 10 ms) were collected and are shown in Figure 19. With increasing mixing time, the OC and OCO carbons remained correlated predominantly with O-alkyl protons, indicating a carbohydrate domain with radii larger than 5 nm that did not equilibrate within the 10-ms mixing time. Though the COO carbons correlated predominantly with O-alkyl protons at t_m = 0.01 ms, they became correlated with alkyl protons with increasing mixing time.

Figure 20 presents the 2D HETCOR spectrum with 0.5-ms HH-CP and 40-μs dipolar dephasing of Winter03 TPIA and corresponding proton slices, providing the nontrivial correlations between abundant nonprotonated carbons and their nearby protons. Though CH_3 carbons were predominantly associated with alkyl protons, the proton spectra associated with nonprotonated carbons such as C_q (53 ppm), OC_{np} (85 ppm), and $OC_{np}O$ (108 ppm) contained nearly equal contributions from alkyl and O-alkyl protons.

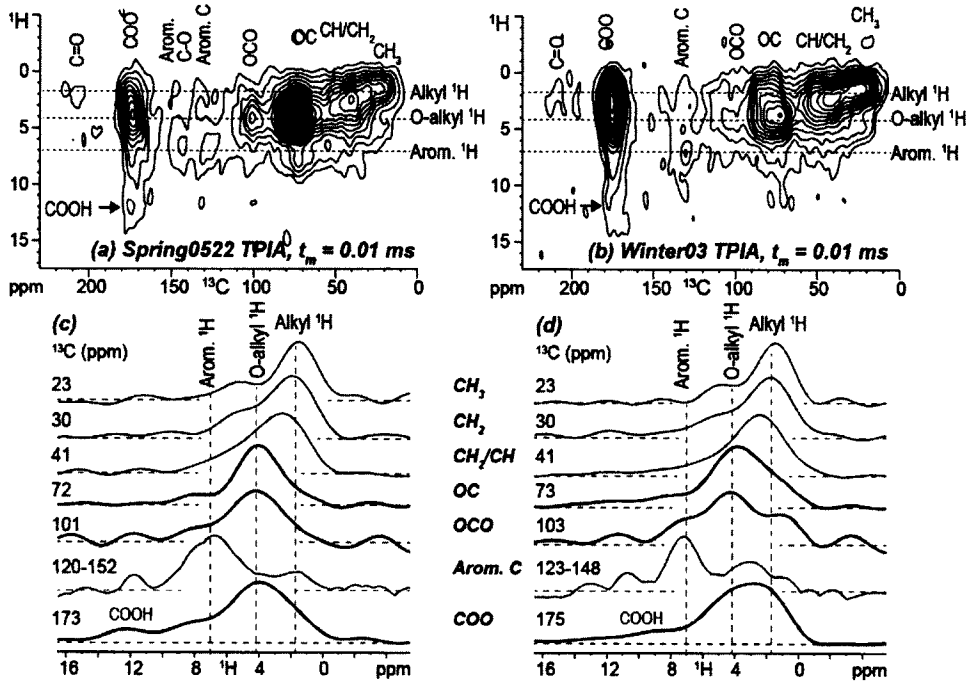

Figure 17. 2D ^{1}H-^{13}C HETCOR spectra with 0.5-ms HH-CP of (a) Spring0522 TPIA and (b) Winter03 TPIA. ^{1}H slices extracted from the 2D spectra: (c) refers to ^{1}H slices of spectrum (a), and (d) to spectrum (b).

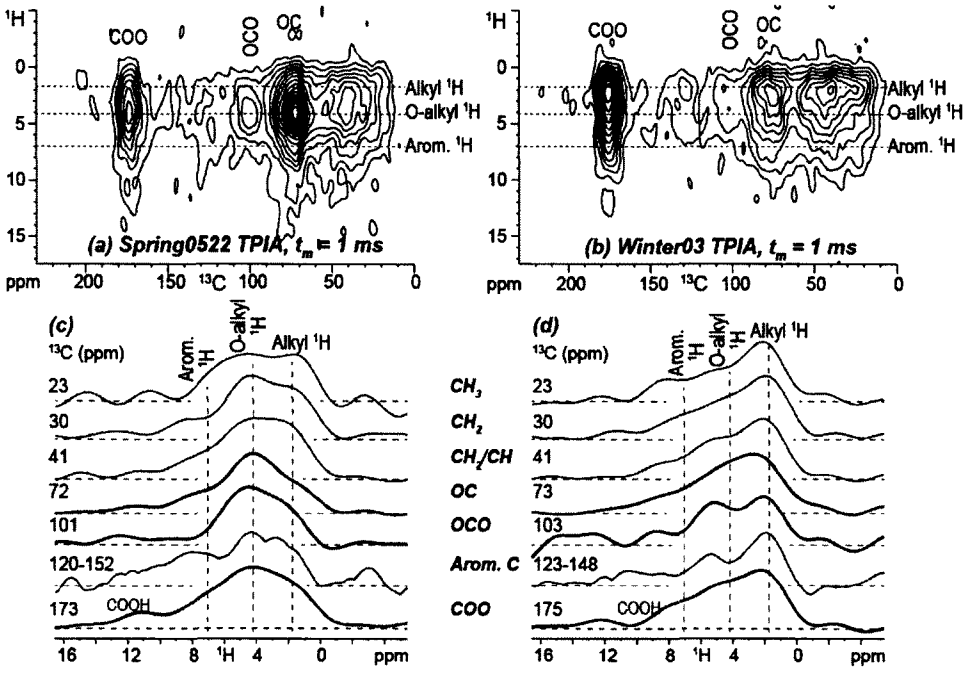

Figure 18. 2D ^{1}H-^{13}C HETCOR spectra with 0.5-ms HH-CP and 1-ms mixing time of (a) Spring0522 TPIA and (b) Winter03 TPIA. ^{1}H slices extracted from the 2D spectra: (c) refers to ^{1}H slices of spectrum (a), and (d) to spectrum (b).

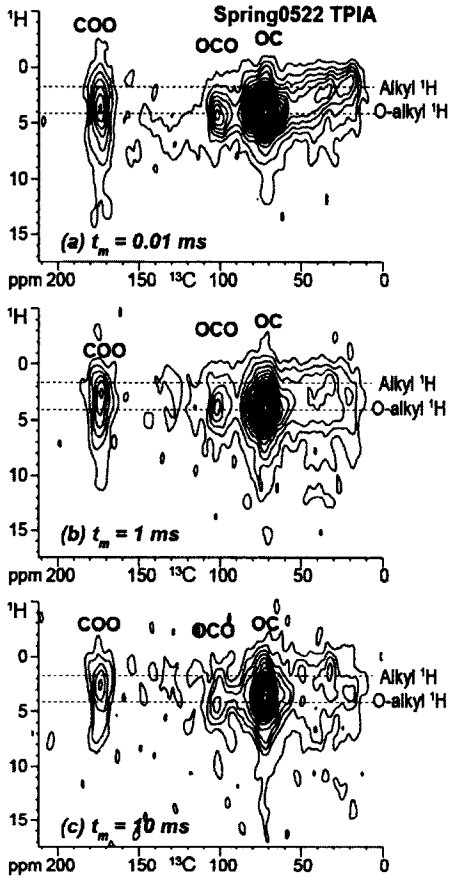

Figure 19. 2D ^{1}H-^{13}C HETCOR spectra of Spring0512 TPIA with 0.5-ms HH-CP (a) and a mixing time of (b) 1 ms and (c) 10 ms.

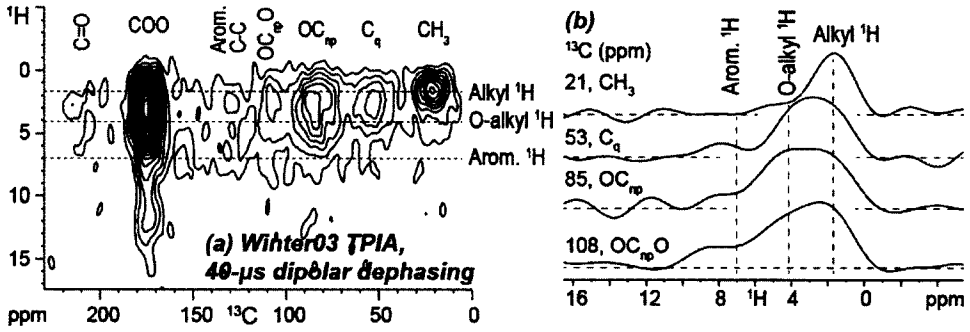

Figure 20. 2D ^{1}H-^{13}C HETCOR spectrum with 0.5-ms HH-CP and 40-µs dipolar dephasing (a) and extracted ^{1}H slices (b) of Winter03 TPIA.

DISCUSSION

Presence of Carbohydrate (-like) Moieties in DOM Across Seasons. The two major DOM fractions (HPOA and TPIA) across different seasons were abundant in O-alkyl C (OC + OCO), which made up 20-21% of HPOA and 29-38% of TPIA isolates, respectively. These O-alkyl C can be further divided into protonated and nonprotonated components, with the nonprotonated O-alkyl C accounting for 9-11% of HPOA and 11-15% of TPIA. The OC and OCO in carbohydrates related to biogenic precursors were primarily protonated, though nonprotonated anomeric (or quaternary anomeric) C had been found in some furanose sugars (Poulin and Lowary, 2010) and keto-deoxyoctulosonate in bacterial lipopolysaccharides (Strain and Armitage, 1985). If present in carbohydrate environments, the immediate proton environments of these nonprotonated OC/OCO carbons would be O-alkyl protons. However, the 2D HECTOR analyses revealed equal or more contributions from alkyl protons as well (Figure 16(b) and Figure 20(b)), indicating that they were unlikely related to carbohydrates.

The protonated OCO made up less than 1% of summer and winter HPOA/TPIA isolates. Even assuming that all protonated OCO occurred as carbohydrates, OCH related to carbohydrates cannot exceed 4-5% of summer and winter HPOA/TPIA. This left the rest of the OCH pool (4-5% of summer and winter HPOA, 8-9% of summer and winter TPIA) associated with other components than carbohydrates. The protonated OCO and OC comprised 1-2% and ~11% of spring HPOA isolates, respectively. Most of the OCH can be associated with carbohydrates based on the same assumption. Therefore there were at most 2 sugar rings per 100 C. This was generally consistent with results from 2D analyses which suggested the absence of carbohydrate moieties containing more than 3

sugar rings. Both protonated OC and OCO were greatly enriched in spring TPIA isolates (Spring0512 in particular). Assume that all 5% and 3% protonated OCO were associated with carbohydrates in Spring0512 and Spring0522, and then there were at most 5 and 3 sugar rings per 100 C in Spring0512 TPIA and Spring0522 TPIA, respectively, consistent with the presence of carbohydrate domains in Spring0512 based on 2D data analysis.

Presence of Carboxyl-Rich Alicyclic Molecules (CRAM) in DOM Across Seasons. The two major DOM fractions (HPOA and TPIA) across different seasons were carboxyl (16-21% of total C in HPOA/TPIA isolates) and alkyl rich (33-41% of HPOA and 28-36% of TPIA). In addition, all HPOA/TPIA isolates contained considerable amounts of nonprotonated OC and OCO aliphatic components (9-11% of HPOA and 11-15% of TPIA) that unlikely occur in carbohydrates. Though the COO/NC=O signals can arise from carboxyls, amides and aliphatic esters, it was estimated based on atomic C/N ratios that amides accounted for at most 1-2% of the total C in all HPOA isolates. The 2D HETCOR data also confirmed the presence of carboxylic acids and suggested the presence of aliphatic esters insignificant (Figures 14 and 17). Further aliphatic ethers may less likely survive the strong acidic conditions involved in the XAD isolation. The correlations of COO and alkyl/O-alkyl revealed in the 2D HETCOR spectra of spring HPOA and winter HPOA/TPIA, were also consistent with the presence of COO-bonded alkyl/O-alkyl, characteristic of terpenoid-derived structures or CRAM (Hertkorn et al., 2006; Leenheer et al., 2003). In addition, with 1-ms mixing time, all C components correlated with alkyl protons resonating near 2 ppm (Figure 15(c, d) and Figure 18(d)),

which was consistent with the proton chemical shift range assigned to CRAM (2.2-3.2 ppm) (Hertkorn et al., 2006; Hertkorn et al., 2013).

The carbohydrate-rich nature of the two spring TPIA isolates (Spring0512 in particular) might have masked the presence of the CRAM signature. The COO was predominantly correlated with O-alkyl protons (Figure 17(a, c) and Figure 19(a)), suggesting the presence of COO-bonded O-alkyl, commonly found in carboxylated carbohydrates such as uronic acids and muramic acids. As mixing time increased, cross peak of COO and alkyl protons became evident (Figure 18(a, c) and Figure 19(b, c)), suggesting the presence of CRAM in spring TPIA too.

Presence of Aromatic Moieties in DOM Across Seasons. The aromaticity (total fraction of protonated, nonprotonated, and oxygen-substituted aromatic C) was higher in the HPOA (19-26%) than in the TPIA isolates (12-17%), and was linearly related to the $SUVA_{254}$ ($R^2 = 0.97$). Aromatic moieties in the HPOA isolates could be derived from lignin as characteristic peaks associated with lignin were evident in the spring HPOA and visible in the summer HPOA samples. This agreed with previous observations of maximum dissolved lignin phenol concentrations in HPOA during the spring flush (Spencer et al., 2008). In addition, these lignin residues were in close proximity with aliphatic components (or CRAM) (Figures 14 and 15). Sources of aromatics in TPIA isolates were not clear, but these aromatics might also originate from lignin residues which are highly altered and have lost the associated lignin signatures so that they cannot be recognized by NMR spectroscopy.

Nonprotonated aromatic C represented the largest fraction of aromatic C, nearly the sum of protonated and O-substituted aromatic C, in all HPOA/TPIA isolates (Table 4). Recently, dissolved black carbon, characteristic of prevalent hydrogen deficient molecules with a large aromaticity index, has been identified by Fourier transform ion cyclotron resonance mass spectrometry throughout the oceans (Dittmar and Koch, 2006; Dittmar and Stubbins, 2014). Our results showed that these nonprotonated aromatics were in close proximity to both aromatic and aliphatic protons (Figure 16). This indicated that most of them unlikely occurred in condensed aromatic structures, otherwise contributions of aliphatic protons would be much less significant than those of aromatic protons, based on conceptual models of condensed aromatics (Dittmar and Koch, 2006; Hertkorn et al., 2013) and 2D HETCOR data of soils with abundant char residues (Mao et al., 2012a).

Implications for DOM Sources and Biodegradability Across Seasons. NMR analyses of two major DOM fractions (HPOA and TPIA, together accounting for 64-74% of DOC) have shown that, spring DOM was more enriched in lignin residues (within HPOA fractions) and carbohydrates (within TPIA fractions), representing contributions from fresh organic materials, than summer and winter DOM. This is consistent with observations from previous studies, such as the maximum concentrations of lignin phenols during the spring flush (Spencer et al., 2008), and younger organic matter pools than at other times of year (Aiken et al., 2014; Neff et al., 2006; Raymond et al., 2007). In addition, CRAM represented a more refractory DOC pool that is present in DOM across different seasons.

DOC isotopic composition ($\delta^{13}C$ and $\Delta^{14}C$) provides information on sources, ages, and transformations of DOC. The HPOA isolates had the following order of increasing apparent age: spring DOM, summer-fall DOM, and winter DOM, consistent with previously published data for total DOC collected at the same site during 2004-2005 (Aiken et al., 2014). During the spring flush period, inputs from leached plant materials and upper soil horizons dominate the DOM pool, consistent with the modern age. In the late summer period, as the influence of organic matter derived from organic rich upper soil horizons becomes much less, DOM is less aromatic, and contains lower lignin phenol yields than during the spring flush period (Spencer et al., 2008). The oldest DOC was reported during the winter months when low flow is dominated by groundwater, associated with more extensively degraded DOM.

In terms of DOM biodegradability, recent incubation studies have given contrasting results: while others found higher biodegradability of spring flush DOM (Holmes et al., 2008; Mann et al., 2012), Wickland et al. (2012) pointed to the greater biodegradability of winter DOM from Arctic rivers than spring and summer samples. From the point view of the major structural components present in DOM across seasons, higher biodegradability would be expected for spring DOM samples which were associated with more lignin residues and carbohydrates than summer and winter samples. However, DOM samples across different seasons all shared relatively more refractory components such as CRAM, and nonprotonated OC and OCO pool which can be very likely to be associated with CRAM. The CRAM were more dominant in summer and winter DOM samples than in spring samples where they were diluted by the presence of abundant carbohydrates in particular in TPIA fractions. Nonprotonated OC and OCO

carbons have been proposed as a potential index of humification (Mao et al., 2012b). Specifically, nonprotonated OCO carbons have been shown to be present and preserved in biologically refractory carbohydrates (Helms, 2012). The combined fractions of nonprotonated OC and OCO carbons were more abundant in summer and winter DOM samples than spring samples, though nonprotonated OC fractions were similar or occasionally slightly higher in DOM during spring than other times of the year. This suggested the refractory nature of DOM samples across different seasons.

CHAPTER IV

COMPARISON OF THE CHEMICAL STRUCTURES OF DISSOLVED ORGANIC MATTER IN LAKES DRIVEN BY HYDROLOGY

INTRODUCTION

Substantial evidence has accumulated that lakes are hotspots of carbon cycling though comprising only a small fraction of the Earth's surface (Cole et al., 2007; Sobek et al., 2006; Tranvik et al., 2009). Lakes act as sites of intense organic carbon (OC) mineralization leading to emissions of greenhouse gases such as carbon dioxide and methane to the atmosphere (Cole et al., 1994; Tranvik et al., 2009), and simultaneously sequester large amounts of carbon (~ 820 Pg of OC) in their sediments (Cole et al., 2007; Mulholland and Elwood, 1982). Therefore, lakes may have environmental effects that are disproportional relative to their spatial extent (Sobek et al., 2006).

Dissolved organic matter (DOM) is the largest pool of OC in most lake waters. With the exception of eutrophic lakes, lake DOM is strongly dominated by allochthonous material exported from the catchment (Wilkinson et al., 2013), supplementing the pools generated from autotrophic and heterotrophic in-situ activities (Guillemette and del Giorgio, 2012; Kritzberg et al., 2004). A large share of lake DOM is altered and lost by in-lake processes including microbial respiration/mineralization, photochemical degradation, and flocculation (Bertilsson and Tranvik, 2000; Cory et al., 2007; Koehler et al., 2012; von Wachenfeldt et al., 2009; von Wachenfeldt et al., 2008). The magnitude of these in-lake processes appears to depend heavily on water residence time (WRT), i.e., the amount of time water spends in the lake (Algesten et al., 2004; Hanson et al., 2011;

Kellerman et al., 2014; Köhler et al., 2013; Kothawala et al., 2014; Meili, 1992). Therefore, the molecular composition of lake DOM can be highly variable across landscapes, hydrologies, and climates, reflecting the net influences of DOM source, reactivity, and all the transformation processes occurring within the lake system (Berggren et al., 2007; Cory et al., 2007; Jaffé et al., 2008; Kellerman et al., 2014; Kothawala et al., 2014).

The Shingobee River headwaters area, located in north-central Minnesota, provides a unique opportunity to compare and contrast two lakes (Williams Lake and Shingobee Lake) with similar biologic, geologic, and climatic settings, but different hydrologies. The hydrologically closed Williams Lake, located close to the highest point in the regional flow system, has no surface inlet or outlet. Ground-water inflow represents 58-76% of the annual water input with the rest being from precipitation (LaBaugh et al., 1995). The hydrologically open Shingobee Lake, about 5 kilometers from Williams Lake, has the Shingobee River flowing through it and dominating the annual flux to and from Shingobee Lake. As a result of these differing hydrological conditions, Shingobee Lake has a much shorter WRT (0.3-0.5 years) than Williams Lake (3-4 years) (Stets et al., 2009; Winter and Rosenberry, 1997).

Previous comparison of DOM in these two lakes has revealed that Williams Lake fulvic acid (FA; an operationally defined fraction of DOM by reversible sorption on XAD-8 resin) is more aliphatic and less aromatic than Shingobee Lake FA (Aiken et al., 1997). The fluorescence characteristics of their FA isolates fell between the microbially-derived and terrestrially-derived end members, suggesting DOM sources from both microbially and terrestrially derived organic material (McKnight et al., 2001). Though the

general chemistry of DOM in these two contrasting lakes has been documented, more detailed molecular-level structural information of DOM has yet to be developed. In addition, previous studies have focused only on the relatively hydrophobic FA fraction of DOM (30-40% of total DOC), whereas the more hydrophilic fraction (termed transphilic acid, TPIA), which represents an important piece of the DOC pie (~20% of total DOC), has received little or no attention. To extend this comparison, DOM samples from Manganika Lake, a hypereutrophic lake with anthropogenic influences from two major water inputs (the Virginia wastewater treatment plant and United Taconite mine waters) are also included. The objective of the present study is to compare and contrast chemical characteristics of DOM including both hydrophobic acid and transphilic acid fractions from Williams Lake, Shingobee Lake and Manganika Lake using one- and two-dimensional solid-state nuclear magnetic resonance (NMR) spectroscopy.

MATERIALS AND METHODS

Water Sampling and DOM Isolation. Sampling was conducted in June of 2012 in Manganika Lake, and in September of 2013 in the Williams Lake and Shingobee Lake in north-central Minnesota. More detailed site descriptions can be found elsewhere (Berndt and Bavin, 2011; Winter and Rosenberry, 1997). Large volume (155-415 L) water samples were filtered in the field (0.45 μm) and shipped on ice to the USGS laboratory in Boulder (Colorado, United States) for DOC concentration, absorbance, and excitation-emission fluorescence analyses.

Water samples were then processed by XAD isolation and concentration as described by Aiken et al. (1992). Briefly, samples were acidified to pH 2 with

hydrochloric acid (HCl) and passed first through a column of XAD-8 resin, followed by a column of XAD-4 resin. Each column was then eluted with 0.1 N sodium hydroxide (NaOH) to obtain the XAD-8 (hydrophobic organic acids, HPOA) and XAD-4 (transphilic organic acids, TPIA) fractions, respectively. The eluates were immediately acidified to minimize sample alteration at high pH, desalted, lyophilized, and stored in a desiccator.

Elemental Analyses and Carbon Isotopic Measurements. Elemental analyses (C, H, O, N, S and ash) of DOM isolates were performed by Huffman Laboratories (Golden, Colorado) by the method described in Huffman and Stuber (1985). Stable carbon isotope ratios ($\delta^{13}C$) were determined by isotope ratio mass spectrometry on dried DOM fractions following vapor phase acidification, and are expressed relative to the PDB standard. The radiocarbon ratios of the HPOA isolates were measured by accelerator mass spectrometry at the Center for Accelerator Mass Spectrometry at Lawrence Livermore National Laboratory (California, United States). $\Delta^{14}C$ data (in ‰) were corrected for isotopic fraction using measured $\delta^{13}C$ values. The $\Delta^{14}C$ and radiocarbon age were determined from percent modern carbon using the year of sample analysis according to Stuiver and Polach (1977). Ages are presented as Modern when the fraction modern exceeded 1. Results of elemental analyses and carbon isotopic data of selected samples are given in Table 5.

Ultraviolet and Visible (UV-visible) Absorbance and Fluorescence Measurements. Specific UV absorbance ($SUVA_{254}$) was determined by dividing the UV-visible

absorbance at $\lambda = 254$ nm by DOC concentration and is correlated to DOM aromaticity (Weishaar et al., 2003). Fluorescence measurements were made on solutions of isolated HPOA and TPIA fractions and filtered whole water samples using a Horiba-JY Fluoromax-3 spectrofluorometer with DataMax software. Fluorescence excitation emission matrices (EEMs) were collected at room temperature by measuring fluorescence intensity across excitation wavelengths ranging from 240 to 450 nm (5 nm increments) and emission wavelengths between 300 and 600 nm (2 nm increments). Excitation and emission slit widths were 5 nm, and the instrument was configured to collect fluorescence scans in ratio mode. Both fluorescence EEMs and absorbance scans were blank-corrected with Milli-Q water, and EEMs were corrected for instrument optics, Raman area normalized and corrected for any inner-filter effects (McKnight et al., 2001; Murphy et al., 2010). Resulting EEMs are reported in Raman Units.

NMR Analysis. All ^{13}C NMR experiments were performed at 100 MHz using a Bruker Avance 400 spectrometer equipped with a 4-mm double-resonance probe head. Samples filled the radio-frequency coil from end to end; a cylindrical glass plug of 2-mm height at the bottom of the rotor prevented sample material from being placed outside the coil. The ^{13}C chemical shifts were referenced to tetramethylsilane, using the COO resonance of glycine in the α-modification at 176.46 ppm as a secondary reference.

The multiple-cross polarization (multiCP) technique recently developed by Johnson and Schmidt-Rohr (2014) was used for all samples to obtain quantitative ^{13}C NMR spectra. The spectra were measured at a spinning speed of 14 kHz, where spinning sidebands are fairly small (< 3%) and have litter overlap with centerbands. The 90° pulse

lengths were 4.3 μs for ^{1}H and 4 μs for ^{13}C. All spectra were recorded with a Hahn echo generated by an 180° pulse with EXORCYCLE phase cycling (Bodenhausen et al., 1977) applied one rotation period (t_r) after the end of cross polarization, in order to achieve dead-time-free detection. The ^{1}H decoupling field strength was $|\gamma B_1|/2\pi = 65$ kHz during the period of 2 $t_r = 0.14$ ms duration before the Hahn echo, and approximately 55 kHz during signal detection. The ramp for CP was implemented with 11 steps of 0.1 ms duration and a 1% amplitude increment (90 to 100%). The recycle delays were 0.35 s. The duration of the repolarization period t_z in multiCP was 0.3 s. Corresponding multiCP spectra of nonprotonated C and mobile groups such as rotating CH_3 were obtained after a dipolar dephasing time of 68 μs (multiCP/DD). The number of scans collected was 2048 per spectrum for HPOA isolates and 2560 for TPIA isolates. The total time for multiCP and multiCP/DD experiments was 3-4 h per sample, tremendously less than the measuring time required by quantitative direct polarization experiments.

Both anomeric (O-C-O) and aromatic carbons resonate between 120 and 90 ppm. To resolve the overlapping resonances, the aromatic carbon signals were selectively suppressed by inserting a three-pulse ^{13}C chemical-shift-anisotropy (CSA) filter with a CSA-filter time of 68 μs into the ^{13}C cross polarization and total suppression of sidebands NMR experiments (Mao and Schmidt-Rohr, 2004a). The number of scans averaged was 1536 or 2048 for each spectrum. The CSA filter was also combined with dipolar dephasing (48 μs) to select signals from nonprotonated anomeric carbons. The number of scans averaged for the spectrum of CSA filter coupled with dipolar dephasing was 3072 for each sample.

^{1}H-^{13}C two dimensional heteronuclear correlation (2D HETCOR) NMR experiments (Mao and Schmidt-Rohr, 2006) were performed at a spinning speed of 7.5 kHz. Standard Hartmann-Hahn CP (HH-CP) with 80-μs CP time reveals primarily one-bond ^{1}H-^{13}C connectivities. HH-CP of 0.5 ms allows for some ^{1}H spin diffusion and therefore correlates the carbons with protons within ~ 0.5 nm radius. In addition, a 40-μs dipolar dephasing delay was inserted in the HH-CP HETCOR to reveal ^{1}H-^{13}C proximities for nonprotonated carbons (multi-bond) and mobile groups. The recycle delay was 0.5 s. Longer-range proximities were probed by ^{1}H spin diffusion during a mixing time of 1 ms, correlating the carbons with protons within ~ 1.6 nm radius.

RESULTS

DOC Concentration, Major Chemical Fractions, $SUVA_{254}$, and Elemental Composition. DOC concentrations were greater in Williams Lake (7.2 mg C L^{-1}) than in Shingobee Lake (5.2 mg C L^{-1}), but lower than in Manganika Lake (10.5 mg C L^{-1}) (Table 5). The hydrophobic acids (HPOA) were the dominant DOM fraction (ca. 30-40% of DOC) in all lakes, but were much less abundant in Williams Lake (30% of DOC) than in Shingobee and Manganika (37% and 40% of DOC, respectively) lakes. The fraction of transphilic acids (TPIA) was higher in Williams (21% of DOC) and Shingobee (22% of DOC) lakes than in Manganika Lake (17% of DOC). The $SUVA_{254}$ (indicating aromaticity) associated with HPOA and TPIA isolates showed the same trend, increasing in values from Williams Lake to Shingobee Lake to Manganika Lake. The TPIA isolates always had lower $SUVA_{254}$ values than corresponding HPOA isolates from the same lake.

Table 5

DOC concentrations, $SUVA_{254}$, and major chemical fractions of DOM.

Date	Sample	DOC (mg C L^{-1})	Fraction	% of DOC	$SUVA_{254}$ (L mg C^{-1} m^{-1})	Ash-free elemental contents (%) and C isotopic data (‰)						
						C	H	O	N	S	$\delta^{13}C$	Age (ybp)
9/18/2013	Williams Lake	7.2	HPOA	30	1.9	56.10	5.62	35.71	1.83	0.75	-26.06	>Modern
			TPIA	21	1.2	50.81	5.21	39.59	3.26	1.12	ND	ND
9/4/2013	Shingobee Lake	5.2	HPOA	37	3.1	55.13	5.03	37.15	1.76	0.93	-29.1	315
			TPIA	22	2.2	49.89	4.64	41.74	2.61	1.12	ND	ND
6/26/2012	Manganika Lake	10.5	HPOA	40	4.2	52.21	4.62	40.39	1.66	1.13	ND	ND
			TPIA	17	2.9	45.52	4.60	45.44	2.36	2.08	ND	ND

DOC is dissolved organic carbon, and $SUVA_{254}$ is specific UV absorbance determined at 254 nm. HPOA is hydrophobic acid, and TPIA is transphilic acid. ybp, years before present. ND, not determined.

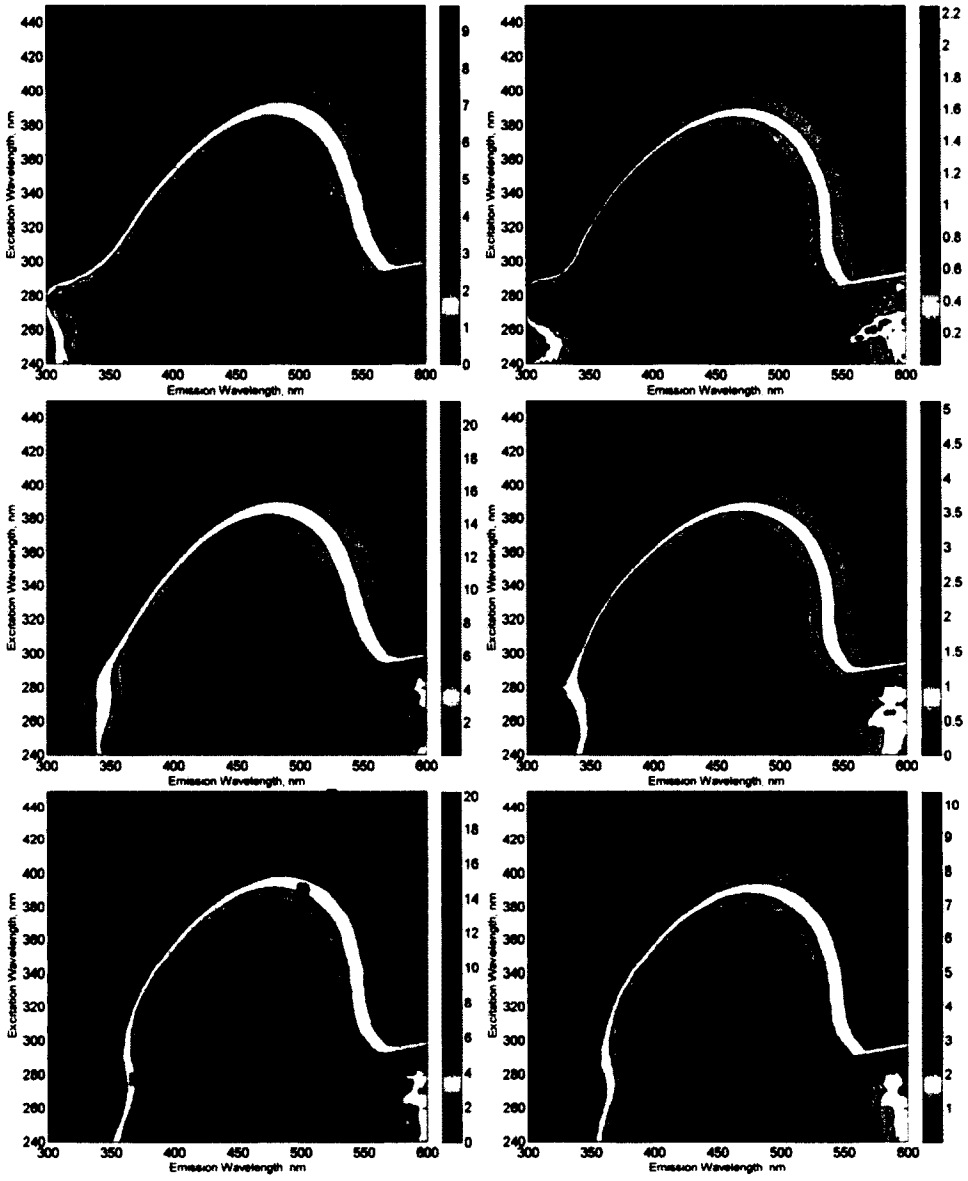

Figure 21. Fluorescence excitation emission spectra for Williams Lake (a, HPOA; d, TPIA), Shingobee Lake (b, HPOA; e, TPIA), and Manganika Lake (c, HPOA; f, TPIA). Peak label and description of fluorophores (B, tyrosine-like and protein-like; T, tryptophan-like and protein-like; A, humic-like; M, marine humic-like; C, humic-like; D, soil fulvic acid; E, soil fulvic acid; N, plankton derived) as summarized in Aiken et al. (2014b).

Elemental analyses show that C and H contents were highest but O content was lowest in HPOA/TPIA from Williams Lake, followed by HPOA/TPIA from Shingobee Lake, and Manganika Lake. In addition, the HPOA isolates were more enriched in C and H, but more depleted in O compared to corresponding TPIA isolates from the same lake. The N contents were low (< 2%) in all HPOA, resulting in atomic C/N values of 35.8-36.7. The TPIA fractions had relatively higher N contents (2-3%), and therefore lower atomic C/N values (18.2-22.5). Sulfur contents were low (0.75-2.08%), and relatively higher, in Manganika Lake than in Shingobee and Williams lakes, and in TPIA isolates than corresponding HPOA isolates from the same lake. Isolates from Manganika Lake may have artificially high sulfur content from sulfate reduction leading to the addition of sulfur to DOM.

The $\delta^{13}C$ values were less negative for Williams HPOA (-26.06‰) than for Shingobee HPOA (-29.1‰), but both indicated terrigenous sources. The Shingobee HPOA had more depleted $\Delta^{14}C$ values than Williams HPOA, which translated to ^{14}C ages of 315 ybp for Shingobee HPOA and modern for Williams HPOA.

Fluorescence Excitation-Emission Matrices (EEMs) of DOM in Different Lakes. The EEMs spectra of HPOA and TPIA isolates from the three lakes are presented in Figure 21. The EEMs data of HPOA isolates had stronger fluorescence intensities than those of corresponding TPIA isolates, indicating that the majority of chromophores and fluorophores in the whole water samples were found in the HPOA fractions. Nevertheless all spectra showed strong fluorescence signals associated with terrestrially derived organic matter, i.e., EEMs dominated by humic and fulvic-like fluorophores (peaks A and

C) (Coble, 1996). Of significance was the presence of fluorescence centers attributed to protein-like materials in HPOA/TPIA from Williams Lake (peak B), indicating contributions from microbial sources.

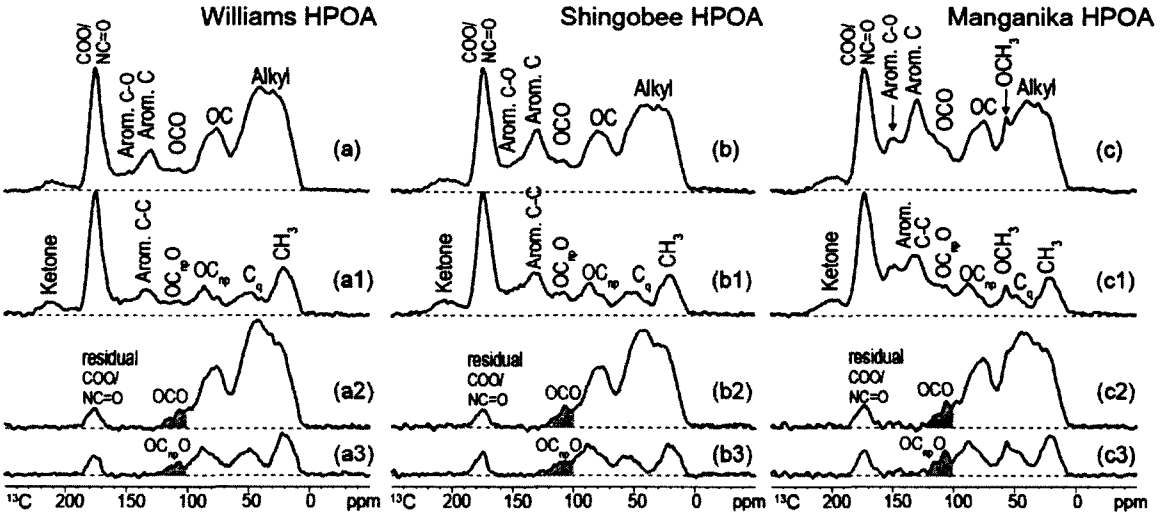

Figure 22. Solid-state ^{13}C multiCP NMR spectra and spectral editing for identification of functional groups obtained for HPOA isolates from three lakes. (a-c) MultiCP spectra showing signals of all C. (a1-c1) MultiCP with dipolar dephasing showing nonprotonated and mobile segments such as CH_3. (a2-c2) Selection of sp^3-hybridized C signals by a ^{13}C CSA filter for the separation of anomeric C (shaded area) from aromatic C. (a3-c3) Selection of nonprotonated sp^3-hybridized C signals and mobile segments for the separation of nonprotonated anomeric C (shaded area) from nonprotonated aromatic C. All multiCP spectra are scaled to match the intensity of the COO/NCO band.

Carbon Functional Group Composition of DOM in Different Lakes. The solid-state ^{13}C spectra of HPOA and TPIA isolates from three different lakes are given in Figures 22 and 23, respectively. The ^{13}C all C multiCP spectra of both HPOA and TPIA isolates (Figure 22(a-c) and Figure 23(a-c)) were dominated by five relatively well-resolved peaks, though varying in intensities, that arose from nonpolar alkyl C (0-64 ppm), O-alkyl C (64-100 ppm), aromatic or olefinic C (100-160 ppm, also containing anomeric C), COO/NC=O (160-190 ppm), and ketone/aldehyde C (190-220 ppm). The multiCP spectra obtained after dipolar dephasing (Figure 22(a1-c1) and Figure 23(a1-c1)), where signals of nonprotonated and mobile C components were retained, were characterized by resonances from CCH_3, quaternary C (CC_q), nonprotonated OC (OC_{np}), nonprotonated anomeric C ($OC_{np}O$), nonprotonated aromatic C-C, aromatic C-O (144-160 ppm), COO/NC=O, and ketone C. Note that ketone signals here were comparable in intensities to ketone/aldehyde C signals in all C spectra (Figure 22(a-c) and Figure 23(a-c)), indicating that the carbonyls were present as ketone C in all HPOA/TPIA isolates. Note that signals from OCH_3 (56 ppm) and aromatic C (including aromatic C-O, ~150 ppm) characteristic of lignin residues were present in the spectra of Manganika HPOA (Figure 22(c, c1)). These characteristic peaks (OCH_3 peak in particular) were not evident in the spectra of Williams and Shingobee HPOA, or spectra of all TPIA isolates. The CP/TOSS spectra after the CSA filtering (Figure 22(a2-c2) and Figure 23(a2-c2)), highlighted signals of anomeric C (OCO, shaded area) while suppressing those of sp^2-hybridized C including aromatic C. Anomeric C signals were observed in spectra of all HPOA/TPIA isolates, and their chemical shifts generally occurred in the region 100-123 ppm. The combination of the CSA filter technique with dipolar dephasing (Figure 22(a3-

c3) and Figure 23(a3-c3)) achieved the selection of nonprotonated anomeric C ($OC_{np}O$, shaded area). Because visual comparison of multipeak spectra can be misleading, comparison of HPOA and TPIA isolates among different lakes was made in terms of the quantitative distributions of specific C functional groups within the samples (Table 6).

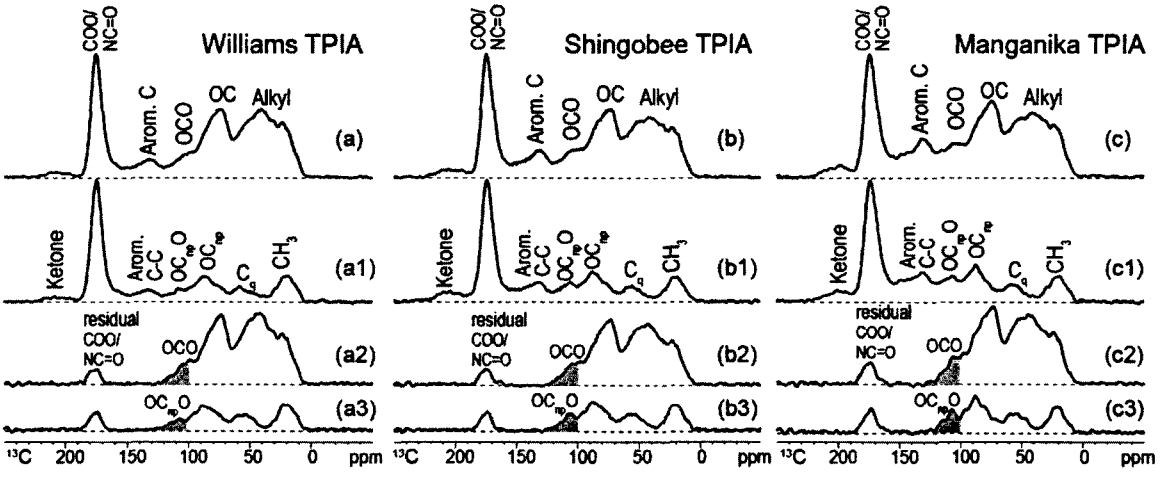

Figure 23. Solid-state ^{13}C multiCP NMR spectra and spectral editing for identification of functional groups obtained for TPIA isolates from three lakes. (a-c) MultiCP spectra showing signals of all C. (a1-c1) MultiCP with dipolar dephasing showing nonprotonated and mobile segments such as CH_3. (a2-c2) Selection of sp^3-hybridized C signals by a ^{13}C CSA filter for the separation of anomeric C (shaded area) from aromatic C. (a3-c3) Selection of nonprotonated sp^3-hybridized C signals and mobile segments for the separation of nonprotonated anomeric C (shaded area) from nonprotonated aromatic C. All multiCP spectra are scaled to match the intensity of the COO/NCO band.

Table 6

Integrated areas (in %) from ^{13}C multiCP NMR spectra for HPOA and TPIA isolates from different lakes, and the assigned structural moieties associated with the spectral region.

Samples		ppm												
		220-190	190-160	160-143	143-100		123-100 (OCO)		100-64 (OC)		64-0 (Alkyl C)			
		Ketone C	COO/ NC=O	Arom. C-O	Arom. C-C[a]	Arom. C-H	$OC_{np}O$[b]	OCHO[b]	OC_{np}[a]	OCH_n	C_q[a]	OCH_3[a]	CH_2/CH/ NCH	CH_3[a]
HPOA	Williams	1.9	17.4	3.0	5.6	4.1	1.8	0.9	6.4	11.0	5.2	0.1	29.0	13.5
	Shingobee	2.6	18.3	4.5	10.0	5.0	2.1	0.8	7.0	9.8	4.4	0.9	23.1	11.5
	Manganika	2.5	16.9	6.7	13.2	7.2	2.5	0.4	6.1	10.3	3.1	1.6	20.4	9.3
TPIA	Williams	1.3	20.8	2.4	3.6	2.4	2.4	1.1	8.9	15.9	4.0	0.0	26.8	10.4
	Shingobee	2.4	21.3	3.2	5.9	3.2	2.9	0.9	9.3	14.9	3.8	0.0	23.3	8.9
	Manganika	2.6	20.0	4.2	8.6	3.2	3.4	0.8	9.4	14.2	3.6	0.0	21.2	8.8

[a] Based on multiCP spectrum with 68-μs dipolar dephasing.

[b] Based on CSA-filtered CP/TOSS spectrum and CSA-filtered CP/TOSS spectrum with dipolar dephasing.

Structural composition of HPOA isolates. HPOA isolates from the three lakes all contained more aliphatic C than aromatic C. The alkyl C (0-64 ppm) accounted for 34-47% of the C in the HPOA isolates. Within the alkyl C pool of all HPOA isolates, protonated alkyl C (i.e., CH_2/CH) has the largest share, followed by methyl C and quaternary C. The OCH_3 comprised only 1-2% of Manganika HPOA, and <1% of HPOA isolates from other two lakes. Both the total alkyl C and its individual sub-components (CH_2/CH, CH_3, C_q) were most enriched in Williams Lake, followed by Shingobee Lake, and Manganika Lake. The total aromatic C fraction (including protonated aromatic C-H, nonprotonated aromatic C-C, and oxygen substituted aromatic C-O; or aromaticity) ranged from 12-27% and increased as alkyl C decreased. Nonprotonated aromatic C-C dominated the aromatic C pool for all HPOA isolates, while aromatic C-H and aromatic C-O contributed less and had similar abundances. The fractions of three types of aromatic C displayed the same trend as aromaticity: largest for Manganida Lake, intermediate for Shingobee Lake, and lowest for Williams Lake. The abundances of O-alkyl C (sum of OC and OCO), were rather constant among three lakes, accounting for 19-20% of total C. The OCO fraction was small, making up 2-3% of all C in all HPOA isolates, and the majority was present in nonprotonated form ($OC_{np}O$, 1-2%). The HPOA isolates from all the lakes were more enriched in protonated OC (OCH_n, 9-11%) than nonprotonated OC (OC_{np}, 6-7%). The COO/NC=O constituted 17-18% of the C in all HPOA isolates. It is estimated that fractions of NC=O were at most 2-3% in all HPOA isolates based on their atomic C/N values (35.8-36.7). The relative fraction of ketone C was small and constant (~2%) in HPOA isolates from three lakes. It is worth noting that all HPOA isolates contained abundant nonprotonated aliphatic C (C_q + OC_{np} + $OC_{np}O$) (11-13%), and CH_3 (9-13%).

Structural composition of TPIA isolates. The dominant component in all TPIA isolates was alkyl C (0-64 ppm), which made up 41%, 36%, and 33%, respectively, of C in TPIA from Williams Lake, Shingobee Lake, and Manganika Lake. The majority of alkyl C was present in the form of CH_2/CH, which was most abundant in Williams Lake TPIA, followed by Shingobee Lake and Manganika Lake TPIA. The methyl C (8-10%) and quaternary C (3-4%) were relatively constant among TPIA isolates from three lakes. The fraction of O-alkyl C (OC + OCO) was rather constant (27-28%) in these TPIA isolates, which contained relatively more protonated OC (OCH_n, 14-15%) than nonprotonated OC (OC_{np}, 8-9%), but less protonated OCO (OCHO, ~1%) than nonprotonated OCO ($OC_{np}O$, 2-3%). Consistent with the intense COO/NC=O peak, it contributed to 20-21% of C in all TPIA isolates. Because the relative abundances of NC=O cannot exceed 4-5% based on their atomic C/N ratios (18.2-22.5), COO contributed at least 15% to C in all TPIA isolates. The total aromatic C comprised 8% of Williams TPIA, 12% of Shingobee TPIA, and 16% of Manganika TPIA. Relative fractions of aromatic C-C and aromatic C-O increased in the same order, whereas that of aromatic C-H did not vary among TPIA isolates from three lakes. Though constituting a very small portion (1-2%) for all TPIA isolates, ketone C was clearly more depleted in Williams Lake than in other two lakes. Notably, nonprotonated aliphatic C (C_q + OC_{np} + $OC_{np}O$) made up a significant fraction, 15-16%, of C in all TPIA isolates.

Proximities of Functional Groups in DOM in Different Lakes. Two-dimensional ^1H-^{13}C heteronuclear correlation (2D HETCOR) NMR provides through-space ^1H-^{13}C correlations and information on proximities or connectivities of different functional

groups. The 2D HETCOR spectra of HPOA/TPIA isolates from the three lakes were presented in Figures 24-29, with ^{1}H slices at different ^{13}C chemical shifts shown below 2D spectra to facilitate observation of the ^{1}H-^{13}C correlations.

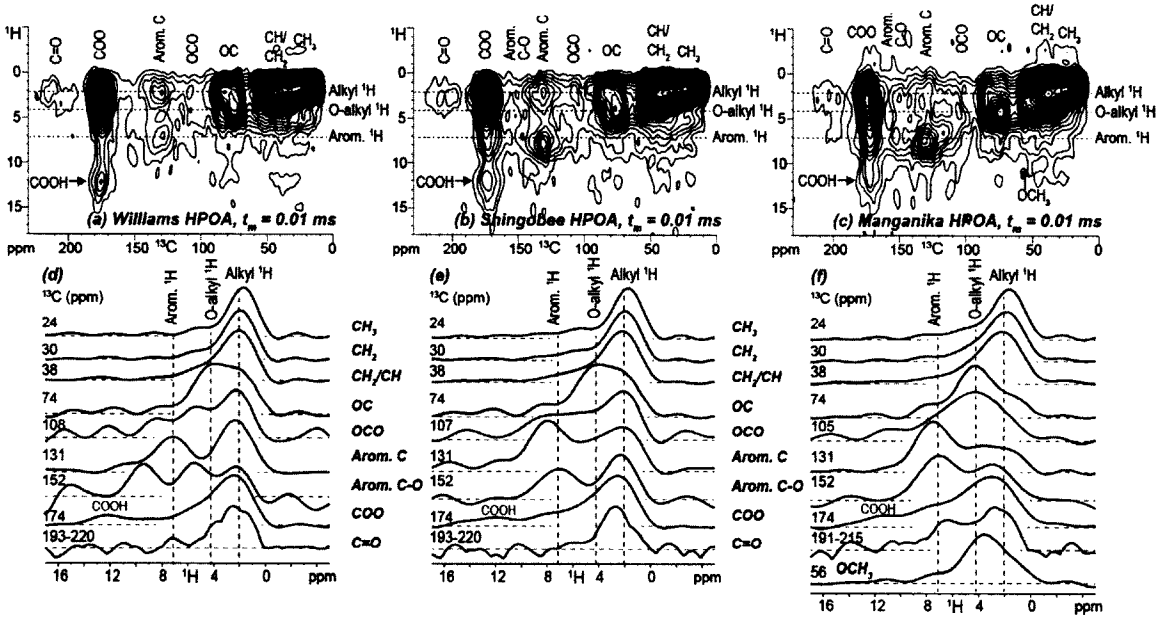

Figure 24. 2D ^{1}H-^{13}C HETCOR spectra with 0.5-ms HH-CP of HPOA isolates from (a) Williams Lake, (b) Shingobee Lake, and (c) Manganika Lake. ^{1}H slices extracted from the 2D spectra: (d) refers to ^{1}H slices of spectrum (a), (e) to spectrum (b), and (f) to spectrum (c).

HPOA isolates. Figure 24 shows the 2D HETCOR spectra of HPOA isolates from Williams Lake (Figure 24(a)), Shingobee Lake (Figure 24(b)) and Manganika Lake (Figure 24(c)) with HH-CP of 0.5 ms, showing ^{1}H-^{13}C correlations within ~ 0.5 nm radius. All spectra showed cross peaks of CH_3 and CH_2/CH with their own alkyl protons resonating at 1-3 ppm. In addition, the spectrum of Manganika Lake HPOA (Figure 24(c)) contained the cross peak of OCH_3, which was absent in the spectra of Williams and Shingobee lakes, consistent with their ^{13}C multiCP spectra. The correlations of other carbon functional groups with their directly attached or neighboring protons can be better illustrated in their corresponding proton slices (Figure 24(d-f)).

For HPOA isolates from Williams and Shingobee lakes, the ^{1}H spectra associated with OC carbons contained resonances from both O-alkyl protons and alkyl protons of similar intensities (Figure 24(d, e)). In addition, the OCO carbons showed primarily correlations with alkyl protons, indicating that both OC and OCO carbons were in close proximity to alkyl protons, and therefore, alkyl carbons. The corresponding proton slices for Manganika Lake HPOA (Figure 24(f)) showed that, both OC and OCO carbons correlated mainly with O-alkyl protons, and the contribution from alkyl protons was also seen but not as significant as for Williams and Shingobee lakes. The ^{1}H slices extracted at the chemical shifts of aromatic C (131 ppm) indicated correlations of aromatic C with both aromatic and alkyl protons for all HPOA isolates from three lakes (Figure 24(d-f)), indicating close association of aromatic and alkyl components. Whereas the alkyl protons contributed more than aromatic protons to the ^{1}H spectrum associated with aromatic C for Williams HPOA (Figure 24(d)), its relative intensities decreased and became less than those of aromatic protons in corresponding ^{1}H spectra for Shingobee and Manganika

HPOA (Figure 24(e, f)). The ^{1}H spectrum associated with aromatic C-O was rather noisy for Williams HPOA, but indicated contributions from both aromatic and alkyl/O-alkyl protons for HPOA isolates from Shingobee and Manganika lakes. Note that the contribution of O-alkyl protons was more evident for Manganika Lake, suggesting aromatic C–O–CH_3 linkages in lignin-like structures (Figure 24(f)). In addition, its ^{1}H spectrum extracted at OCH_3 site was dominated by directly attached OCH_3 protons resonating at ~3.5 ppm. The COO carbons showed correlations primarily with alkyl protons near 2-3 ppm, with additional contribution from O-alkyl protons, indicating that they were attached mostly to alkyl and O-alkyl carbons. Linkages between COO and O-alkyl groups can be either $\underline{C}$(=O)–O–$C\underline{H}_n$ or O–$C\underline{H}_n$–$\underline{C}$(=O)–O–. The latter carboxyl linkage was more likely because it involves a shorter C–H distance (two-bond C– –H) than the former ester linkage (three-bond C– – –H), and favored the rapid H-to-C cross polarization observed in the experiments. In addition, the cross peaks of COO carbons with the acidic COOH protons (~12 ppm) were prominent in all 2D HETCOR spectra (Figure 24(a-c)), further confirming the presence of carboxylic acids. Ketone C appeared to mainly correlate with aliphatic protons indicating that they were attached to aliphatic carbons, though the cross peaks of ketone C and their neighboring protons were very weak and corresponding proton spectra were noisy.

The 2D HETCOR with a 1-ms mixing time, which allows for proton magnetization transfer from more distant sites, further enabled the examination of ^{1}H-^{13}C correlations on a longer length scale (~ 1.6 nm radius) (Figure 25(a-c)). The HPOA isolates from the three lakes had very similar 2D spectral patterns, and proton slices (Figure 25(d-f)). Generally, the ^{1}H spectra associated with all types of C were dominated

by alkyl protons near 2 ppm (Figure 25(d-f)), indicating that all C sites were in close proximity to alkyl protons. Correlations of these different C sites with O-alkyl protons were also observed for all, but to a greater extent in ^{1}H spectra for Manganika HPOA (Figure 25(f)).

Nonprotonated aliphatic carbons (C_q + OC_{np} + $OC_{np}O$, 11-13% of all C) were shown to be abundant in HPOA isolates from all three lakes. These nonprotonated carbons are separated by at least two bonds from their nearby protons, and this type of ^{1}H-^{13}C correlations can be observed with a 2D HETCOR spectrum with 0.5-ms HH-CP and 40-μs dipolar dephasing (Figure 26(a-c)) and corresponding proton slices (Figure 26(d-f)). For all HPOA isolates, the ^{1}H slices extracted at 48 ppm (C_q) all showed primarily correlations with alkyl protons (~2 ppm). The ^{1}H spectra associated with OC_{np} (86 ppm) all contained major contributions from alkyl protons, but their proximity with O-alkyl protons was also observed, which was more pronounced for Manganika HPOA (Figure 26(f)) than Williams and Shingobee HPOA isolates (Figure 26(d, e)). The proton slices extracted at $OC_{np}O$ (108 ppm) were noisy due to their low abundance. But these carbons appeared to predominantly associate with alkyl protons in HPOA isolates from Williams and Shingobee lakes. For Manganika HPOA, the contribution from O-alkyl protons and aromatic protons was also seen. These results suggested that nonprotonated OC and OCO carbons were not present in carbohydrate environments. Both aromatic and alkyl protons contributed to the ^{1}H slices of nonprotonated aromatic C, though the relative intensities of aromatic protons varied: highest for Manganika HPOA, intermediate for Shingobee HPOA, and lowest for Williams HPOA. The ^{1}H slices extracted at ketone C for all HPOA isolates demonstrated that these carbons were mainly

associated with alkyl protons. The proton spectra of aromatic C-O and OCH_3 were also extracted for Manganika HPOA; that of aromatic C-O showed contributions from aromatic protons, O-alkyl (~3.5 ppm) and alkyl protons, while that of OCH_3 showed correlations predominantly with O-alkyl protons at ~3.5 ppm and with aromatic protons. These correlations were consistent with the presence of lignin residues.

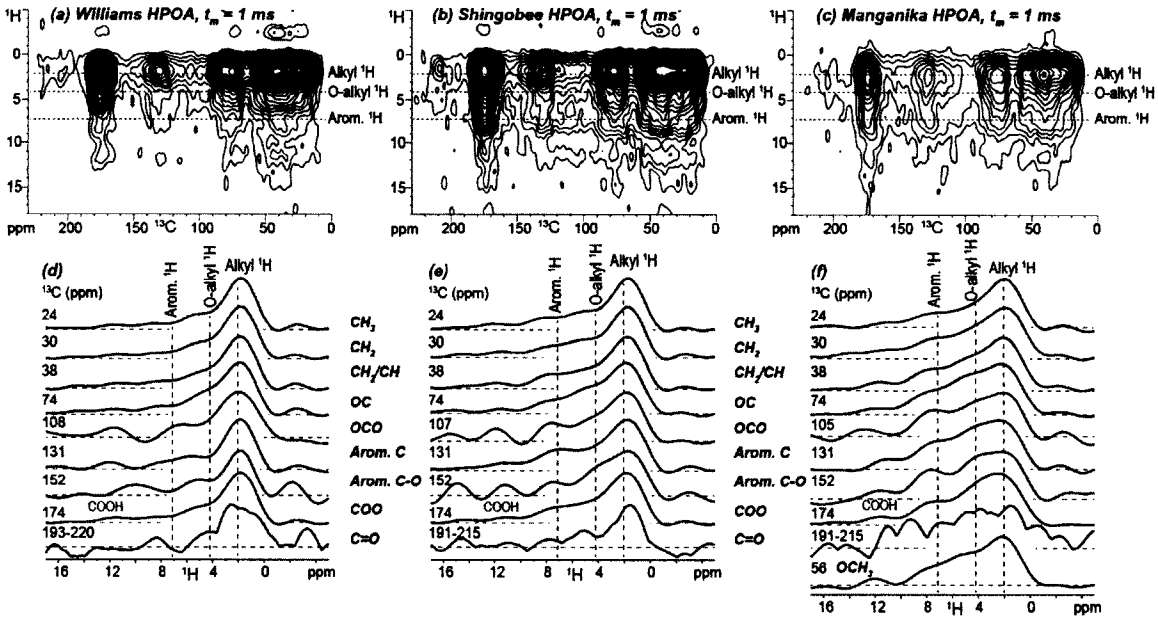

Figure 25. 2D ^{1}H-^{13}C HETCOR spectra with 0.5-ms HH-CP and 1-ms mixing time of HPOA isolates from (a) Williams Lake, (b) Shingobee Lake, and (c) Manganika Lake. ^{1}H slices extracted from the 2D spectra: (d) refers to ^{1}H slices of spectrum (a), (e) to spectrum (b), and (f) to spectrum (c).

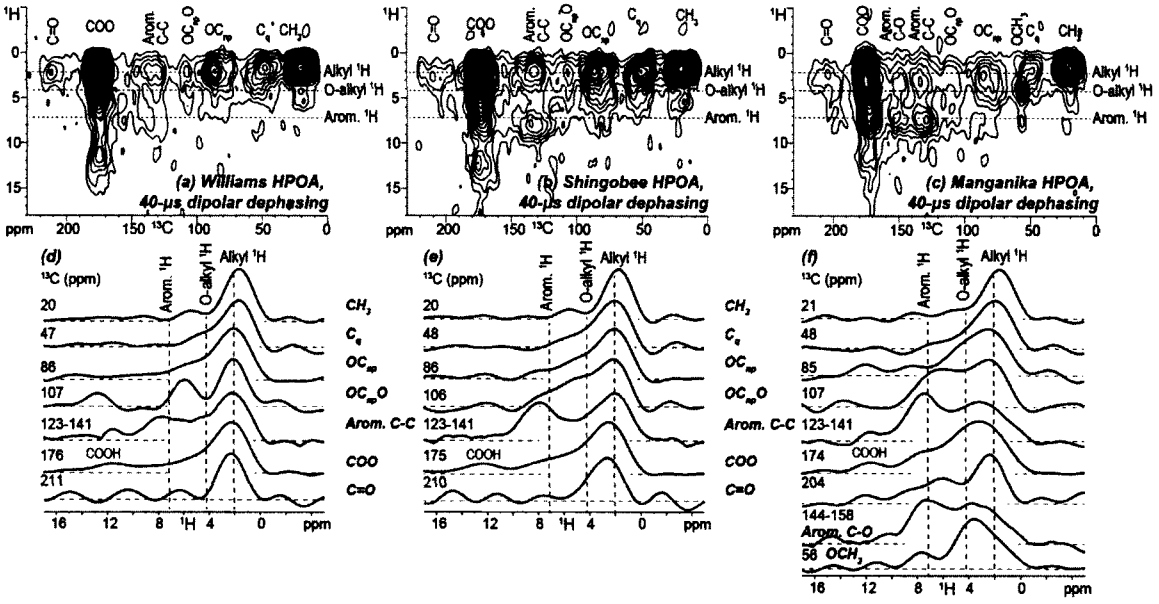

Figure 26. 2D ^{1}H-^{13}C HETCOR spectrum with 0.5-ms HH-CP and 40-μs dipolar dephasing of HPOA isolates from (a) Williams Lake, (b) Shingobee Lake, and (c) Manganika Lake. ^{1}H slices extracted from the 2D spectra: (d) refers to ^{1}H slices of spectrum (a), (e) to spectrum (b), and (f) to spectrum (c).

TPIA isolates. The 2D HETCOR spectra of TPIA isolates from Williams Lake, Shingobee Lake, and Manganika Lake are presented in Figure 27(a-c), with their corresponding proton slices extracted at different ^{13}C chemical shifts shown in Figure 27(d-f), respectively. These 2D spectra shared strong cross peaks of alkyl (CH_3, CH_2, and CH) and OC carbons with their directly attached protons (i.e., alkyl and O-alkyl protons, respectively). In addition, the cross peaks of protonated anomeric C (OCHO) were evident in all the spectra. The cross peaks of aromatic C were generally weak in all spectra. The ^{1}H spectra associated with aromatic C showed contributions from both

aromatic and non-aromatic protons, with that of Manganika TPIA containing relatively more resonances from aromatic protons than those of Shingobee TPIA, and Williams TPIA. The ^{1}H slices extracted at COO (174 ppm) all showed a major band centered at 2-3 ppm and correlations with O-alkyl protons, suggesting that COO groups were mostly attached to alkyl and O-alkyl carbons. The cross peaks of COO carbons with acidic COOH protons (~12 ppm) prominent in all spectra further supported that these COO groups were more likely present in carboxyls rather than esters. The ^{1}H slices of ketones were not extracted due to the low signal-to-noise ratio.

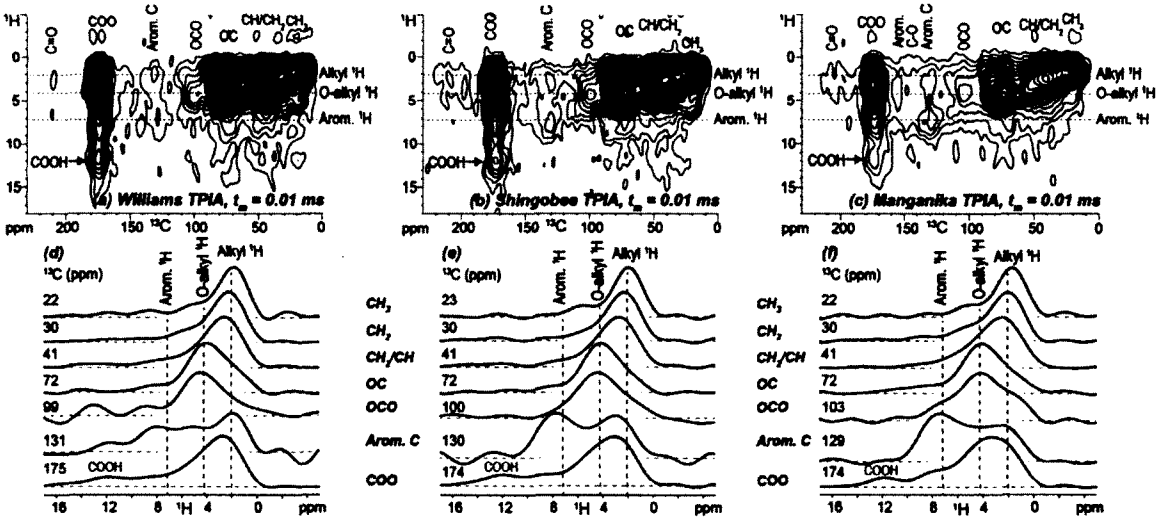

Figure 27. 2D ^{1}H-^{13}C HETCOR spectra with 0.5-ms HH-CP of TPIA isolates from (a) Williams Lake, (b) Shingobee Lake, and (c) Manganika Lake. ^{1}H slices extracted from the 2D spectra: (d) refers to ^{1}H slices of spectrum (a), (e) to spectrum (b), and (f) to spectrum (c).

The 2D HETCOR spectra with 1-ms spin diffusion time of all TPIA isolates are shown in Figure 28. For all TPIA isolates, the proton slices extracted at alkyl (CH_3, CH_2, CH) and COO carbons showed that these C sites remained associated primarily with alkyl protons. The dominant resonances in ^1H spectra associated with aromatic C were from alkyl protons. The ^1H spectra associated with O-alkyl C for all TPIA isolates showed increasing resonances from alkyl protons, which became the dominant band in the ^1H spectra for Williams TPIA and Shingobee TPIA, compared to those spectra obtained without mixing time (Figure 27(d, e)). This indicated the proximity of alkyl and O-alkyl components. Similarly, increasing contributions from alkyl protons were also seen for the ^1H slices extracted at OCO (~100 ppm), but to a greater extent for Williams TPIA and Shingobee TPIA than Manganika TPIA.

Figure 29 presents the 2D HETCOR spectra with 0.5-ms HH-CP and 40-μs dipolar dephasing of all TPIA isolates (Figure 29(a-c)) and corresponding proton slices (Figure 29(d-f)), which showed the nontrivial correlations between nonprotonated carbons and their nearby protons. For all TPIA isolates, their ^1H spectra extracted at quaternary C (C_q) indicated the proximity of C_q carbons to both alkyl and O-alkyl protons. The ^1H slices associated with OC_{np} (~86 ppm) all showed major contributions from alkyl protons, but their proximity with O-alkyl protons was also observed. The $OC_{np}O$ carbons appeared to correlate primarily with alkyl protons in TPIA isolates from Williams and Shingobee lakes. For Manganika TPIA, the contribution from O-alkyl protons was equally, if not more, important. The ^1H slices of nonprotonated aromatic C contained resonances from both aromatic and non-aromatic protons. Aromatic proton resonances contributed relatively more to the ^1H spectrum for Manganika TPIA than for Shingobee

TPIA, and Williams TPIA. The ^{1}H slices extracted at ketone C for all TPIA isolates demonstrated that these carbons were attached to alkyl protons.

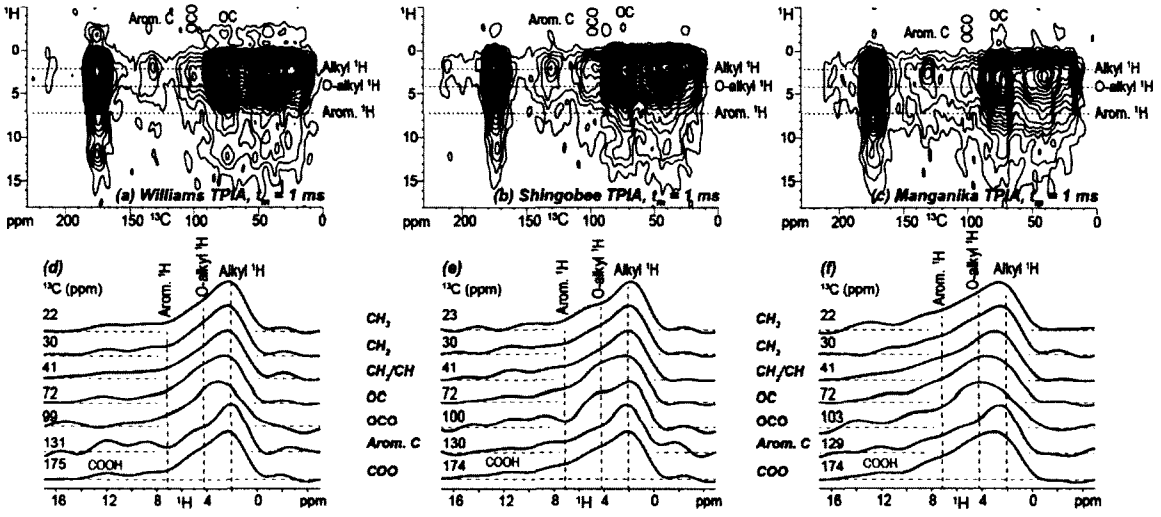

Figure 28. 2D ^{1}H-^{13}C HETCOR spectra with 0.5-ms HH-CP and 1-ms mixing time of TPIA isolates from (a) Williams Lake, (b) Shingobee Lake, and (c) Manganika Lake. ^{1}H slices extracted from the 2D spectra: (d) refers to ^{1}H slices of spectrum (a), (e) to spectrum (b), and (f) to spectrum (c).

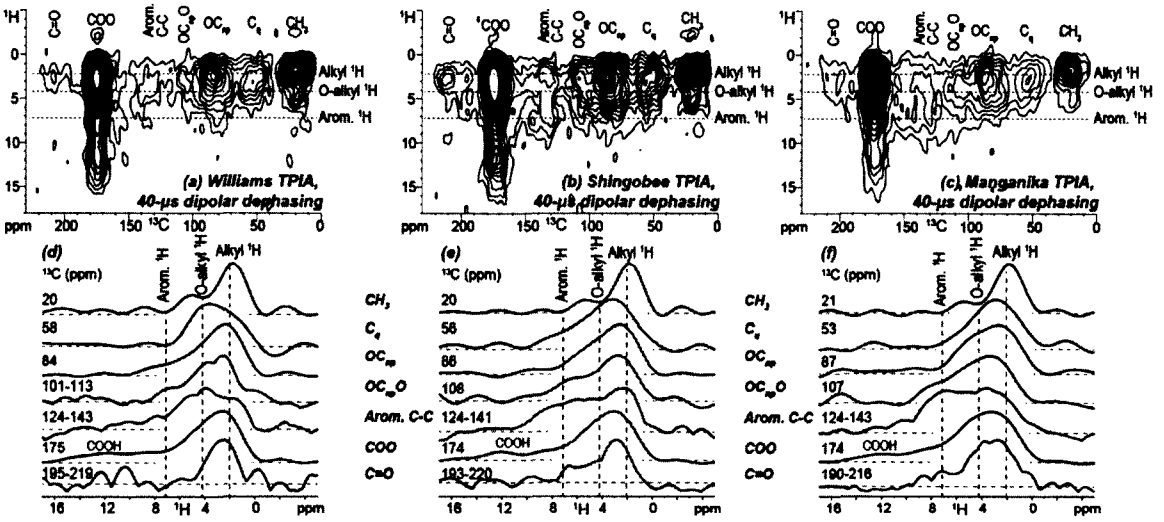

Figure 29. 2D ^{1}H-^{13}C HETCOR spectrum with 0.5-ms HH-CP and 40-μs dipolar dephasing of TPIA isolates from (a) Williams Lake, (b) Shingobee Lake, and (c) Manganika Lake. ^{1}H slices extracted from the 2D spectra: (d) refers to ^{1}H slices of spectrum (a), (e) to spectrum (b), and (f) to spectrum (c).

DISCUSSION

Major Structural Components of DOM in Lakes. The structural components present in two major DOM fractions (HPOA and TPIA) isolated from three lakes as revealed by ^{13}C 1D and ^{1}H-^{13}C 2D NMR both included COO-bonded alkyl/O-alkyls, aromatic compounds, and O-alkyl structures indicative of carbohydrate-like materials, though of varying abundances in respective HPOA and TPIA isolates. HPOA isolates were more enriched in aromatic compounds but depleted in carbohydrate-like materials than corresponding TPIA isolates. This is consistent with the lower H/C and O/C atomic values of HPOA isolates relative to respective TPIA isolates, and NMR measurements on

DOM isolates from rivers and groundwaters (Aiken et al., 1992). The higher aromatic signature of HPOA isolates also agreed with previous findings that ~90% of the lignin phenols were recovered in the HPOA fractions (Spencer et al., 2010; Spencer et al., 2008).

Though O-alkyl carbons (OC and OCO) accounted for ~20% and ~28% of C in HPOA and TPIA isolates respectively, approximately 1/3 to 1/2 of them occurred as nonprotonated forms, not normally seen in carbohydrates. The 2D NMR further revealed their proximity to alkyl protons (Figures 26 and 29), suggesting that they were unlikely present in carbohydrate environment. Nonprotonated O-alkyl carbons have been proposed as a potential index of humification (Mao et al., 2012b), as humification leads to greater substitution, branching, and cross-linking of C structures. The abundance of these nonprotonated O-alkyl C in both HPOA (8-9%) and TPIA (11-12%) isolates suggested that they could be subject to similar humification. The remaining protonated O-alkyl C (OCH_n + OCHO) may not be completely associated with carbohydrates as well, due to the very low abundance of protonated anomeric C (~1% in both HPOA and TPIA isolates), and proximity between O-alkyl carbons and alkyl protons (Figures 23, 24, 27 and 28). This is not surprising because, unlike ultrafiltration which recovers a carbohydrate-rich ultrafiltered DOM (UDOM) or high-molecular-weight (HMW) DOM, XAD isolation with XAD-8 resins (HPOA fraction) does not normally retain HMW carbohydrates. Though the occurrence of carbohydrates in TPIA fraction was more likely, our data suggested that carbohydrates were a very minor component in TPIA isolates.

Both HPOA and TPIA isolates contained abundant COO/NC=O (17-18% and 20-21% of all C, respectively), with NC=O contributing at most 2-3%, and 4-5%, and therefore COO accounted for ~15% and ~16% of all C in HPOA and TPIA isolates,

respectively. The 2D NMR data confirmed the presence of COOH and suggested the insignificant presence of ester groups. In addition, COO groups were found to be closely associated with alkyl protons resonating at ~2-3 ppm, typically assigned to carboxyl-rich alicyclic materials (CRAM) in proton spectra (Hertkorn et al., 2006; Hertkorn et al., 2013). Alkyl C (0-64 ppm) accounted for 34-47% and 33-41% of all C in HPOA and TPIA isolates, after subtracting potential NCH contributions. If we regard the alkyl C and COO substructures as characteristic of CRAM, its C-based relative percentages in HPOA and TPIA isolates were 48-62% and 48-56%, respectively. This estimation is not optimal as it is realized that some alkyl C such as CH_3 may not, yet some O-alkyl C (OC_{np} and $OC_{np}O$ in particular), can be associated with CRAM. Our results, however, are not directly comparable to reported estimates of CRAM contribution to DOM in previous studies where different DOM fractions were investigated and various estimation protocols existed (Hertkorn et al., 2006; Hertkorn et al., 2013; Woods et al., 2011; Zigah et al., 2014). Overall, CRAM represented a more important component in DOM isolated by solid phase extraction with XAD resins or PPL resins (Hertkorn et al., 2013) or diethylaminoethyl-cellulose (Woods et al., 2011) than in ultrafiltered DOM (Hertkorn et al., 2006; Zigah et al., 2014).

Effects of Hydrology on DOM Structure in Lakes. Recently published studies have explored chemical composition of DOM from hundreds of lakes distributed across a wide range of land-use, hydrology, and climate gradients in Sweden using fluorescence spectroscopy (Kothawala et al., 2014) and Fourier transform ion cyclotron resonance mass spectrometry (FT-ICR MS) (Kellerman et al., 2014). Characterization of DOM

from lakes in a small headwaters watershed in Minnesota, United States, at more localized scales in the present work enables us to decipher the importance of lake hydrological setting in driving DOM chemical composition.

DOM in the closed lake (Williams) was more aliphatic and less aromatic than DOM in the open lake (Shingobee). This is consistent with independent UV-absorbance measurements which showed that DOM in Shingobee Lake was associated with much higher $SUVA_{254}$ values, and previous observations (Aiken et al., 1997). DOM from Manganika Lake, a more humic lake, was more enriched in aromatics and had even higher $SUVA_{254}$ values. These aromatics were at least partially derived from lignin residues based on 1D ^{13}C and 2D ^{1}H-^{13}C NMR data of Manganika HPOA which demonstrated characteristic peaks of lignin (OCH_3 and aromatic C-O) (Figure 22(c, c1)), and linkages of aromatic C–O–CH_3 (Figure 24(c, f)), respectively. Nevertheless these lignin signatures were not immediately evident with NMR data of HPOA from Williams Lake or Shingobee Lake. Quantitative NMR data showed that aromatic C-O and OCH_3 were less abundant in HPOA from Shingobee Lake than Manganika Lake, and further depleted in Williams Lake HPOA (Table 6). These differences can be attributed to the differences in DOM sources and in-lake processing (Aiken et al., 1997). It has been commonly assumed that DOM in Shingobee Lake and Williams Lake arises from primarily allochthonous, and primarily autochthonous sources, respectively (Aiken et al., 1997). However, the $\delta^{13}C$ values for the HPOA isolates from these two lakes (-29.1‰ for Shingobee, -26.06‰ for Williams) were indicative of terrigenous or allochthonous source contributions. Shingobee Lake HPOA was more depleted in ^{13}C by about 3‰ relative to Williams Lake HPOA, which had $\delta^{13}C$ value comparable to those reported at multiple

sites in Lake Superior (Zigah et al., 2012). Shingobee Lake receives terrestrial inputs from Shingobee River, which supplied more aromatic DOM than groundwater entering Williams Lake (Aiken et al., 1997). Manganika Lake yet receives more terrestrial inputs from the Virginia wastewater treatment plant and United Taconite mine waters. Moreover, Williams Lake has a much longer water residence time which very likely facilitates the accumulation of autochthonous DOM (Köhler et al., 2013; Kothawala et al., 2014) and increases photo-exposure (Aiken et al., 1997). For instance, Kellerman et al. (2014), by examining the distribution of DOM molecules in 120 lakes across Sweden, concluded that terrestrially derived DOM such as polyphenols, known to be sensitive to photodegradation (Helms et al., 2014; Kujawinski et al., 2004; Stubbins et al., 2010), was selectively lost with increasing residence time. Therefore, Williams Lake DOM may be more depleted in aromatics than Shingobee Lake and Manganika Lake DOM, in part due to photodegradation. Previous studies also observed the enrichment of ^{13}C in DOM after light exposure (Opsahl and Zepp, 2001; Vahatalo and Wetzel, 2008), and the $\delta^{13}C$-DOC enrichment and loss of lignin phenols during irradiation was reported to be strongly correlated (Spencer et al., 2009b). These observations could account for the ^{13}C enrichment of Williams Lake HPOA relative to Shingobee Lake HPOA. Surprisingly, ^{14}C analyses indicated that Williams Lake HPOA which receives groundwater input was younger in age than Shingobee Lake HPOA (modern vs. 315 ybp). While Williams Lake receives groundwater discharge from flowpaths that are approximately 1 km long, Shingobee Lake also receives groundwater discharge from a mix of flowpath lengths, with some of those flowpaths being ~5 or ~10 km long (Donald Rosenberry, personal

communication, September 22, 2014). Therefore, the older ^{14}C age associated with Shingobee Lake HPOA is likely due to deeper groundwater contributions.

On the other hand, the enrichment of aliphatic components in DOM from Williams Lake, relative to that from Shingobee Lake and Manganika Lake, could be attributed to the in-lake production of aliphatic compounds (Gonsior et al., 2009; Köhler et al., 2013; Stubbins et al., 2010), or an indirect consequence of the depletion of aromatic components. Though NMR data presented here cannot evaluate the relative importance of these two effects, they provided information on the identity of these aliphatic moieties, which were found to be mainly associated with CRAM. Estimation of CRAM indicated that they were more enriched in Williams Lake (62% of HPOA and 48% of TPIA) than in Shingobee Lake (55% of HPOA and 52% of TPIA), and in Manganika Lake (48% of HPOA and 48% of TPIA). CRAM have also been identified in DOM from several other lakes (Lam et al., 2007; McCaul et al., 2011; Zigah et al., 2014). Their alicyclic and highly branched structures confer their resistance to both biodegradation and photodegradation (Hertkorn et al., 2006; Leenheer, 1994); therefore CRAM can persist in DOM from lakes with longer water residence times. Though an FT-ICR MS study indicated that CRAM were also highly photo-labile, they were not as photoreactive as aromatic compounds (Stubbins et al., 2010). Furthermore, as the authors readily admitted, the MS peaks assigned as CRAM might contain both aromatic and CRAM isomers.

Abundances of O-alkyl carbons indicative of carbohydrate-like materials stayed rather constant among different lakes. As previously described, a small fraction of them can be actually attributed to carbohydrates. Note that carbohydrates appeared to

contribute relatively more to DOM from Lake Manganika (primarily in its TPIA fraction) than to DOM from other lakes as suggested by the more evident O-alkyl carbon and proton correlations from 2D data (Figures 27 and 28). The nonprotonated O-alkyl carbon fractions, which represented more humified components than carbohydrates, were distributed rather evenly among three lakes. Their abundance further suggests their resistance to photolysis and other degradation processes.

Lake hydrological settings influence the DOM source inputs and its in-lake processing (Aiken et al., 1997), which leads to the differences observed in DOC structure among the three lakes, such as the diminished terrestrial detritus (i.e., lignin residues) signatures from Lake Manganika to Shingobee and Williams. This agrees with previous findings that terrestrially derived DOM (i.e., polyphenols and other highly unsaturated compounds) was selectively and preferentially lost with increasing lake water residence time (Kellerman et al., 2014; Köhler et al., 2013; Kothawala et al., 2014). DOM from Lake Manganika also contained relatively more contribution from carbohydrates than from other lakes. Despite these differences, our results have revealed the structural similarity of DOC among three lakes such as the occurrence of CRAM as the major component, and prevalence of humified nonprotonated O-alkyl components. This is consistent with the identification of CRAM in several lakes (Lam et al., 2007; McCaul et al., 2011; Zigah et al., 2014). Our results also agree with the observations of Jaffé et al. (2012) that ultrafiltered DOM in headwater streams from six different biomes in North America shared clear similarities in the chemical and molecular characteristics, and those of Kellerman et al. (2014) which indicated the presence of an abundant core of reoccurring molecules in DOM from most lakes over a large spatial scale.

CHAPTER V

UBIQUITY OF CARBOXYL-RICH ALICYCLIC MOLECULES IN DISSOLVED ORGANIC MATTER FROM VARIOUS SOURCES

INTRODUCTION

Major efforts have been undertaken in the past decade for a molecular-level understanding of chemistry of dissolved organic matter (DOM), an exceedingly complex and heterogeneous continuum of freshly released to highly degraded/altered biomolecules with different solubilities and reactivities. This continued and growing interest in DOM research is justified not only because DOM is a quantitatively and functionally important component, but also for its informational richness (Hedges, 2002). Thousands of diverse organic molecules present in DOM pool carry the signatures of their origins and diagenetic alterations that have occurred during transport (Hedges, 2002; Mopper et al., 2007). A number of advanced analytical techniques, among which two most influential spectroscopic methods—nuclear magnetic resonance (NMR) spectroscopy and Fourier transform ion cyclotron resonance mass spectrometry (FT-ICR MS), have been applied to read these molecular messages and provided exciting new insights into DOM composition.

Arguably, one of the most important contributions was the identification of a major refractory component of oceanic ultrafiltered DOM (UDOM, cutoff 1 kDa), termed carboxyl-rich alicyclic molecules (CRAM) (Hertkorn et al., 2006), based on evidence from multidimensional NMR and FT-ICR MS analyses. CRAM comprise a set of carboxylated and fused alicyclic structures with a carboxyl-C to aliphatic-C ratio of 1:2 to

1:7 (Hertkorn et al., 2006), and are structurally more heterogeneous than other biopolymers such as carbohydrates and peptides. NMR data provided strong evidence for the presence of carboxylic acids and aliphatic branching, while FT-ICR MS revealed a substantial degree of unsaturation in excess of carboxyl groups pointing to the alicyclic nature (Hertkorn et al., 2006). Lam et al. (2007) demonstrated similar key features arising from CRAM in $^{1}H/^{13}C$ NMR spectra of DOM extracted by diethylaminoethyl (DEAE)-cellulose resin from Lake Ontario and defined a second aliphatic fraction, material derived from linear terpenoids. The concept of CRAM thereafter widely appeared in DOM literature. The identification of CRAM in subsequent studies mostly relies on the application of NMR spectroscopy or FT-ICR MS. For instance, CRAM are associated with the ^{13}C NMR resonances (C<u>C</u>H 0-47 ppm and <u>C</u>OX 167-187 ppm) or ^{1}H NMR regions (~1.9-2.7 ppm) (Hertkorn et al., 2006; Hertkorn et al., 2013; Woods et al., 2010; Zigah et al., 2014). In terms of FT-ICR MS, CRAM tend to occupy a certain, however restricted area (double bond equivalence (DBE)/C = 0.30–0.68, DBE/H = 0.20–0.95, and DBE/O = 0.77–1.75) within the van Krevelen diagram (Hertkorn et al., 2006; Stubbins et al., 2010). The CRAM can be hugely abundant, making up ~8% of marine DOC (Hertkorn et al., 2006), ~50% of marine DOC extracted using PPL (a styrene divinyl copolymer) resins (Hertkorn et al., 2013), and 16-25% of ultrafiltered DOC in Lake Superior (Zigah et al., 2014), or likely accounting for more than 40% of DOC isolated by DEAE-cellulose resins in freshwater estimated by solution-state ^{1}H NMR analyses (Mitchell et al., 2013; Woods et al., 2011).

At present it remains unclear as to the sources of CRAM. Most likely CRAM originate from cyclic terpenoids such as steroids and hopanoids that have undergone

carboxylation either biologically or chemically (Hertkorn et al., 2006; Lam et al., 2007; Leenheer, 2009; Leenheer et al., 2003). For instance, hopane products diagnostic of bacteriohopanepolyols were found in the microscale sealed vessel pyrolysate of DOM from the Great Salt Lake by gas chromatography–mass spectrometry (Greenwood et al., 2006). Woods et al. (2012) detected oxidized sterol- and hopanoid-like structures similar to cholic acid in DOM by two dimensional hydrophilic interaction chromatography combined with multidimensional NMR spectroscopy. CRAM with branched- and condensed alicyclic-ring structures are among the most resistant structures to biodegradation, but even these structures can degrade biologically or photochemically (Leenheer, 2009; Stubbins et al., 2010).

The objective of this study is to prove the ubiquity of CRAM in aquatic systems using solid-state NMR spectroscopy coupled with FT-ICR mass spectrometry. There are several motivations for our study. First, since Hertkorn's pioneering work (Hertkorn et al., 2006; Hertkorn et al., 2013), assignment and estimates of CRAM in most subsequent studies are solely based on one-dimensional $^{1}H/^{13}C$ NMR or FT-ICR MS, which does not suffice the differentiation of CRAM from other components. For instance, the proton chemical shifts assigned to CRAM (1.6-3.2 ppm) also contain resonances from acetyl and peptide aliphatics (Hertkorn et al., 2006). CRAM also cluster within a similar section of the van Krevelen diagram as poly phenolic or lignin-like or tannin-like compounds (Sleighter and Hatcher, 2008). Second, previous detailed investigations of CRAM have only focused on DOM samples from single aquatic environment (mostly ocean waters). It would be of interest to examine the presence of CRAM in DOM isolated from diverse aquatic environments representing different sources (autochthonous and allochthonous).

Third, most detailed investigations have been made on the ultrafiltered DOM (Hertkorn et al., 2006), which is known to be carbohydrate-rich (accounting for > 50% of ultrafiltered DOC). A recent study has focused on DOM samples obtained by solid phase extraction (SPE) using PPL resins, from only ocean waters though (Hertkorn et al., 2013). The present study selects samples extracted by SPE using XAD-8 resins. Because XAD resins preferentially bind more hydrophobic material, large polysaccharides are not well retained while CRAM-like structures, upon sample acidification, should be retained well by hydrophobic phases (Minor et al., 2014). Fourth, previously proposed models of CRAM neglected abundant C-O signals. While in our preliminary study, we found the presence of significant alkyl C-O segments associated with CRAM, but not related to carbohydrates. Therefore, the present study attempted a more comprehensive model of CRAM based on NMR and FT-ICR MS.

MATERIALS AND METHODS

Description of DOM Isolates and Elemental Analyses. DOM samples were isolated from a wide range of aquatic environments (Table 7) by using Amerlite XAD resins according to Aiken et al. (1992). Briefly, large volume water samples passed through Gelman AquaPrep 600 capsule filters (0.45 μm) were acidified to pH 2 with hydrochloric acid (HCl) and passed through an XAD-8 resin column. The hydrophobic acid (HPOA) fraction, which contained both humic acid (HA) and fulvic acid (FA), was retained on the XAD-8 column, and back eluted with 0.1 N sodium hydroxide (NaOH). The eluate was desalted and hydrogen saturated using cation exchange resin, lyophilized, and stored in a desiccator. For some samples, the HPOA fraction was further separated

into FA and HA by acidifying the XAD-8 eluate to pH <1 using HCl. The supernatant containing FA was then desalted, hydrogen saturated, lyophilized, and stored in a desiccator. The FA fraction generally accounts for 90–95% of the HPOA fraction.

The XAD isolates (HPOA/FA) were distributed between three broad types of aquatic DOM (depending on the dominant DOM source) as autochthonous DOM (AU; in situ microbial sources, including algae and bacteria), allochthonous DOM (AL; higher plant and soil derived), and a mixture of both (M; Table 7). The predominantly allochthonous samples were from streams and rivers in the United States where terrestrial plant and soil OM were the dominant precursor sources, including the Penobscot River (at Eddington, Maine), two sites from the St. Louis River Watershed in Minnesota (West Swan River and Long Lake Creek), and blackwater-dominated rivers from the Yukon River Basin, Alaska (Koyakuk River and Forty Mile River). The predominantly autochthonous-derived samples included the Lake Fryxell (an ice bound Antarctic lake) FA from 9-m depth (Aiken et al., 1996; McKnight et al., 1991), and the Pacific Ocean FA (eastern equatorial Pacific Ocean near Hawaii from a depth of about 200 m) (Malcolm, 1990). The other samples represent mixed sources, including samples from the Water Conservation Area (WCA) 2A and 3A of the Florida Everglades, an area of subtropical wetland environment containing peat soils, cattail and saw grass vegetation, and significant microbial activity. Three ground water samples, Biscayne FA (Biscayne aquifer near Miami, Florida), Laramie-Fox Hills FA (Laramie-Fox Hills aquifer near Boulder, Colorado), and Rifle HPOA (an alluvial aquifer on Colorado River in Rifle, Colorado) were also included to cover the most diverse set of DOM samples. This study

encompassed the significant variation in both DOM quantity and quality that may be encountered in aquatic systems.

Elemental analyses (C, H, O, N, S and ash) of isolates were performed by Huffman Laboratories (Golden, Colorado) per methods described previously (Huffman and Stuber, 1985). Results of elemental analyses are given in Table 7.

Solid-State NMR Analyses. NMR experiments were performed using a Bruker Avance 400 spectrometer at 100 MHz (400 MHz ^{1}H frequency). All the experiments were run with a 4-mm double-resonance probehead. The ^{13}C chemical shifts were referenced to tetramethylsilane, using the COO resonance of glycine in the α-modification at 176.46 ppm as a secondary reference.

The multiple cross polarization/magic angle spinning (multiCP/MAS) technique (Johnson and Schmidt-Rohr, 2014) was applied at a spinning frequency of 14 kHz for acquisition of quantitative ^{13}C NMR spectra with good signal-to-noise ratios. The 90° pulse lengths were 4.3 μs for ^{1}H and 4 μs for ^{13}C. To achieve dead-time-free detection, all spectra were recorded with a Hahn echo generated by an 180° pulse with EXORCYCLE phase cycling (Bodenhausen et al., 1977) applied one rotation period (t_r) after the end of cross polarization. The ^{1}H decoupling field strength was $|\gamma B_1|/2\pi = 65$ kHz during the period of $2\ t_r = 0.14$ ms duration before the Hahn echo, and approximately 55 kHz during signal detection. The ramp for CP was implemented with 11 steps of 0.1 ms duration and a 1% amplitude increment (90 to 100%). The recycle delays were 0.35 s for all the samples except 0.5 s for Lake Fryxell FA. The duration of the repolarization period t_z in multiCP was 0.3 s for all except 0.5 s for Lake Fryxell FA. Corresponding multiCP

spectra of nonprotonated and mobile segments were obtained after 68-μs of dipolar dephasing (multiCP/DD). The number of scans averaged per spectrum was between 1536 and 5120.

To resolve the overlapping resonances of anomeric (O-C-O) and aromatic carbons in the 90-120 ppm region, the aromatic carbon signals were selectively suppressed using a three-pulse ^{13}C chemical-shift-anisotropy (CSA) filter with a CSA-filter time of 68 μs (Mao and Schmidt-Rohr, 2004b). The CSA filter was also combined with a dipolar dephasing time of 48 μs to select nonprotonated anomeric carbons. The number of scans averaged was 768-2048 per CSA-filtered spectrum, and 1536-4096 per spectrum of CSA filter coupled with dipolar dephasing.

Two dimensional (2D) ^{1}H-^{13}C heteronuclear correlation (HETCOR) NMR experiments (Mao and Schmidt-Rohr, 2006) were performed at a spinning speed of 7.5 kHz. Two kinds of CP were employed. Lee-Goldburg cross polarization (LG-CP) of 0.5 ms was used to suppress ^{1}H-^{1}H spin diffusion during polarization transfer, and the spectra show three- or less bond ^{1}H-^{13}C connectivities. Standard Hartmann-Hahn CP (HH-CP) with 0.5-ms CP time allows for some ^{1}H spin diffusion and so correlates the carbons with protons within a ~ 4 Å radius. In addition, a 40-μs dipolar dephasing delay was inserted in the LG-CP and HH-CP HETCOR to reveal ^{1}H-^{13}C proximities for nonprotonated carbons (multi-bond) and mobile groups like CH_3. The recycle delay was 0.5 s for Forty Mile River, Everglades 3AM, Rifle aquifer, and Lake Fryxell samples, and 2 s for Biscayne and Laramie-Fox Hills samples.

Table 7

Ash-free elemental compositions (% by wt) and $SUVA_{254}$ (L mg C^{-1} m^{-1}) of DOM isolates.

Site Name	Source	Sampling Date	DOM Fraction	Sample ID	% of DOC	$SUVA_{254}$ (L mg C^{-1} m^{-1})	%C	%H	%O	%N	%S	N atoms per 100 C atoms
St. Louis River	AL	06/27/2012	HPOA	SLR-HPOA	64	4.8	51.39	4.21	42.67	1.20	0.52	2.0
Long Lake Creek	AL	06/26/2012	HPOA	LLC-HPOA	60	4.7	51.11	4.10	42.94	0.98	0.86	1.6
West Swan River	AL	06/26/2012	HPOA	WSR-HPOA	53	ND	51.45	4.43	41.83	1.51	0.78	2.5
Penobscot River	AL	06/23/2008	HPOA	PR-HPOA	59	4.3	52.96	4.80	40.81	0.95	0.48	1.5
Koyakuk River	AL	06/09/2003	HPOA	KR-HPOA	52	4.4	52.03	4.83	41.81	0.93	0.40	1.5
Forty Mile River	AL	06/16/2004	HPOA	FMR-HPOA	55	4.3	ND	ND	ND	ND	ND	ND
Everglades 2AO	M	05/07/2013	HPOA	E-2AO-HPOA	49	4.2	54.28	4.42	38.28	1.99	1.04	3.1
Everglades 3AM	M	05/08/2013	HPOA	E-3AM-HPOA	43	4.2	53.41	4.41	39.19	1.88	1.10	3.0
Everglades 3AC	M	05/07/2013	HPOA	E-3AC-HPOA	45	3.4	54.69	4.80	38.26	1.58	0.67	2.5
Biscayne aquifer	M	11/1979	FA	Biscayne-FA	ND	3.9	56.68	4.24	36.20	1.80	1.08	2.7
Laramie-Fox Hills aquifer	M	08/1982	FA	LFH-FA	ND	1.9	60.12	6.04	32.76	0.47	0.60	0.7
Rifle aquifer	M	03/19/2013	HPOA	Rifle-HPOA	37	1.7	56.41	5.34	36.38	1.16	0.71	1.8
Pacific Ocean	AU	02/1986	FA	PO-FA	ND	0.72	57.49	6.10	34.53	1.48	0.39	2.2
Lake Fryxell	AU	12/1987	FA	LF-FA	22[a]	ND	55.0[a]	5.4[a]	35.3[a]	2.8[a]	1.5[a]	4.4

$SUVA_{254}$ is specific UV absorbance determined at 254 nm. AL is predominantly allochthonous, AU is predominantly autochthonous, and M is considered a mixed source. HPOA, hydrophobic acid; FA, fulvic acid. ND, not determined.

[a] Data from Aiken et al. (1996).

FT-ICR MS Analyses. Four representative samples were analyzed by FT-ICR MS with a custom-built 9.4 T FT-ICR superconducting magnet mass spectrometer at the National High Magnetic Field Laboratory (NHMFL) in Tallahassee, Florida (Kaiser et al., 2011). These samples included HPOA isolate from the Penobscot River, FA isolates from the Pacific Ocean and Lake Fryxell as references for microbially derived DOM, and Laramie-Fox Hills FA. Before analysis, samples were dissolved in 100% MeOH (HPLC grade) and further diluted to a final concentration of 250 μg/mL in methanol.

Negatively charged gaseous analyte ions were produced by electrospray ionization (ESI) prior to MS analysis. 1% (v/v) ammonium hydroxide solution (28% in methanol) was added to aid the deprotonation prior to negative-ion ESI FT-ICR MS analysis. Samples were delivered to the ionization source via a syringe pump at a rate of 500 nL/min through a 50μm i.d. fused silica microESI needle under typical ESI conditions.

Data collection was facilitated by a modular ICR data acquisition system (PREDATOR) (Blakney et al., 2011). Multiple (50-100) individual time-domain transients were co-added, half-Hanning-apodized, zero-filled, and fast Fourier transformed prior to frequency conversion to mass-to-charge ratio to obtain the final mass spectrum in absorption mode (Ledford Jr et al., 1984; Xian et al., 2010).

Spectra were internally calibrated with the use of a highly abundant homologous O_8 series which repeat by 14.01565 Da (or CH_2 units) based on the "walking calibration" (Savory et al., 2011). IUPAC mass can be converted to Kendrick mass (Kendrick mass = IUPAC mass × (14/14.01565)) to sort compounds that differ in mass by 14.01565 Da (mass of CH_2) (Kendrick, 1963). Mass spectral peaks with signal magnitude greater than

six times the baseline root-mean-square noise level were assigned elemental compositions with custom-built MIDAS Analysis software (NHMFL, Tallahassee, USA).

RESULTS

Carbon Functional Group Composition by 1D Quantitative NMR. The solid-state ^{13}C multiCP NMR spectra of representative DOM isolates of predominantly allochthonous sources, mixed sources, and predominantly autochthonous sources are shown in Figure 30. Note that spectra of the Penobscot River and Pacific Ocean samples (Figure 30(e, l)) were obtained with quantitative direct polarization (DP) technique as described in Chapter 2 and shown here for comparison only. In general, five broad peaks were present in the ^{13}C all C spectra (thin lines, Figure 30(a-l)) of all samples. They were assigned to signals from nonpolar alkyl C (0-64 ppm, also including some OCH_3/NCH), O-alkyl C (64-100 ppm), aromatic or olefinic C (100-160 ppm, also containing anomeric C), COO/NC=O (160-190 ppm), and ketone/aldehyde C (190-220 ppm). The spectra of river samples (Figure 30(a-e)) contained additional peaks arising from OCH_3 (~56 ppm) and aromatic C-O (~150 ppm) characteristic of lignin residues. These peaks were not immediately discernable in the spectra of other samples (Figure 30(f-l)), except those of the Everglades 3AM sample (Figure 30(g)). These spectra (Figure 30(f-l)) also had narrower aromatic resonances than those of river samples. In particular, the spectrum of Laramie-Fox Hills sample (LFH-FA, Figure 30(j)) contained a very sharp signal attributed to aromatic/olefinic carbons. Furthermore, the lineshapes of alkyl C resonances of Rifle-HPOA and LFH-FA (Figure 30(i, j)) were similar to those of Lake Fryxell (LF-FA) and Pacific Ocean (PO-FA) samples (Figure 30(k, l)), which contained two slightly

well-resolved peaks with maxima at ~23 ppm and ~40 ppm, in comparison to one broad peak with maximum at ~40 ppm for other samples (Figure 30(a-h)). The multiCP or DP spectra obtained after dipolar dephasing (bold lines, Figure 30(a-l)), which selected signals of nonprotonated and mobile C components, were characterized by resonances from CCH_3, quaternary C (CC_q), nonprotonated OC (OC_{np}), nonprotonated anomeric C ($OC_{np}O$), nonprotonated aromatic C-C, aromatic C-O, COO/NC=O, and ketone C. These spectra further confirmed the presence of OCH_3 and aromatic C-O signals in river samples (Figure 30(a-e)) and in Everglades 3AM sample (Figure 30(g)). The signals due to ketone/aldehyde C in the 190-220 ppm region were retained in the dipolar-dephased spectra (bold lines, Figure 30(a-k)), indicating that the carbonyls were present as ketone C in these samples.

Notice that the signal overlap of aromatic and anomeric (OCO) carbons in the 100-120 ppm region was prominent, in particular for spectra of river samples (Figure 30(a-e)). The CP/TOSS with a ^{13}C CSA filter experiments were performed to suppress signals of sp^2-hybridized C including aromatic C so that signals of anomeric C can be separated and quantified. Such spectra were demonstrated in Figure 31(a-c, bold lines) and overlay on the all C spectra (Figure 31(a-c), thin lines) to show the separation. Anomeric C signals (OCO, shaded area) that occurred in the region 100-123 ppm were observed in the spectra of samples from different sources. The combination of the CSA filter technique with dipolar dephasing (Figure 31(d-f), bold lines) further selected nonprotonated anomeric C ($OC_{np}O$, shaded area). The overlay of CSA-filtered and dipolar dephased spectra (Figure 31(d-f), bold lines) on corresponding dipolar dephased spectra (Figure 31(d-f), thin lines) demonstrated the separation of $OC_{np}O$ and

nonprotonated aromatics. Quantitative distributions of different C functional groups identified by spectral-editing techniques were compiled in Table 8 and allowed more detailed comparisons among DOM samples from different sources.

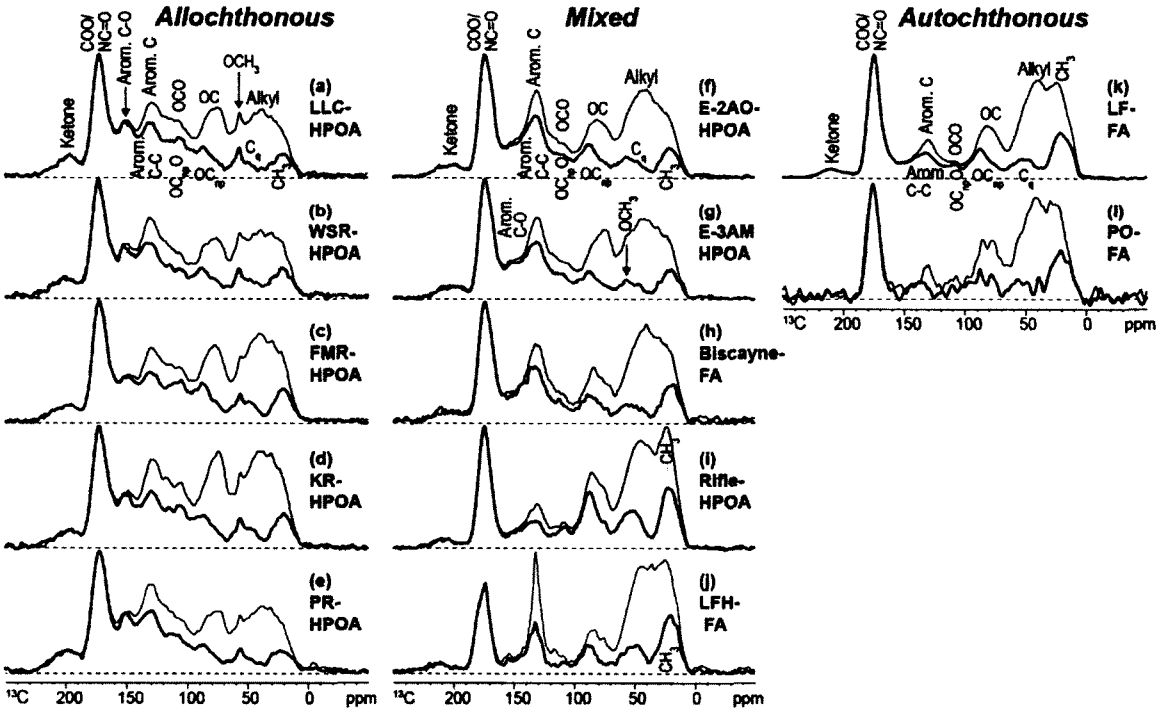

Figure 30. Solid-state ^{13}C multiCP NMR spectra (thin lines) and multiCP with dipolar dephasing (bold lines). Spectra of PR-HPOA and PO-FA were obtained by direct polarization (DP, thin lines) and DP with dipolar dephasing (bold lines). Dipolar dephasing shows primarily nonprotonated and highly mobile carbons.

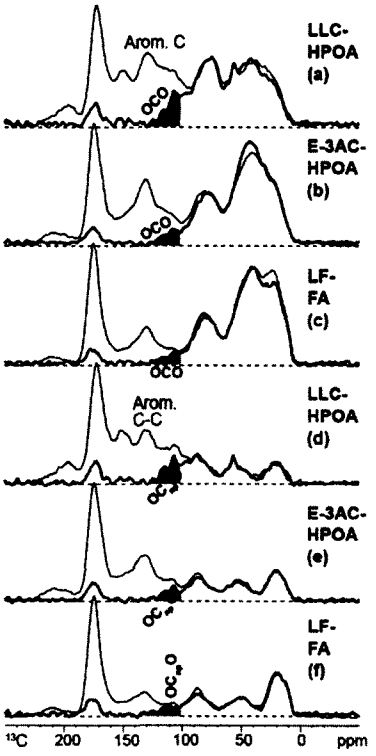

Figure 31. (a-c) Spectra of ^{13}C multiCP (thin lines), and ^{13}C CP/TOSS spectra with a ^{13}C CSA-filter (bold lines) for the separation of anomeric C (OCO, shaded area) from aromatic C. (d-f) Spectra of ^{13}C multiCP with dipolar dephasing (thin lines) and ^{13}C CP/TOSS NMR spectra with a CSA-filter and dipolar dephasing (bold lines) for the separation of nonprotonated anomeric C ($OC_{np}O$, shaded area) from nonprotonated aromatic C.

Table 8

Integrated areas (in %) from ^{13}C multiCP NMR spectra for all samples, and the assigned structural moieties associated with the spectral regions.

	Samples	ppm												
		220-190	190-160	160-143	143-100		123-100 (OCO)		100-64 (OC)		64-0 (Alkyl C)			
		Ketone C	COO/ NC=O	Arom. C-O	Arom. C-C[a]	Arom. C-H	$OC_{np}O$[b]	OCHO[b]	OC_{np}[a]	OCH_n	C_q[a]	OCH_3[a]	$CH_2/CH/NCH$	CH_3[a]
AL	LLC-HPOA	3.4	18.0	7.9	13.5	7.0	3.8	0.8	6.9	11.7	2.4	2.1	16.3	6.3
	WSR-HPOA	3.5	18.6	7.5	13.7	7.6	2.7	0.5	6.4	9.9	3.6	1.5	16.3	8.1
	PR-HPOA[c]	3.6	17.5	8.8	15.1	10.1	3.1	0.1	6.4	9.7	2.9	0.9	15.4	6.4
	FMR-HPOA	3.0	16.8	6.4	12.2	7.3	3.4	0.0	7.9	10.7	3.2	1.7	19.4	8.1
M	E-2AO-HPOA	2.7	18.2	5.5	13.6	6.5	2.3	0.0	7.3	8.5	4.0	0.0	23.2	8.2
	E-3AC-HPOA	2.9	18.5	5.0	11.5	5.8	2.2	0.0	6.7	9.1	4.2	0.0	24.9	9.4
	E-3AM-HPOA	2.5	17.9	5.9	13.1	7.1	2.1	0.2	6.1	11.6	2.0	2.4	21.2	8.1
	Biscayne-FA	2.1	18.5	5.1	12.8	6.0	1.8	0.0	6.3	7.5	3.8	0.0	25.4	10.7
	LFH-FA	1.3	13.8	2.5	7.9	8.5	1.1	0.1	5.8	5.5	6.4	0.0	29.3	17.8
	Rifle-HPOA	1.7	15.8	2.6	5.6	4.0	2.3	0.1	10.8	7.8	7.4	0.0	26.3	15.5
AU	LF-FA	2.1	19.0	3.1	6.3	3.5	2.0	0.1	7.0	8.2	4.8	0.0	29.0	14.8
	PO-FA[c]	0.0	18.1	1.8	2.9	4.0	2.0	0.4	6.5	11.6	4.8	0.0	32.0	15.8

AL is predominantly allochthonous, AU is predominantly autochthonous, and M is considered a mixed source.

[a] Based on multiCP spectrum with 68-μs dipolar dephasing; [b] Based on CSA-filtered CP/TOSS spectrum and CSA-filtered CP/TOSS spectrum with dipolar dephasing; [c] Based on DP and DP spectra with 68-μs dipolar dephasing.

The DOM isolates from rivers (AL category) with predominantly allochthonous sources had similar compositions of functional groups (Table 8). The alkyl C (0-64 ppm, also included some OCH_3 and NCH in 45-64 ppm region) accounted for 26-32% of the C in these samples. Within the alkyl C pool, CH_2/CH/NCH has the largest share, followed by methyl C and quaternary C. The OCH_3 comprised 1-2% of all C in these samples, while the fraction of NCH was estimated to be no more than ~2% based on elemental C and N contents (Table 7). The total aromatic C fractions (including protonated aromatic C-H, nonprotonated aromatic C-C, and oxygen substituted aromatic C-O; or aromaticity) ranged from 26-29% for the other three but were much higher in PR-HPOA (34%). Because the spectra of PR-HPOA were obtained by direction polarization (DP) technique instead of multiCP technique as used for the other three samples, this difference could be due to the slight enhancement of aliphatic C associated with multiCP spectra versus DP spectra as documented in Chapter III. Nonprotonated aromatic C-C dominated the aromatic C pool for all the DOM isolates in AL category, while aromatic C-H and aromatic C-O contributed less and had similar abundances. The abundances of O-alkyl C (OC + OCO) accounted for 19-23% of total C. The OCO fraction made up 3-5% of all C in DOM isolates from rivers, and the majority was present in nonprotonated form ($OC_{np}O$, 3-4%). These DOM isolates were more enriched in protonated OC (OCH_n, 10-12%) than nonprotonated OC (OC_{np}, 6-8%). The COO/NC=O constituted 17-19% of total C, with abundances of NC=O estimated to be at most 2-3% of total C (Table 7). The relative fraction of ketone C was ~3% in these samples.

The DOM isolates from Lake Fryxell (LF-FA) and Pacific Ocean (PO-FA) (AU category) with predominantly autochthonous sources showed similar distributions in C

functional groups except that PO-FA contained relatively more protonated OC and $CH/CH_2/NCH$ but less aromatics and no ketone C (Table 8). The alkyl C (0-64 ppm, also included some NCH) accounted for approximately 50% of the C in these two samples. The relative fractions of CH_3 were ~15%, which were about twice of those in samples from AL category. The aromatics were much more depleted in LF-FA (~13%) and PO-FA (~9%) compared with samples from the AL category (26-34%). The abundances of O-alkyl C (OC + OCO) were slightly lower in LF-FA than in other samples. The OCO fraction dominated by $OC_{np}O$ made up ~2% of all C in LF-FA and PO-FA. Similar to samples from the AL category, there were more protonated OC (OCH_n, ~12%) than nonprotonated OC (OC_{np}, ~6%) in the PO-FA, while the protonated and nonprotonated OC were distributed almost equally in LF-FA. In addition, the COO/NC=O constituted 18-19% of the C, with fractions of NC=O estimated to be at most ~2% for PO-FA and ~4% for LF-FA (Table 7).

The DOM isolates in M category with mixed sources can be further grouped into two subcategories based on their C functional group distributions: (i) E-2AO/E-3AC/E-3AM and Biscayne-FA, and (ii) LFH-FA and Rifle-HPOA. The dominant component in samples from Everglades and Biscayne aquifer was alkyl C (0-64 ppm), which made up 34-40% of all C. The majority of alkyl C occurred as $CH_2/CH/NCH$ (21-25% of total C), where the fraction of NCH can be at most 2-3% of all C (Table 7). The methyl C comprised 8-11%. The fractions of quaternary C comprised ~4% for other three samples, except ~2% for E-2AM-HPOA, which also contained some OCH_3 groups (~2%). The aromatics made up 22-26% of C in all the samples from Everglades and Biscayne aquifer. Relative abundances of both aromatic C-H and aromatic C-O were around 5-7%, whereas

those of aromatic C-C were much higher and ranged from 11-14%. The O-alkyl C (OC + OCO) comprised 16-20% of C in these samples. There seemed to be slightly more protonated OC than nonprotonated OC, in particular for E-3AM-HPOA. The contribution of protonated OCO was negligible. The COO/NC=O contributed to ~18% of C in these samples, where the relative abundances of NC=O cannot exceed 3% (Table 7). Ketone C constituted 2-3% of all C in these samples. In general, the ground water sample (Biscayne-FA) had very similar structures as surface water samples from Everglades (E-2AO-HPOA and E-3AC-HPOA in particular). Furthermore, these DOM samples were compositionally more similar to samples in the AL category than those in the AU category. Compared to DOM samples in the AL category, Everglades and Biscayne samples contained more alkyl C but less aromatic C and O-alkyl C.

By contrast, two other groundwater samples, LFH-FA and especially Rifle-HPOA, showed compositions resembling the DOM samples in the AU category. The differences between Rifle-HPOA and LF-FA were that Rifle-HPOA contained more OC carbons but less COO/NCO than LF-FA. Though the relative abundances of alkyl C were comparable between the two, Rifle-HPOA contained more quaternary C but less $CH/CH_2/NCH$ than LF-FA. The LFH-FA was as alkyl-rich as Rifle-HPOA and samples from AU category (LF-FA and PO-FA), but it was distinct from the other three samples in that it contained much more aromatics but much less O-alkyl C.

Proximities of Functional Groups by 2D HETCOR NMR. Two-dimensional ^{1}H-^{13}C heteronuclear correlation (2D HETCOR) spectra of DOM isolates from different sources were presented in Figures 32-35, with the extracted ^{1}H slices at different ^{13}C

chemical shifts shown below the corresponding 2D spectra to facilitate observation of the ^{1}H-^{13}C correlations.

Figure 32 shows the 2D HETCOR spectra of FMR-HPOA (Figure 32(a)), E-3AM-HPOA (Figure 32(b)) and LF-FA (Figure 32(c)) with HH-CP of 0.5 ms, showing ^{1}H-^{13}C correlations within ~ 0.5 nm radius. The 2D spectra of FMR-HPOA and E-3AM-HPOA looked similar, and showed more complex spectral patterns than that of LF-FA. The correlations of C functional groups with their directly attached or neighboring protons were better illustrated in their corresponding proton slices (Figure 32(d-f)).

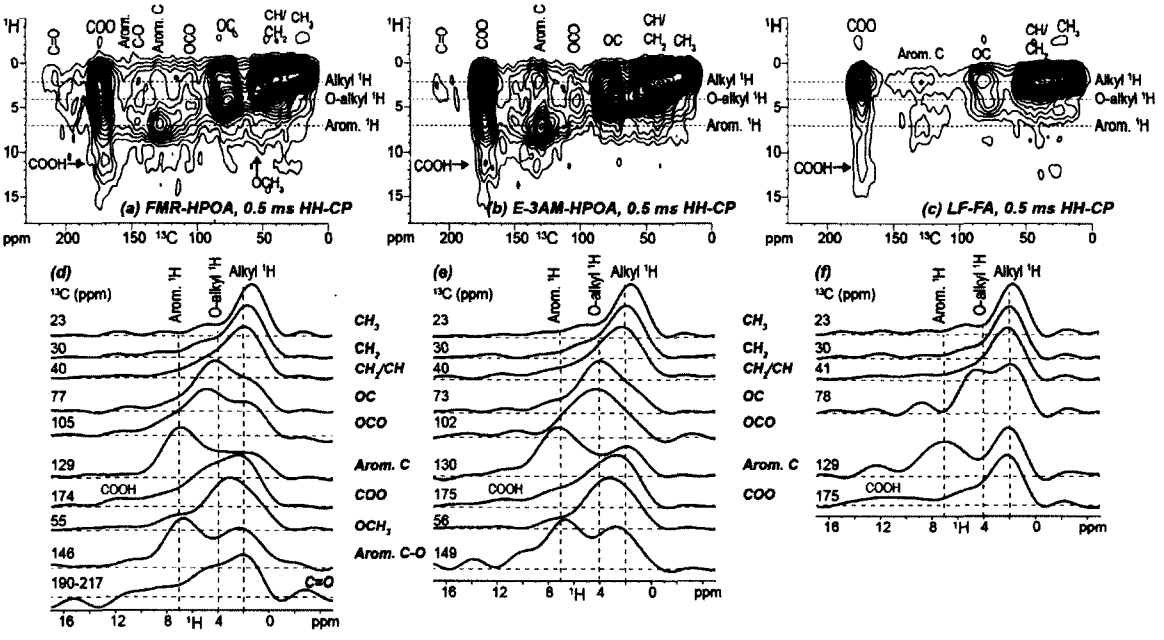

Figure 32. 2D ^{1}H-^{13}C HETCOR spectra with 0.5-ms HH-CP of samples from Forty Mile River (a), Everglades 3AM (b), and Lake Fryxell (c). ^{1}H slices extracted from the 2D spectra: (d) refers to ^{1}H slices of spectrum (a), (e) to spectrum (b), and (f) to spectrum (c).

All types of alkyl carbons (CH_3, CH_2, and CH_2/CH) were found to correlate with their own alkyl protons resonating at 1-3 ppm for all samples. The proton spectra associated with OC carbons showed some differences among three samples: the proton slices were dominated by O-alkyl protons for FMR-HPOA, and especially E-3AM-HPOA, whereas for LF-FA the proton spectrum contained approximately equal contributions from alkyl and O-alkyl protons. This likely has to do with the higher fractions of protonated OC relative to nonprotonated OC in E-3AM-HPOA and FMR-HPOA than in LF-FA (Table 8). The cross peak of OCO was visible in the 2D spectra of FMR-HPOA and E-3AM-HPOA but absent in spectrum of LF-FA. These OCO carbons were found in close proximity to O-alkyl protons for E-3AM-HPOA, and to both O-alkyl and alkyl protons for FMR-HPOA. The ^1H slices extracted at the chemical shifts of aromatic C (129/130 ppm) indicated correlations of aromatic C with both aromatic and alkyl/O-alkyl protons for all three samples (Figure 32(d-f)), indicating close association of aromatic and aliphatic components. Whereas aromatic protons contributed more than non-aromatic protons to the ^1H spectra for FMR-HPOA and E-3AM-HPOA (Figure 32(d, e)), the relative intensity of aromatic protons decreased and became comparable to or less than that of alkyl protons in corresponding ^1H spectrum for LF-FA (Figure 32(f)). For all the samples, the COO carbons showed correlations primarily with alkyl protons near 2-3 ppm, with additional contribution from O-alkyl protons, indicating that they were attached mostly to alkyl and O-alkyl carbons. The cross peaks of COO carbons with the acidic COOH protons (~12 ppm) were also prominent in the spectra of all samples (Figure 32(a-c)). In addition, the proton slices were extracted at the chemical shifts of OCH_3 and aromatic C-O for FMR-HPOA and E-3AM-HPOA. The ^1H spectra associated

with aromatic C-O indicated contributions from both aromatic and alkyl/O-alkyl protons. Those associated with OCH_3 site were dominated by O-alkyl protons resonating at 3-4 ppm, but their proximity to aromatic protons was also indicated by the shoulders at ~7 ppm (Figure 32(d, e)). Ketone C had weak and noisy cross peaks in spectra of FMR-HPOA and E-3AM-HPOA (Figure 32(a, b)), but they appeared to mainly correlate with aliphatic protons, indicating that they were attached to aliphatic carbons.

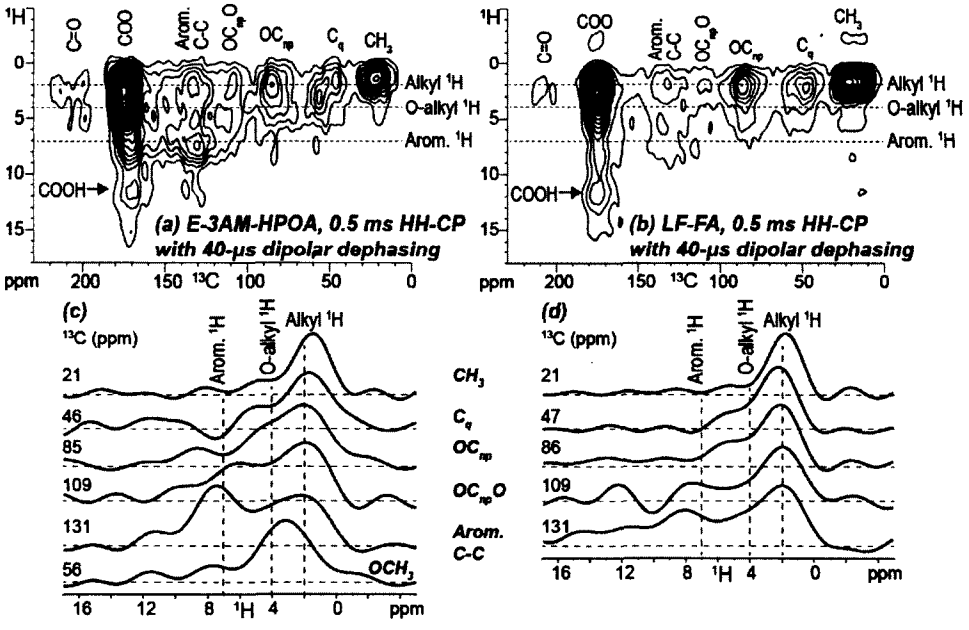

Figure 33. 2D ^{1}H-^{13}C HETCOR spectrum with 0.5-ms HH-CP and 40-μs dipolar dephasing of samples from Everglades 3AM (a) and Lake Fryxell (b). ^{1}H slices extracted from the 2D spectra: (c) refers to ^{1}H slices of spectrum (a), and (d) to spectrum (b).

The 2D HETCOR spectra with 0.5-ms HH-CP and 40-μs dipolar dephasing of E-3AM-HPOA and LF-FA were presented in Figure 33(a, b), which showed correlations of nonprotonated carbons and their neighboring protons that are separated by at least two bonds. For both samples, the ^{1}H slices extracted at C_q (46/47 ppm), OC_{np} (85/86 ppm), and $OC_{np}O$ (109 ppm) showed primarily correlations with alkyl protons (~2 ppm) (Figure 33(c, d)). The proximity of these C sites to O-alkyl protons was also indicated, and possibly more pronounced for FMR-HPOA because its proton spectra (Figure 33(c)) contained more O-alkyl proton resonances relative to those of LF-FA (Figure 33(d)). Both aromatic and alkyl protons contributed to the ^{1}H slice of nonprotonated aromatic C for E-3AM-HPOA, while alkyl protons dominated the proton spectrum for LF-FA. The 2D spectrum of E-3AM-HPOA contained an additional cross peak at ^{13}C chemical shifts of 55 ppm, likely due to the presence of OCH_3 groups.

The 2D HETCOR spectra of three groundwater samples from Biscayne, Laramie-Fox Hills, and Rifle aquifers were shown in Figure 34. The 2D spectrum and corresponding proton slices of Biscayne-FA (Figure 34(a, d)) had generally broader spectral lines than those of LFH-FA and Rifle-HPOA (Figure 34(b, c, e, f)). The proton spectra extracted at alkyl C sites (CH_3, CH_2, and CH_2/CH) were dominated by alkyl protons for all three samples. Note that spectrum of Rifle-HPOA was obtained with LG-CP, which does not allow spin diffusion, instead of HH-CP used for all other samples. Under this condition, ^{1}H-^{13}C correlations were probed at a relatively shorter length scale. This likely explained why the peak maximum of the proton spectrum associated with CH_3 appeared at a relatively lower chemical shift for Rifle-HPOA (Figure 34(f)) than Biscayne-FA and LFH-FA (Figure 34(d, e)). Though the proton spectra extracted at OC

carbons contained relatively more resonances from alkyl protons than O-alkyl protons for LFH-FA and Rifle-HPOA (Figure 34(e, f)), the corresponding proton spectrum for Biscayne-FA (Figure 34(d)) had nearly equal contributions from alkyl and O-alkyl protons. The aromatic C correlated with both aromatic and alkyl/O-alkyl protons for Biscayne-FA suggesting the close association of aliphatic and aromatic components, while aromatic proton signals dominated the ^{1}H slices for LFH-FA and Rifle-HPOA. It is worth noting that for Biscayne-FA, and LFH-FA in particular, their proton spectra (Figure 34(d, e)) contained resonances from COOH protons at ~12 ppm, indicating that some COOH can be attached to aromatic carbons. For all the samples, the COO carbons correlated primarily with alkyl protons at ~2 ppm, in addition to O-alkyl, aromatic, and COOH protons. But the O-alkyl proton signals were much more prominent in ^{1}H spectrum associated with COO for Biscayne-FA relative to LFH-FA and Rifle-HPOA.

Figure 35 presents the 2D HETCOR spectra of Biscayne-FA and LFH-FA with 0.5-ms HH-CP and 40-μs dipolar dephasing and of Rifle-HPOA with 0.5-ms LG-CP and 40-μs dipolar dephasing (Figure 35(a-c)) and corresponding proton slices (Figure 35(d-f)), which showed the nontrivial correlations between nonprotonated carbons and their nearby protons. For all the three samples, their ^{1}H spectra extracted at quaternary C (C_q) indicated the proximity of C_q carbons to alkyl protons. The ^{1}H slices associated with OC_{np} (~85 ppm) all showed major contributions from alkyl protons, but their proximity with O-alkyl protons was also observed for Biscayne-FA. The ^{1}H slices of nonprotonated aromatic C contained resonances from both aromatic and non-aromatic protons, and were quite noisy for Rifle-HPOA. Aromatic proton resonances contributed relatively more to the ^{1}H spectrum for Biscayne-FA than for LFH-FA.

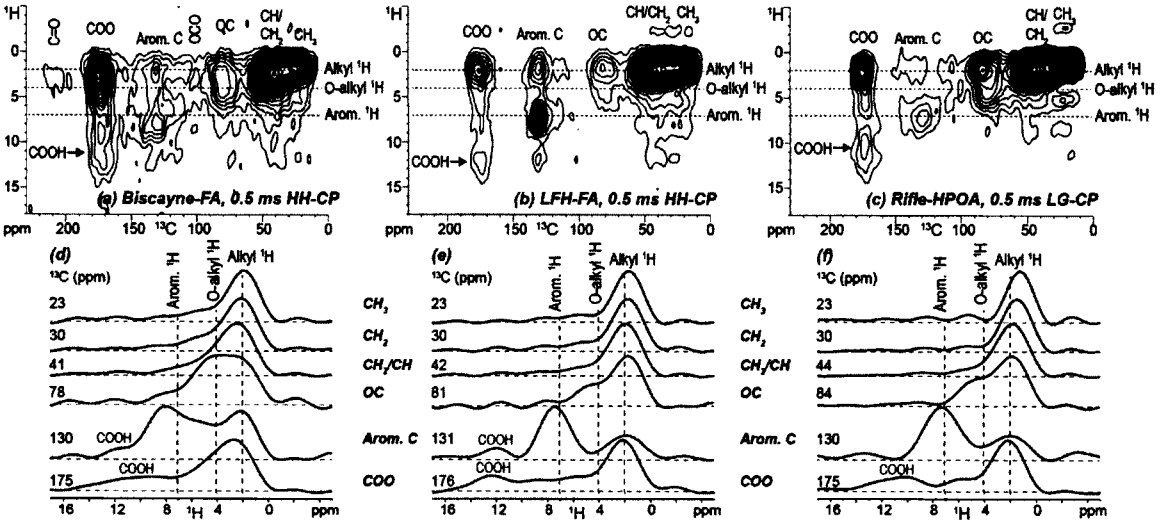

Figure 34. 2D ^{1}H-^{13}C HETCOR spectra with 0.5-ms HH-CP of samples from Biscayne aquifer (a), Laramie-Fox Hills aquifer (b), and Rifle aquifer (c). ^{1}H slices extracted from the 2D spectra: (d) refers to ^{1}H slices of spectrum (a), (e) to spectrum (b), and (f) to spectrum (c).

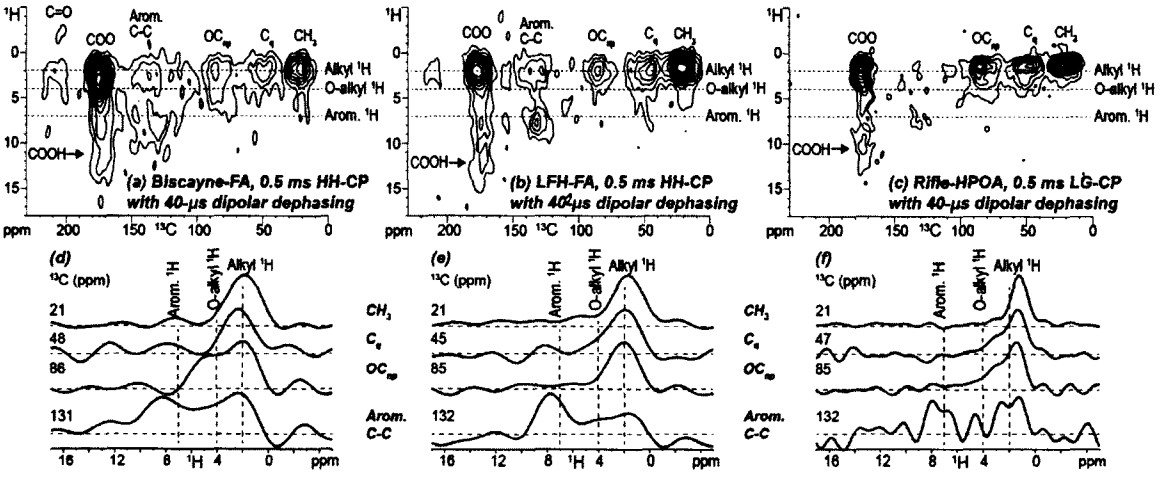

Figure 35. 2D ^{1}H-^{13}C HETCOR spectra with 0.5-ms HH-CP and 40-μs dipolar dephasing of samples from Biscayne aquifer (a), Laramie-Fox Hills aquifer (b), and Rifle aquifer (c). ^{1}H slices extracted from the 2D spectra: (d) refers to ^{1}H slices of spectrum (a), (e) to spectrum (b), and (f) to spectrum (c).

General Characteristics of FT-ICR Mass Spectra. The negative ion ESI mass spectra of four samples (PR-HPOA, PO-FA, LF-FA, and LFH-FA) are shown in Figure 36. Their mass distributions all spanned the same range ($200 < m/z < 700$), confirming the previously proposed small size of DOM molecules (Aiken and Malcolm, 1987; Simpson, 2002). Though the mass spectra of all other samples showed roughly Gaussian distributions centered around m/z 380, the LF-FA distribution was skewed somewhat toward ~m/z 320. PR-HPOA yielded the highest number of assigned mass peaks (17, 644), followed by LFH-FA (9, 859), and LF-FA (9, 837), while PO-FA had the lowest numbers of peaks (7, 861, respectively). Though this difference could be due to slightly different DOC concentration levels analyzed and varying ionization efficiencies, it might

also indicate more diversified structures associated with PR-HPOA than others, in particular PO-FA (Chen et al., 2014).

Heteroatom Class Distributions and van Krevelen Diagram Analyses. After exact elemental formulae had been assigned, compounds were grouped into heteroatom classes within a sample based on their heteroatom content. Figure 37 shows the heteroatom class distribution for species of >1% relative abundance in the ESI FT-ICR mass spectra for the four samples. Mass spectral peaks were normalized to the most abundant peak in each mass spectrum. Compounds containing 8-9 oxygen atoms (O_8 and O_9 classes) were generally the most abundant in all the samples. Those with 10 oxygen atoms (O_{10} class) were nearly equally abundant as compounds in O_8/O_9 classes for PR-HPOA and PO-FA, but less abundant than O_8/O_9 classes in LF-FA and LFH-FA. These two samples (LF-FA and LFH-FA) contained relatively more compounds in O_7 than O_{10} class. The N_1 class (molecules containing one nitrogen atom) was the only N-containing class of >1% relative abundance in all samples except LF-FA, with the N_1O_8/N_1O_9 classes being most abundant for PR-HPOA and PO-FA, and N_1O_8/N_1O_7 for LF-FA and LFH-FA. In addition, LF-FA contained some compounds with two nitrogen atoms (N_2O_7/N_2O_8 classes), consistent with its relatively higher N elemental content than other samples.

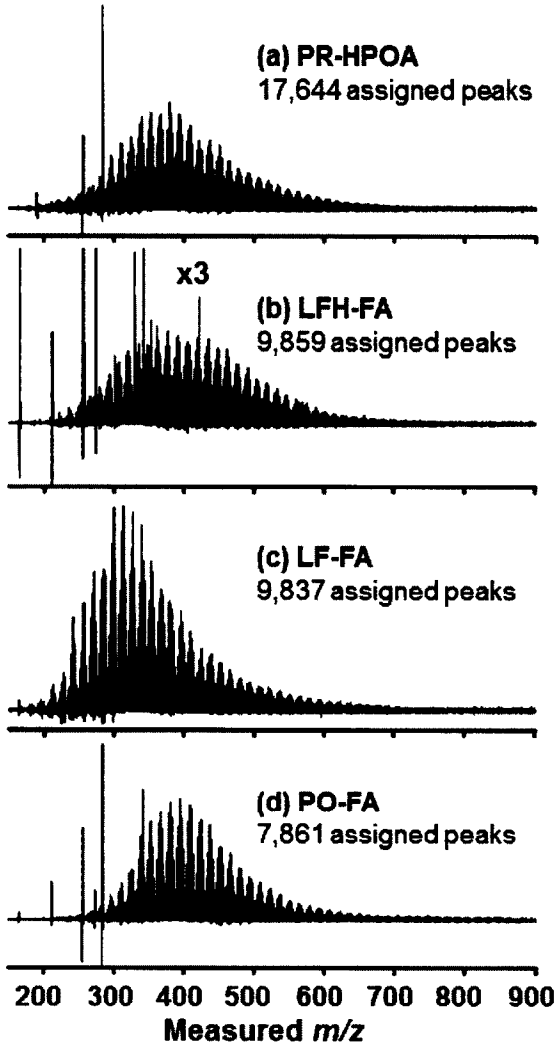

Figure 36. Ultrahigh resolution electrospray ionization Fourier transform ion cyclotron mass spectra for (a) PR-HPOA, (b) LFH-FA, (c) LF-FA, and (d) PO-FA.

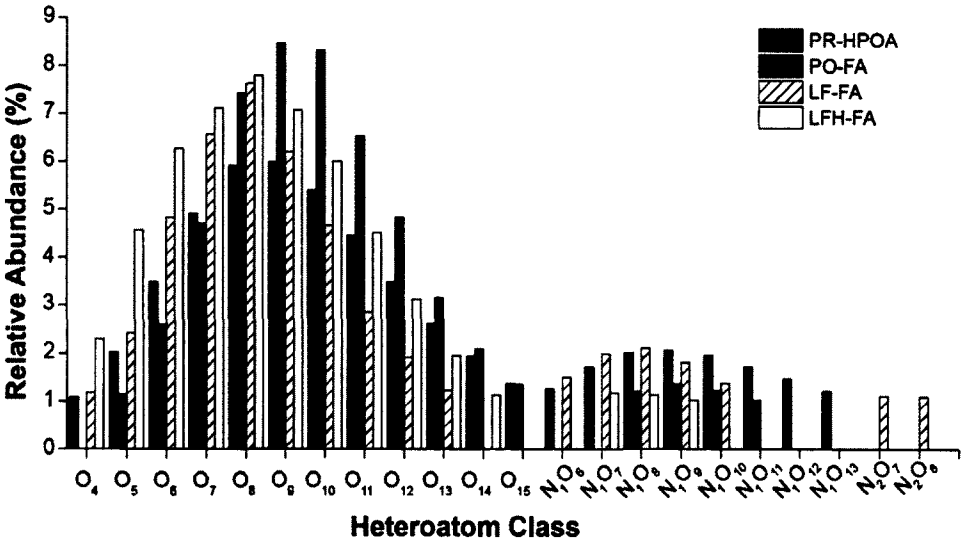

Figure 37. Heteroatom class distribution (heteroatom content) of species of > 1% relative abundance in PR-HPOA, PO-FA, LF-FA, and LFH-FA.

Molecules containing only C, H, and O represented the majority of DOM molecules and were projected on van Krevelen (vK) diagrams (Figure 38) in which atomic ratios of hydrogen to carbon are plotted on the y-axis and oxygen to carbon ratios on the x-axis (Kim et al., 2003a). The CHO formulas were further divided into groups by compound class, on the basis that each class has characteristic H/C and O/C ratios and therefore clusters within specific regions of the diagram. Double bond equivalents (DBE = double bonds + rings = 1 + C – 0.5 H) were calculated from molecular formulae to facilitate defining some of the following compound classes. They are (i) aliphatics (molecular formulas with DBE/C < 0.3 and H/C 1.0-3.0) (Perdue, 1984), (ii) carbohydrates (molecular formulas with O/C 0.7-1 and H/C 1.6-2 within the aliphatics group) (Chen et al., 2014), (iii) carboxyl-rich alicyclic molecules-like (CRAM-like) compounds (DBE/C = 0.30-0.68, DBE/H = 0.20-0.95, and DBE/O = 0.77-1.75)

(Hertkorn et al., 2006), (4) lignin-like compounds (H/C = 1.0-1.4, O/C = 0.35-0.50) (Kim et al., 2006), and (5) tannin-like compounds (H/C = 0.55-1.40, O/C = 0.60-0.95) (Sleighter and Hatcher, 2007). In areas where overlap of tannin-like and CRAM-like compounds occurred, the molecular formulas were assigned to CRAM-like rather than tannin-like. Unfortunately the overlap of CRAM-like and lignin-like cannot be handled similarly because lignins were known to be present in at least PR-HPOA (Figure 30(e), Table 8, and Chapter II). Therefore, molecular formulas that can be categorized as both CRAM-like and lignin-like are grouped into a separate class as CRAM/lignin-like. The compound classes were denoted as "-like" because different isomer structures exist solely based on elemental formulas; for instance, CRAM-like compounds likely contain both aromatic and CRAM (alicyclic) isomers (Sleighter and Hatcher, 2008), while tannin-like compounds could be high O-content aromatics/CRAM (Chen et al., 2014). Included in the vK plots were aromaticity thresholds defined by aromaticity index (AI). Formulas with an $AI > 0.5$ unambiguously contain aromatic structures, while compounds with $AI \geq 0.67$ contain condensed aromatic structures (Koch and Dittmar, 2006).

The four compound classes (aliphatics, CRAM-like only, lignin-like only, and tannin-like) were well distinguished in various regions of the vK diagrams for the four samples (Figure 38). There were nearly no CHO formulas (< 2) identified as carbohydrates in any of these four samples, likely due to a paucity of carbohydrates in these DOM samples, or their inefficient ionization in negative-mode ESI (Stubbins et al., 2010). All vK diagrams contained a region of CHO molecular formulas assigned to CRAM/lignin-like compounds (black points), though the contribution of lignin-like compounds was negligible in LFH-FA, LF-FA, and PO-FA. Notable differences were

observed among vK diagrams of different samples under the regions below the AI lines. All samples contained formulas characteristic of other aromatics (i.e., grey circles between AI > 0.5 and AI ≥ 0.67 lines) that are not lignin-like or tannin-like compounds, though much fewer such aromatics were identified in LF-FA, and PO-FA in particular, in general agreement with their lower aromatic abundances from the ^{13}C NMR data (Table 8). Condensed aromatic compounds (i.e., grey circles under AI ≥ 0.67 line) expected from black carbon were identified in PR-HPOA, further depleted in LFH-FA, and nearly absent in LF-FA and PO-FA.

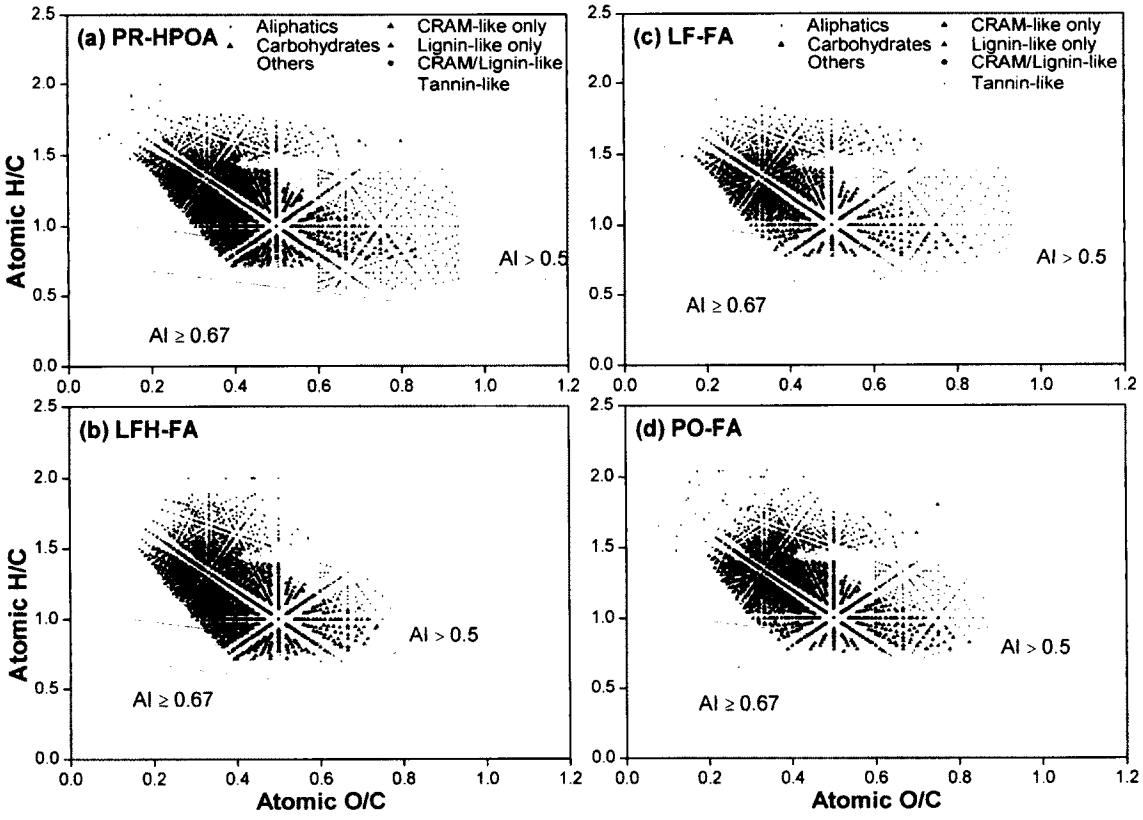

Figure 38. van Krevelen diagrams using CHO formulas for (a) PR-HPOA, (b) LFH-FA, (c) LF-FA, and (d) PO-FA.

DISCUSSION

Based on the ^{13}C 1D and ^{1}H-^{13}C 2D NMR data, carbons present in the DOM samples were distributed among the following structural components: CRAM-like, aromatic compounds, carbohydrate-like, and N-containing compounds. CRAM-like group was associated with the following functional groups listed in Table 8: $CH_3/CH_2/CH/C_q$, OC_{np}, OC_{np}/O, COO, and ketone C. Note that contributions from NCH in 0-64 ppm and NC=O in 160-190 ppm regions were estimated based on elemental C and N contents and excluded from estimation of CRAM-like group. Aromatic compound group included contributions from aromatic C-H/C-C/C-O (100-160 ppm) and OCH_3. The carbohydrate-like compound group was associated with protonated OC and OCO (i.e., OCH_n and OCHO). N-containing compounds were estimated from N elemental contents and it was assumed that each N atom was attached to two C atoms. Though the classification scheme is operational and likely an oversimplification, it has been deemed useful to define compound classes for comparison among samples. What distinguishes our work from that of others (Abdulla et al., 2010b; Zigah et al., 2014) is the fact that our classification is based on 2D NMR data which provide information on functional group connectivities. The relative abundances of these four component groups were given in Table 9. Molecular formula number-based percentages of different compound classes from FT-ICR MS analyses were shown in Table 10 for comparative purposes although we recognized that they were not quantitative.

Table 9

The relative carbon percentages of four structural components in the DOM samples based on NMR data.

	Sample	CRAM-like	Aromatic	Carbohydrate-like	N-containing
AL	LLC-HPOA	53.8	30.5	12.5	3.2
	WSR-HPOA	54.3	30.3	10.4	5.0
	PR-HPOA[a]	52.3	34.9	9.8	3.0
	FMR-HPOA	57.8	27.5	10.7	4.0[b]
M	E-2AO-HPOA	59.7	25.6	8.5	6.2
	E-3AC-HPOA	63.7	22.2	9.1	5.0
	E-3AM-HPOA	53.7	28.4	11.8	6.0
	Biscayne-FA	63.2	23.9	7.5	5.4
	LFH-FA	74.1	19.0	5.6	1.4
	Rifle-HPOA	76.3	12.2	7.8	3.6
AU	LF-FA	70.0	12.9	8.3	8.8
	PO-FA	74.8	8.7	12.0	4.4

[a] Based on DP and DP spectra with 68-μs dipolar dephasing.

[b] Estimated based on N element content of 2%.

Table 10

Fractions of different compound classes of CHO molecular formulas based on numbers of elemental formulas in PR-HPOA, LFH-FA, LF-FA, and PO-FA.

Sample	CRAM-like only	CRAM /lignin-like	Tannin -like	Lignin-like only	Other aromatics	Condensed aromatics	Carbo-hydrates	Ali-phatics	Not defined
PR-HPOA	31.7	15.5	8.8	0.6	7.7	4.3	0.1	11.4	19.9
LFH-FA	38.9	17.3	2.3	0.6	4.6	0.2	0.0	16.4	19.7
LF-FA	34.2	20.0	8.5	0.7	1.7	0.0	0.1	17.9	16.8
PO-FA	34.3	22.8	6.9	1.0	0.3	0.0	0.1	22.3	12.3

CRAM-like compounds had the highest C percentages in all the samples (Table 9). The NMR estimated CRAM-like contents were 52-58% and > 70%, respectively, of DOM isolates from AL category and AU category. The CRAM-like contents of samples from Everglades and Biscayne had intermediate values, while those of LFH-FA and Rifle-HPOA had similar or even higher CRAM-like percentages than samples from AU category. The number-based percentages of CRAM-like only formulas of the four samples showed the similar trend (Table 10), though the percentages were significantly lower. Because NMR signals associated with lignins were insignificant in the spectra of LFH-FA, LF-FA and PO-FA (Figure 30(j-l)), the CRAM/lignin-like compounds may be reasonably counted toward CRAM-like only, resulting in corrected CRAM-like only fractions of 54-57% in LFH-FA, LF-FA and PO-FA. Our estimates were comparable to those of Chen et al. (2014) on a set of oceanic DOM isolated by reverse osmosis coupled

with electro-dialysis, where CRAM-like CHO formulas represented 50-65% of CHO formulas.

Aromatic compounds represented 27-35% and 9-13% of DOM isolates from AL category and AU category, respectively (Table 9). Those Everglades and Biscayne samples had relatively lower aromatic contents than samples from AL category. Their less aromatic character could be related to their higher exposure to sunlight in Florida, USA than samples in AL category from higher latitude states such as Minnesota, Alaska and Maine. Aromatic contents of LFH-FA and Rifle-HPOA were even lower as compared to river samples, Everglades and Biscayne samples, though those of LFH-FA were considerably higher than those of Rifle-HPOA, LF-FA and PO-FA. Aromatic compounds were divided into different groups based on FT-ICR MS analyses, i.e., tannin-like, lignin-like only, other aromatics, and condensed aromatics (Table 10). These fractions were summed to yield the content of aromatic compounds, which were 21% for PR-HPOA, and 8-11% for LFH-FA, LF-FA and PO-FA. These estimates were generally consistent with NMR-based estimates. The aromatic contents can be much higher for PR-HPOA as some of CRAM/lignin-like compounds can be solely associated with lignin-like only. The percentages of tannin-like compounds were much lower in LFH-FA than in other samples, consistent with its lower O content than all other samples (Table 7). The fractions of CHO formulas associated with lignin-like only compounds were ca. 1% for all four samples, but for PR-HPOA, it was expected to be higher after including lignin contributions from CRAM/lignin-like compounds. Contributions from other aromatics to all CHO formulas were lower than 8%, decreasing in the order from PR-HPOA, to LFH-FA, LF-FA, and to PO-FA. PR-HPOA also contained some condensed aromatics (ca.

4%), which were negligible in other samples. This was expected due to the more aromatic character of PR-HPOA than other samples, in particular LF-FA and PO-FA which represented microbially derived DOM (Table 8). D'Andrilli et al. (2013) characterized the FA isolates from Antarctic Pony Lake (PL-FA) derived solely from microbial sources, and Suwannee River (SR-FA) derived from terrigenous sources, using FT-ICR MS. Surprisingly, they reported higher abundance of condensed aromatics for PL-FA than SR-FA, and attributed this observation to more extensive photochemical degradation of condensed aromatics in SR-FA vs. PL-FA. Estimates of condensed aromatics were not available based on our collected NMR data. Nonprotonated aromatics, essential in condensed aromatic structures, were more abundant in PR-HPOA than in LFH-FA, LF-FA, and PO-FA in particular (Table 8). However, not all nonprotonated aromatics were associated with condensed aromatics because 2D NMR data also showed the correlation of these nonprotonated aromatics with aliphatic components (Figure 33(c, d) and Figure 35(d-f)).

The NMR-estimated abundances of the carbohydrate-like compound showed less variation than those of other compounds among different samples, ranging from 6-12%. Most of these compounds were not expected to associate with carbohydrates due to the extremely low abundance of protonated anomeric carbons (Table 8), and the correlations observed between OC carbons with alkyl protons (Figures 32 and 34). Carbohydrates were estimated to be nearly absent in all samples from MS data (Table 10). Evidence from both NMR and FT-ICR MS indicated that carbohydrates were a negligible component though FT-ICR MS can underrepresent the contribution of carbohydrates to DOM.

The N-containing compounds were not well defined from NMR or FT-ICR MS. But they had minor contributions to these DOM isolates. N-containing compounds were most abundant in LF-FA but most depleted in LFH-FA (Table 9). These N atoms were mostly found in highly oxygenated species with 7-9 O atoms (Figure 37). In addition, FT-ICR MS data also separated an "aliphatics" component (Table 10), which accounted for 11-22% of all CHO formulas, and appeared to be more abundant in PO-FA than in other samples, especially PR-HPOA.

The following discussion mainly focused on the structural characteristics of three DOM isolates (Biscayne-FA, LFH-FA and Rifle-HPOA) from groundwater, which have received little attention. The 1D and 2D NMR data revealed that structures of Biscyane-FA resembled those of Everglades samples, while LFH-FA and Rifle-HPOA were more similar to microbially derived LF-FA and PO-FA. The Rifle-HPOA sample had similar NMR spectral characteristics as infiltrated groundwater samples (Leenheer et al., 2003). Aromatic C-O structures associated with lignins in Rifle-HPOA and LFH-FA were not as evident as in river samples or Everglades and Biscayne samples, while NMR signals from methyl and quaternary aliphatic carbons indicative of terpenoid precursor structures were prominent, consistent with previous findings (Leenheer et al., 2003). The aromatic structures in groundwater FA may therefore not arise from lignins but are produced during degradation of alicyclic rings by bacteria (Leenheer et al., 2003). For instance, abietic acid can be converted to dehydroabietic acid (one aromatic ring) and retene (three aromatic rings) during abiotic oxidative reactions in pine tar (Leenheer et al., 2003).

Previous studies on FA isolates from the Biscayne and Laramie-Fox Hills aquifers concluded that they were derived from distinct sources (Murphy, 1987; Thurman, 1985).

Biscayne is a shallow aquifer in carbonate sandstone, with recharge from the Everglades which contain humic-rich surface water (Thurman, 1985). Based on its similar elemental composition, $\delta^{13}C$ values, and Infra-red spectra to those of DOM from surface waters, Biscayne-FA was considered to originate from recharge waters which leached OM in overlying soils and transported it to the aquifer (Thurman, 1985). The NMR evidence that Biscayne-FA and Everglades samples shared similar structural characteristics supported this hypothesis.

The Laramie-Fox Hills aquifer, in contrast, is marine sand, and could have accumulated OM from marine and algal sources (Thurman, 1985). It has been proposed that FA from this aquifer was leached from kerogen in the sediment of the aquifer. Two lines of supporting evidence were provided (Murphy, 1987; Thurman, 1985). First, FA from the Laramie-Fox Hills groundwater had a more kerogen-like elemental analysis (i.e., enriched in C and H and depleted in O) and was more aliphatic than FA Biscayne aquifer. Second, it showed a ^{14}C age of 16, 980 ± 380 versus 800 ± 250 years before present (ybp) for Biscayne-FA, and appeared to contain a component of dead carbon or kerogen from the aquifer matrix (Murphy, 1987). The LFH-FA sample studied here showed a similar old age (17, 070 ± 50 ybp) as previously reported. However, the kerogen signature was not very evident in LFH-FA in terms of its C structure. Although kerogen structure in this aquifer has not been examined, kerogen from marine sources typically contains condensed aromatics (Mao et al., 2010), which were nearly absent in LFH-FA based on FT-ICR MS data (Table 10). Therefore, the contribution of kerogen to LFH-FA may be minor. Though the aromatic structures in LFH-FA were not resolved, their formation from bacterial degradation of alicyclic structures such as CRAM cannot be excluded.

In conclusion, the NMR analyses of DOM samples from vastly different environments all revealed three key features characteristic of CRAM structures: a high degree of carboxylation, presence of abundant methyl, quaternary and nonprotonated aliphatic structures, and COO bonded alkyl/O-alkyl structures. The estimates of CRAM-like contents based on NMR and FT-ICR MS data showed the same trend, i.e., CRAM-like compounds were more enriched in Lake Fryxell and Pacific Ocean samples than in river samples. The groundwater sample from the shallow Biscayne aquifer had chemical characteristics resembling river samples and Everglades samples, while the other two samples from Rifle and Laramie-Fox Hills aquifers were more similar in structures to microbially derived end members such as those from Lake Fryxell and Pacific Ocean.

CHAPTER VI

SUMMARY AND CONCLUSIONS

CONCLUSIONS AND SUMMARY OF RESEARCH

The work of this dissertation was focused upon investigating the chemical structure of dissolved organic matter (DOM) by advanced solid-state nuclear magnetic resonance (NMR) spectroscopy and Fourier transform ion cyclotron resonance mass spectrometry (FT-ICR MS) techniques, to shed light on the linkages between DOM sources and DOM composition. In particular it was of my interest to evaluate the hypotheses of the chemical homogenization of DOM relative to source material and the ubiquity of carboxyl-rich alicyclic molecules (CRAM) in DOM in aquatic environments. Unique and extensive sets of DOM samples studied here were isolated from diverse aquatic systems, including end-member environments in which DOM is considered as autochthonous and microbially derived (Pacific Ocean, and Lake Fryxell in Antarctica), or is terrestrially derived and allochthonous (Penobscot River, Forty Mile River, and West Swan River), and areas in which DOM has characteristics falling somewhere between the two end members (Shingobee Lake, Williams Lake, and Florida Everglades etc.). In addition to DOM from surface waters, representative samples isolated from groundwater systems (Biscayne aquifer, Laramie-Fox Hills aquifer, and Rifle aquifer) which have received much less attention, were also covered in this dissertation. Chapters II to IV each focused on the characterization of a set of DOM samples within the same watershed/basin environment by solid-state NMR to address additional site-related

questions, while Chapter V studied a more diverse set of DOM samples from different aquatic systems by solid-state NMR and FT-ICR MS.

The fate of terrestrial DOM in the marine waters has remained enigmatic. The chemical-structural changes of DOM samples collected from the Penobscot River, Penobscot Bay, Gulf of Maine, and the Pacific Ocean were investigated to provide insights into the role of terrestrial DOM in the marine system (Chapter II). Characteristic NMR signals of CRAM were identified in all these samples based on one-dimensional (1D) quantitative NMR and a range of spectral editing techniques, coupled with two-dimensional heteronuclear correlation (2D HETCOR) NMR. The 1D NMR analyses found carboxyl-rich, and highly branched structures such as methyl groups, quaternary alkyl, nonprotonated O-alkyl and anomeric carbons, while 2D NMR revealed COO-bonded alkyl structures consistent with CRAM. The alicyclic nature was indicated by the high chemical shift of CCH carbons (peak maximum 45-50 ppm), which according to analyses from CNMR predictor software, can have up to six β carbons and are therefore most likely present in fused cyclic systems. Moreover, a selective loss of aromatic compounds was observed throughout the sequence of riverine, coastal, and open-ocean DOM. Specifically, characteristic peaks of aromatic C-O (~150 ppm) and OCH_3 (~57 ppm) associated with lignin were distinct in Penobscot River DOM, reduced in abundances in the Penobscot Bay DOM, and further more depleted in the Gulf of Maine and Pacific Ocean samples. These results were consistent with reported trends in measured concentrations of dissolved lignin phenols from similar sites in the Penobscot River, Penobscot Bay and the Gulf of Maine (Spencer et al., 2010). Loss of aromatic structures such as isotopically "light" lignin may be attributed to photooxidation, and

likely accounted for observed changes in the carbon stable-isotope composition from riverine (-27.6‰) to ocean DOM (-23.0‰). By contrast, the absence of chromophoric structures in CRAM confers resistance to degradation by UV radiation while the alicyclic structures of CRAM are resistant to biological oxidation (Leenheer, 1994). These structural features associated with CRAM and their presence as the major structural units in DOM samples from the Penobscot River to Gulf of Maine transect and the Pacific Ocean imply that CRAM may cycle on time scales long enough to be transported into the ocean.

Arctic rivers export large quantities of DOM, approximately 10% of the global river discharge, to the Arctic Ocean. Growing evidence indicates that Arctic rivers exhibit striking seasonal patterns in water discharge, DOC concentration, chemical composition, and age. However, detailed structural information of DOM, especially across different seasons, in these rivers is currently lacking. By including samples across distinct phases of the Yukon River hydrograph (spring freshet, summer-autumn, and winter), detailed seasonal variability in chemical structure of DOM was captured by advanced 1D and 2D solid-state NMR spectroscopy, coupled with isotopic measurements and UV-visible spectroscopy (Chapter III). Two major DOM fractions including the hydrophobic organic acids (HPOA) and transphilic organic acids (TPIA) from XAD isolation were studied. They together accounted for 64-74% of DOM. The structures of HPOA and TPIA samples showed seasonal variations. HPOA isolates from the spring freshet period were characterized by greater contributions from lignin residues and carbohydrate-like materials than those from summer-autumn and winter. The NMR spectra of spring freshet TPIA samples indicated a predominance of carbohydrates in their structures, which was

much less evident in the structures of summer-autumn and winter TPIA isolates. The carboxyl-rich alicyclic molecules represented a major structural component in HPOA/TPIA samples regardless of sampling time. In terms of DOM sources, spring DOM, which was more abundant in lignin residues (within HPOA fraction) and carbohydrates (within TPIA fraction), was representative of inputs from leached plant materials and upper soil horizons, consistent with the modern age. These relatively fresh organic materials were depleted in summer-fall and winter samples, indicating that summer-fall and especially winter DOM were associated with more extensively degraded DOM and older DOM pools. All DOM samples shared relatively more refractory components such as CRAM, and nonprotonated OC and OCO pool, suggesting the refractory nature of DOM samples across different seasons.

Freshwater lakes are hotspots of carbon cycling through both organic carbon mineralization and sequestration. DOM is the largest pool of organic matter in most lakes, and its reactivity is inherently tied to its chemical composition, which is further controlled by climate, hydrology and land use variables. The DOM structures from three hydrologically distinct lakes from Minnesota, United States, were investigated to decipher the importance of lake hydrological setting in driving DOM chemical composition (Chapter IV). The hydrologically closed Williams Lake, and hydrologically open Shingobee Lake and Manganika Lake have contrasting water residence times (3-4 years for Williams, 0.3-0.5 years for Shingobee, and several months for Manganika). Both the HPOA (30-40% of DOC) and TPIA (17-22% of DOC) fractions of DOM were studied with 1D ^{13}C and 2D ^{1}H-^{13}C NMR spectroscopy. The major structural components present in HPOA and TPIA from three lakes included CRAM, aromatic compounds, and

carbohydrate-like materials. Aromatic compounds such as lignin residues and phenols were much more enriched in HPOA fractions than corresponding TPIA fractions of DOM, and their relative carbon percentages decreased from Manganika Lake HPOA/TPIA, to Shingobee Lake HPOA/TPIA, and Williams Lake HPOA/TPIA. Carbohydrate-like materials were more depleted in HPOA than TPIA fractions, and their C percentages stayed rather constant in DOC from three lakes. Among those, carbohydrates were a very minor component, and appeared to be more important in Manganika DOM than in other lakes. DOM from all lakes however contained significant amounts of nonprotonated O-alkyl C, which represented a more humified component than carbohydrate. It was estimated that CRAM accounted for 48-62% of C in HPOA and 48-56% of C in TPIA, and they appeared to be more enriched in Williams Lake relative to Shingobee Lake and Manganika Lake, respectively. The structural differences observed in DOM among the three lakes indicated the selective loss of terrestrially derived DOM (i.e., polyphenols and other highly unsaturated compounds) with increasing lake water residence time. Nevertheless, the occurrence of CRAM as the major component, and prevalence of humified nonprotonated O-alkyl component in DOM from three lakes pointed to the structural similarity of DOM in lakes, which is consistent with previous finding of an abundant core of reoccurring molecules in most lakes over a large spatial scale.

Though solid-state NMR spectroscopy allows for quantitative and comprehensive structural information of complex DOM, it remains regarded as bulk-level characterization tool, has lower sensitivity, and offers limited molecular-level information. The FT-ICR mass spectroscopy is capable of resolving thousands of molecular formulae directly out of the DOM mixture; however it has considerable

selectivity depending on sample handling and ionization method used. NMR spectroscopy coupled with FT-ICR mass spectrometry provides complementary information on molecular-level DOM composition and structure. Chapter V applied advanced NMR and FT-ICR MS spectroscopic methods to investigate the presence of CRAM in DOM from diverse aquatic environments, such as rivers receiving predominantly terrestrial sources of DOM, an Antarctic lake and open ocean with microbial sources of DOM, and understudied environments like groundwaters. The NMR analyses of these DOM samples all revealed three key features characteristic of CRAM structures: a high degree of carboxylation, presence of abundant methyl, quaternary and nonprotonated aliphatic structures, and COO bonded alkyl/O-alkyl structures. The NMR estimated CRAM-like contents were > 50% for DOM isolates with predominantly terrestrial sources, and > 70% for DOM isolates with predominantly microbial sources. Estimates based on FT-ICR MS data, though yielded relatively lower CRAM percentages than NMR estimates, showed the same trend, i.e., CRAM-like compounds were more abundant in Lake Fryxell and Pacific Ocean samples than in river samples. The groundwater sample from the shallow Biscayne aquifer had chemical characteristics resembling river samples and Everglades samples, while the other two samples from Rifle and Laramie-Fox Hills aquifers were more similar in structures to microbially derived end members such as those from Lake Fryxell and Pacific Ocean. The precursors of aromatic structures in DOM from Laramie-Fox Hills remain unresolved. The contribution of kerogen from marine sources to LFH-FA may not be as significant as previously postulated, due to the paucity of condensed aromatic structures revealed by FT-ICR MS data.

The research in my dissertation clearly revealed the ubiquity of CRAM in DOM from across different biomes, ecosystem types, and with a large range of autochthonous, allochthonous, and anthropogenic influences. Even in freshwater environments lignin residues represented a small fraction of total DOM because they have been shown to be susceptible to both photochemical and microbial degradation. Carbohydrates were also proved to be a minor component in DOM isolates, with the exception of spring DOM (TPIA isolates) from the Yukon River. Admittedly, the abundances of carbohydrates in DOM greatly depend on the isolation method used; and DOM isolates studied here were obtained with XAD adsorption method which does not typically retain high-molecular-weight DOM. It is worth noting that nonprotonated aliphatic carbons such as quaternary C, nonprotonated OC and anomeric carbons were prevalent in DOM from various environments. These structures were very likely associated with CRAM from 2D NMR analyses. Overall, the chemical and molecular characteristics of DOM, from vastly different environments with different source strengths, featured clear general similarities. This implies the chemical homogenization of DOM relative to source material in aquatic environments under the influence of diagenetical degradation processes. All compounds in DOM go through different diagenetic processes, which serve as "microbial and photochemical filters" to remove the more labile compounds, leaving behind more refractory components such as CRAM and nonprotonated aliphatic carbons.

FUTURE DIRECTIONS

The most logical extension of this work focuses on an investigation into the origins of CRAM. CRAM have been proposed to arise from cyclic terpenoids such as

steroids and hopanoids that have undergone biological or chemical carboxylation (Hertkorn et al., 2006; Lam et al., 2007; Leenheer, 2009; Leenheer et al., 2003). In addition, these structures could be derived from polyunsaturated lipid precursors that are oxidatively coupled and cyclized by free-radical mechanisms (Harvey et al., 1983). Few attempts have currently been undertaken to identify individual compounds in the CRAM group. These studies typically involved chromatographic methods to reduce the DOM heterogeneity. For instance, gas chromatography–mass spectrometry analyses identified hopane products diagnostic of bacteriohopanepolyols in the microscale sealed vessel pyrolysate of DOM from the Great Salt Lake (Greenwood et al., 2006). Woods et al. (2012) detected oxidized sterol and hopanoid-like structures similar to cholic acid in DOM by two dimensional hydrophilic interaction chromatography combined with multidimensional NMR spectroscopy. Arakawa and Aluwihare (2014) recently reported a method to chemically reduce DOM, which enabled the detection of terpenoid derived compounds. Although their results were preliminary and have not been published yet, they showed great promise for identifying individual terpenoid derived compounds. Elucidation of CRAM structures in more detail, and comparison of similar structures in fresh/degraded terrestrial/marine biomass with those in DOM, have the potential to decipher their organic precursors, diagenetic processes and reactivities.

Further work to assess the microbial and photochemical degradation of CRAM is also warranted. Due to their alicyclic and highly branched structures, CRAM are considered as a more refractory component than other biomolecules such as carbohydrates and proteins though very few studies have been initiated to confirm their refractory nature. One available study through FT-ICR MS analyses of Congo River

DOM pre- and post-irradiation indicated that molecular signatures consistent with CRAM were also highly photo-labile, though not as photoreactive as aromatic compounds (Stubbins et al., 2010). This finding was surprising, but as the authors readily admitted, the MS peaks assigned to CRAM might contain both aromatic and CRAM isomers. Therefore it is essential in future similar studies to include NMR spectroscopy as a more diagnostic tool for unambiguously tracking the structural changes of CRAM.

REFERENCES

Aagaard, K., Carmack, E., 1989. The role of sea ice and other fresh water in the Arctic circulation. Journal of Geophysical Research: Oceans 94, 14485-14498.

Abdulla, H.A.N., Minor, E.C., Dias, R.F., Hatcher, P.G., 2010a. Changes in the compound classes of dissolved organic matter along an estuarine transect: A study using FTIR and C-13 NMR. Geochimica et Cosmochimica Acta 74, 3815-3838.

Abdulla, H.A.N., Minor, E.C., Hatcher, P.G., 2010b. Using two-dimensional correlations of C-13 NMR and FTIR to investigate changes in the chemical composition of dissolved organic matter along an estuarine transect. Environmental Science & Technology 44, 8044-8049.

Ågren, G.I., Bosatta, E., 1996. Quality: A Bridge between Theory and Experiment in Soil Organic Matter Studies. Oikos 76, 522-528.

Ahuja, S., 2013. Comprehensive Water Quality and Purification. Elsevier Science.

Aiken, G., McKnight, D., Harnish, R., Wershaw, R., 1996. Geochemistry of aquatic humic substances in the Lake Fryxell Basin, Antarctica. Biogeochemistry 34, 157-188.

Aiken, G.R., 2014a. 1.11 - Dissolved organic matter in aquatic systems. In: Ahuja, S. (Ed.), Comprehensive Water Quality and Purification. Elsevier, Waltham, pp. 205-220.

Aiken, G.R., 2014b. Fluorescence and dissolved organic matter: a chemist's perspective. In: Coble, P., Lead, J., Baker, A., Reynolds, D., Spencer, R.G.M. (Eds.), Aquatic Organic Matter Fluorescence. Cambridge University Press, New York, pp. 35-74.

Aiken, G.R., Malcolm, R.L., 1987. Molecular weight of aquatic fulvic acids by vapor pressure osmometry. Geochimica et Cosmochimica Acta 51, 2177-2184.

Aiken, G.R., McKnight, D.M., Thorn, K.A., Thurman, E.M., 1992. Isolation of hydrophilic organic acids from water using nonionic macroporous resins. Organic Geochemistry 18, 567-573.

Aiken, G.R., McKnight, D.M., Winter, T., 1997. The influence of hydrological factors on the nature of organic matter in the Williams and Shingobee Lake Systems. Interdisciplinary research initiative: hydrological and biogeochemical research in the Shingobee River headwaters area, north-central Minnesota. Document, 96-4215.

Aiken, G.R., Spencer, R.G., Striegl, R.G., Schuster, P.F., Raymond, P.A., 2014. Influences of glacier melt and permafrost thaw on the age of dissolved organic carbon in the Yukon River basin. Global Biogeochemical Cycles 28, 525-537.

Aitkenhead-Peterson, J., McDowell, W., Neff, J., 2003. Sources, production, and regulation of allochthonous dissolved organic matter inputs to surface waters. In: Findlay, S.E., Sinsabaugh, R.L. (Eds.), Aquatic Ecosystems: Interactivity of Dissolved Organic Matter. Academic Press, San Diego, pp. 25-70.

Algesten, G., Sobek, S., Bergström, A.K., Ågren, A., Tranvik, L.J., Jansson, M., 2004. Role of lakes for organic carbon cycling in the boreal zone. Global Change Biology 10, 141-147.

Aluwihare, L.I., Repeta, D.J., Chen, R.F., 1997. A major biopolymeric component to dissolved organic carbon in surface sea water. Nature 387, 166-169.

Aluwihare, L.I., Repeta, D.J., Pantoja, S., Johnson, C.G., 2005. Two chemically distinct pools of organic nitrogen accumulate in the ocean. Science 308, 1007-1010.

Amon, R., Rinehart, A., Duan, S., Louchouarn, P., Prokushkin, A., Guggenberger, G., Bauch, D., Stedmon, C., Raymond, P., Holmes, R., 2012. Dissolved organic matter sources in large Arctic rivers. Geochimica et Cosmochimica Acta 94, 217-237.

Amon, R.M.W., 2004. The Role of Dissolved Organic Matter for the Organic Carbon Cycle in the Arctic Ocean. In: Stein, R., MacDonald, R.W. (Eds.), The Organic Carbon Cycle in the Arctic Ocean. Springer, New York, pp. 83-99.

Amon, R.M.W., Benner, R., 1996. Photochemical and microbial consumption of dissolved organic carbon and dissolved oxygen in the Amazon River system. Geochimica et Cosmochimica Acta 60, 1783-1792.

Amon, R.M.W., Meon, B., 2004. The biogeochemistry of dissolved organic matter and nutrients in two large Arctic estuaries and potential implications for our understanding of the Arctic Ocean system. Marine Chemistry 92, 311-330.

Arakawa, N.K., Aluwihare, L.I., 2014. Examining the distribution of degraded terpenoids in terrestrial DOM following chemical reduction. Abstract., Joint Aquatic Sciences Meeting 2014, Portland, Oregon.

Bauer, J.E., 2002. Carbon isotopic composition of DOM. In: Hansell, D.A., Carlson, C.A. (Eds.), Biogeochemistry of Marine Dissolved Organic Matter. Academic Press, San Diego, pp. 405-453.

Bauer, J.E., Bianchi, T.S., 2011. Dissolved organic carbon cycling and transformation. In: Wolanski, E., McLusky, D.S. (Eds.), Treatise on Estuarine and Coastal Science. Academic Press, Waltham, pp. 7-67.

Benner, R., 2002. Chemical composition and reactivity. In: Hansell, D.A., Carlson, C.A. (Eds.), Biogeochemistry of Marine Dissolved Organic Matter. Academic Press, San Diego, pp. 59-90.

Benner, R., 2003. Molecular indicators of the bioavailability of dissolved organic matter. In: Findlay, S.E., Sinsabaugh, R.L. (Eds.), Aquatic Ecosystems: Interactivity of Dissolved Organic Matter. Academic Press, San Diego, pp. 121-138.

Benner, R., 2004. What happens to terrestrial organic matter in the ocean? Marine Chemistry 92, 307-310.

Benner, R., Benitez-Nelson, B., Kaiser, K., Amon, R.M.W., 2004. Export of young terrigenous dissolved organic carbon from rivers to the Arctic Ocean. Geophysical Research Letters 31, L05305.

Benner, R., Biddanda, B., Black, B., McCarthy, M., 1997. Abundance, size distribution, and stable carbon and nitrogen isotopic compositions of marine organic matter isolated by tangential-flow ultrafiltration. Marine Chemistry 57, 243-263.

Benner, R., Kaiser, K., 2011. Biological and photochemical transformations of amino acids and lignin phenols in riverine dissolved organic matter. Biogeochemistry 102, 209-222.

Benner, R., Louchouarn, P., Amon, R.M.W., 2005. Terrigenous dissolved organic matter in the Arctic Ocean and its transport to surface and deep waters of the North Atlantic. Global Biogeochemical Cycles 19, GB2025.

Benner, R., Pakulski, J.D., McCarthy, M., Hedges, J.I., Hatcher, P.G., 1992. Bulk chemical characteristics of dissolved organic matter in the ocean. Science 255, 1561-1564.

Bennett, A.E., Rienstra, C.M., Auger, M., Lakshmi, K., Griffin, R.G., 1995. Heteronuclear decoupling in rotating solids. The Journal of Chemical Physics 103, 6951-6958.

Berggren, M., Laudon, H., Jansson, M., 2007. Landscape regulation of bacterial growth efficiency in boreal freshwaters. Global Biogeochemical Cycles 21, GB4002.

Berndt, M.E., Bavin, T.K., 2011. Sulfate and Mercury Cycling in Five Wetlands and a Lake Receiving Sulfate from Taconite Mines in Northeastern Minnesota. Minnesota Department of Natural Resources, Division of Lands and Minerals, St. Paul, MN.

Bertilsson, S., Jones, J., 2003. Supply of dissolved organic matter to aquatic ecosystems: autochthonous sources. In: Findlay, S., Sinsabaugh, R. (Eds.), Aquatic Ecosystems: Interactivity of Dissolved Organic Matter. Academic Press, San Diego, pp. 3-24.

Bertilsson, S., Tranvik, L.J., 2000. Photochemical transformation of dissolved organic matter in lakes. Limnology and Oceanography 45, 753-762.

Berwick, L., Greenwood, P.F., Smernik, R.J., 2010. The use of MSSV pyrolysis to assist the molecular characterisation of aquatic natural organic matter. Water Research 44, 3039-3054.

Blakney, G.T., Hendrickson, C.L., Marshall, A.G., 2011. Predator data station: a fast data acquisition system for advanced FT-ICR MS experiments. International Journal of Mass Spectrometry 306, 246-252.

Blough, N.V., Del Vecchio, R., 2002. Chromophoric DOM in the coastal environment. In: Hansell, D.A., Carlson, C.A. (Eds.), Biogeochemistry of Marine Dissolved Organic Matter. Academic Press, San Diego, pp. 509-546.

Bodenhausen, G., Freeman, R., Turner, D.L., 1977. Suppression of artifacts in two-dimensional *J* spectroscopy. Journal of Magnetic Resonance (1969) 27, 511-514.

Bovey, F.A., 1987. Nuclear Magnetic Resonance Spectroscopy. Academic Press, San Diego.

Brabets, T.P., Wang, B., Meade, R.H., 2000. Environmental and hydrologic overview of the Yukon River Basin, Alaska and Canada. US Department of the Interior, US Geological Survey.

Catalán, N., Obrador, B., Felip, M., Pretus, J.L., 2013. Higher reactivity of allochthonous vs. autochthonous DOC sources in a shallow lake. Aquatic Sciences 75, 581-593.

Cauwet, G., Sidorov, I., 1996. The biogeochemistry of Lena River: organic carbon and nutrients distribution. Marine Chemistry 53, 211-227.

Chen, H., Stubbins, A., Perdue, E.M., Green, N.W., Helms, J.R., Mopper, K., Hatcher, P.G., 2014. Ultrahigh resolution mass spectrometric differentiation of dissolved organic matter isolated by coupled reverse osmosis-electrodialysis from various major oceanic water masses. Marine Chemistry 164, 48-59.

Coble, P.G., 1996. Characterization of marine and terrestrial DOM in seawater using excitation-emission matrix spectroscopy. Marine Chemistry 51, 325-346.

Coble, P.G., 2007. Marine optical biogeochemistry: the chemistry of ocean color. Chemical Reviews 107, 402-418.

Coble, P.G., Green, S.A., Blough, N.V., Gagosian, R.B., 1990. Characterization of dissolved organic matter in the Black Sea by fluorescence spectroscopy. Nature 348, 432-435.

Cole, J.J., Caraco, N.F., Kling, G.W., Kratz, T.K., 1994. Carbon dioxide supersaturation in the surface waters of lakes. Science 265, 1568-1570.

Cole, J.J., Prairie, Y.T., Caraco, N.F., McDowell, W.H., Tranvik, L.J., Striegl, R.G., Duarte, C.M., Kortelainen, P., Downing, J.A., Middelburg, J.J., 2007. Plumbing the global carbon cycle: integrating inland waters into the terrestrial carbon budget. Ecosystems 10, 172-185.

Cory, R.M., McKnight, D.M., Chin, Y.P., Miller, P., Jaros, C.L., 2007. Chemical characteristics of fulvic acids from Arctic surface waters: microbial contributions and photochemical transformations. Journal of Geophysical Research: Biogeosciences 112, G04S51.

D'Andrilli, J., Foreman, C.M., Marshall, A.G., McKnight, D.M., 2013. Characterization of IHSS Pony Lake fulvic acid dissolved organic matter by electrospray ionization Fourier transform ion cyclotron resonance mass spectrometry and fluorescence spectroscopy. Organic Geochemistry 65, 19-28.

Dalzell, B.J., Minor, E.C., Mopper, K.M., 2009. Photodegradation of estuarine dissolved organic matter: a multi-method assessment of DOM transformation. Organic Geochemistry 40, 243-257.

Davis, J.C., Proctor, I.D., Southon, J.R., Caffee, M.W., Heikkinen, D.W., Roberts, M.L., Moore, T.L., Turteltaub, K.W., Nelson, D.E., Loyd, D.H., Vogel, J.S., 1990. LLNL/UC AMS facility and research program. Nuclear Instruments and Methods in Physics Research Section B 52, 269-272.

Del Giorgio, P., Davis, J., 2003. Patterns in dissolved organic matter lability and consumption across aquatic ecosystems. Aquatic Ecosystems: Interactivity of Dissolved Organic Matter. Academic Press, San Diego, pp. 399-424.

Dittmar, T., Kattner, G., 2003. The biogeochemistry of the river and shelf ecosystem of the Arctic Ocean: a review. Marine Chemistry 83, 103-120.

Dittmar, T., Koch, B., Hertkorn, N., Kattner, G., 2008. A simple and efficient method for the solid-phase extraction of dissolved organic matter (SPE-DOM) from seawater. Limnology and Oceanography: Methods 6, 230-235.

Dittmar, T., Koch, B.P., 2006. Thermogenic organic matter dissolved in the abyssal ocean. Marine Chemistry 102, 208-217.

Dittmar, T., Paeng, J., 2009. A heat-induced molecular signature in marine dissolved organic matter. Nature Geoscience 2, 175-179.

Dittmar, T., Stubbins, A., 2014. 12.6 - Dissolved organic matter in aquatic systems. In: Holland, H.D., Turekian, K.K. (Eds.), Treatise on Geochemistry (second ed.). Elsevier, Oxford, pp. 125-156.

Dittmar, T., Whitehead, K., Minor, E.C., Koch, B.P., 2007. Tracing terrigenous dissolved organic matter and its photochemical decay in the ocean by using liquid chromatography/mass spectrometry. Marine Chemistry 107, 378-387.

Dixon, W.T., 1982. Spinning-sideband-free and spinning-sideband-only NMR spectra in spinning samples. Journal of Chemical Physics 77, 1800-1809.

Druffel, E.R., Williams, P.M., Bauer, J.E., Ertel, J.R., 1992. Cycling of dissolved and particulate organic matter in the open ocean. Journal of Geophysical Research: Oceans 97, 15639-15659.

Eglinton, T., Repeta, D., 2004. Marine organic geochemistry. Treatise on geochemistry 7, 145-180.

Esteves, V.I., Otero, M., Duarte, A.C., 2009. Comparative characterization of humic substances from the open ocean, estuarine water and fresh water. Organic Geochemistry 40, 942-950.

Fellman, J.B., Hood, E., Spencer, R.G., 2010. Fluorescence spectroscopy opens new windows into dissolved organic matter dynamics in freshwater ecosystems: a review. Limnology and Oceanography 55, 2452-2462.

Feng, X., Benitez-Nelson, B.C., Montlucon, D.B., Prahl, F.G., McNichol, A.P., Xu, L., Repeta, D.J., Eglinton, T.I., 2013. ^{14}C and ^{13}C characteristics of higher plant biomarkers in Washington margin surface sediments. Geochimica et Cosmochimica Acta 105, 14-30.

Findlay, S.E., Sinsabaugh, R.L., 2003. Aquatic Ecosystems: Interactivity of Dissolved Organic Matter. Academic Press, San Diego, CA.

Frey, K.E., McClelland, J.W., 2009. Impacts of permafrost degradation on arctic river biogeochemistry. Hydrological Processes 23, 169-182.

Gaskell, S.J., 1997. Electrospray: principles and practice. Journal of Mass Spectrometry 32, 677-688.

Goñi, M.A., Eglinton, T.I., 1996. Stable carbon isotopic analyses of lignin-derived CuO oxidation products by isotope ratio monitoring-gas chromatography-mass spectrometry (irm-GC-MS). Organic Geochemistry 24, 601-615.

Gonsior, M., Peake, B.M., Cooper, W.T., Podgorski, D., D'Andrilli, J., Cooper, W.J., 2009. Photochemically induced changes in dissolved organic matter identified by ultrahigh resolution Fourier transform ion cyclotron resonance mass spectrometry. Environmental Science & Technology 43, 698-703.

Green, N.W., Perdue, E.M., Aiken, G.R., Butler, K.D., Chen, H., Dittmar, T., Niggemann, J., Stubbins, A., 2014. An intercomparison of three methods for the large-scale isolation of oceanic dissolved organic matter. Marine Chemistry 161, 14-19.

Green, S.A., Blough, N.V., 1994. Optical absorption and fluorescence properties of chromophoric dissolved organic matter in natural waters. Limnology and Oceanography 39, 1903-1916.

Greenwood, P.F., Leenheer, J.A., McIntyre, C., Berwick, L., Franzmann, P.D., 2006. Bacterial biomarkers thermally released from dissolved organic matter. Organic Geochemistry 37, 597-609.

Grosse, G., Harden, J., Turetsky, M., McGuire, A.D., Camill, P., Tarnocai, C., Frolking, S., Schuur, E.A., Jorgenson, T., Marchenko, S., 2011. Vulnerability of high - latitude soil organic carbon in North America to disturbance. Journal of Geophysical Research: Biogeosciences (2005 - 2012) 116, G00K06.

Gruber, N., Friedlingstein, P., Field, C.B., Valentini, R., Heimann, M., Richey, J.E., Lankao, P.R., Schulze, E.-D., Chen, C.-T.A., 2004. The vulnerability of the carbon cycle in the 21st century: an assessment of carbon-climate-human interactions. Scope 62, 45-76.

Guillemette, F., del Giorgio, P.A., 2012. Simultaneous consumption and production of fluorescent dissolved organic matter by lake bacterioplankton. Environmental Microbiology 14, 1432-1443.

Guo, L., Cai, Y., Belzile, C., Macdonald, R.W., 2012. Sources and export fluxes of inorganic and organic carbon and nutrient species from the seasonally ice-covered Yukon River. Biogeochemistry 107, 187-206.

Guo, L., Striegl, R.G., Macdonald, R., 2013. Composition and fluxes of carbon and nutrient species from the Yukon River basin in a changing environment. In: Bianchi, T.S., Allison, M.A., Cai, W.-J. (Eds.), Biogeochemical Dynamics at Major River-Coastal Interfaces. Cambridge University Press, New York, pp. 503-529.

Gurtler, B.K., Vetter, T.A., Perdue, E.M., Ingall, E., Koprivnjak, J.F., Pfromm, P.H., 2008. Combining reverse osmosis and pulsed electrical current electrodialysis for improved

recovery of dissolved organic matter from seawater. Journal of Membrane Science 323, 328-336.

Hansell, D.A., Kadko, D., Bates, N.R., 2004. Degradation of terrigenous dissolved organic carbon in the western Arctic Ocean. Science 304, 858-861.

Hanson, P.C., Hamilton, D.P., Stanley, E.H., Preston, N., Langman, O.C., Kara, E.L., 2011. Fate of allochthonous dissolved organic carbon in lakes: a quantitative approach. PLoS One 6, e21884.

Harvey, G.R., Boran, D.A., Chesal, L.A., Tokar, J.M., 1983. The structure of marine fulvic and humic acids. Marine Chemistry 12, 119-132.

Hedges, J.I., 1992. Global biogeochemical cycles: progress and problems. Marine Chemistry 39, 67-93.

Hedges, J.I., 2002. Why dissolved organics matter. In: Hansell, D.A., Carlson, C.A. (Eds.), Biogeochemistry of Marine Dissolved Organic Matter. Academic Press, San Diego, pp. 1-33.

Hedges, J.I., Eglinton, G., Hatcher, P.G., Kirchman, D.L., Arnosti, C., Derenne, S., Evershed, R.P., Kogel-Knabner, I., de Leeuw, J.W., Littke, R., Michaelis, W., Rullkotter, J., 2000. The molecularly-uncharacterized component of nonliving organic matter in natural environments. Organic Geochemistry 31, 945-958.

Hedges, J.I., Hatcher, P.G., Ertel, J.R., Meyers-Schulte, K.J., 1992. A comparison of dissolved humic substances from seawater with Amazon River counterparts by 13C-NMR spectrometry. Geochimica et Cosmochimica Acta 56, 1753-1757.

Hedges, J.I., Keil, R.G., Benner, R., 1997. What happens to terrestrial organic matter in the ocean? Organic Geochemistry 27, 195-212.

Hedges, J.I., Oades, J.M., 1997. Comparative organic geochemistries of soils and marine sediments. Organic Geochemistry 27, 319-361.

Helms, J.R., 2012. Spectroscopic Characterization of Dissolved Organic Matter: Insights into Composition, Photochemical Transformation and Carbon Cycling. Old Dominion University, Virginia, USA., p. 234.

Helms, J.R., Mao, J., Stubbins, A., Schmidt-Rohr, K., Spencer, R.G., Hernes, P.J., Mopper, K., 2014. Loss of optical and molecular indicators of terrigenous dissolved organic matter during long-term photobleaching. Aquatic Sciences, 353-373.

Helms, J.R., Stubbins, A., Ritchie, J.D., Minor, E.C., Kieber, D.J., Mopper, K., 2008. Absorption spectral slopes and slope ratios as indicators of molecular weight, source, and photobleaching of chromophoric dissolved organic matter. Limnology and Oceanography 53, 955.

Hernes, P.J., Benner, R., 2003. Photochemical and microbial degradation of dissolved lignin phenols: Implications for the fate of terrigenous dissolved organic matter in marine environments. Journal of Geophysical Research: Oceans 108, 3291.

Hernes, P.J., Benner, R., 2006. Terrigenous organic matter sources and reactivity in the North Atlantic Ocean and a comparison to the Arctic and Pacific oceans. Marine Chemistry 100, 66-79.

Hertkorn, N., Benner, R., Frommberger, M., Schmitt-Kopplin, P., Witt, M., Kaiser, K., Kettrup, A., Hedges, J.I., 2006. Characterization of a major refractory component of marine dissolved organic matter. Geochimica et Cosmochimica Acta 70, 2990-3010.

Hertkorn, N., Harir, M., Koch, B., Michalke, B., Schmitt-Kopplin, P., 2013. High-field NMR spectroscopy and FTICR mass spectrometry: powerful discovery tools for the molecular level characterization of marine dissolved organic matter. Biogeosciences 10, 1583-1624.

Holmes, R.M., Coe, M.T., Fiske, G.J., Gurtovaya, T., McClelland, J.W., Shiklomanov, A.I., Spencer, R.G., Tank, S.E., Zhulidov, A.V., 2013. Climate change impacts on the hydrology and biogeochemistry of Arctic rivers. In: Goldman, C.R., Kumagai, M., Robarts, R.D. (Eds.), Climatic Change and Global Warming of Inland Waters: Impacts and Mitigation for Ecosystems and Societies. John Wiley & Sons, Ltd., Chichester, UK., pp. 3-26.

Holmes, R.M., McClelland, J.W., Peterson, B.J., Tank, S.E., Bulygina, E., Eglinton, T.I., Gordeev, V.V., Gurtovaya, T.Y., Raymond, P.A., Repeta, D.J., Staples, R., Striegl, R.G., Zhulidov, A.V., Zimov, S.A., 2012. Seasonal and Annual Fluxes of Nutrients and Organic Matter from Large Rivers to the Arctic Ocean and Surrounding Seas. Estuaries and Coasts 35, 369-382.

Holmes, R.M., McClelland, J.W., Raymond, P.A., Frazer, B.B., Peterson, B.J., Stieglitz, M., 2008. Lability of DOC transported by Alaskan rivers to the arctic ocean. Geophysical Research Letters 35, L03402.

Hu, W.G., Mao, J.D., Xing, B.S., Schmidt-Rohr, K., 2000. Poly(methylene) crystallites in humic substances detected by nuclear magnetic resonance. Environmental Science and Technology 34, 530-534.

Huffman, E., Stuber, H., 1985. Analytical methodology for elemental analysis of humic substances. In: G. R. Aiken, D. M. McKnight, R. L. Wershaw, McCarthy, P. (Eds.),

Humic substances in soil, sediment and water: geochemistry, isolation, and characterization. John Wiley & Sons, New York, pp. 433-455.

Jaffé, R., Boyer, J., Lu, X., Maie, N., Yang, C., Scully, N., Mock, S., 2004. Source characterization of dissolved organic matter in a subtropical mangrove-dominated estuary by fluorescence analysis. Marine Chemistry 84, 195-210.

Jaffé, R., McKnight, D.M., Maie, N., Cory, R., McDowell, W., Campbell, J., 2008. Spatial and temporal variations in DOM composition in ecosystems: the importance of long - term monitoring of optical properties. Journal of Geophysical Research: Biogeosciences 113, G04032.

Jaffé, R., Yamashita, Y., Maie, N., Cooper, W.T., Dittmar, T., Dodds, W.K., Jones, J.B., Myoshi, T., Ortiz-Zayas, J.R., Podgorski, D.C., Watanabe, A., 2012. Dissolved organic matter in headwater streams: Compositional variability across climatic regions of North America. Geochimica et Cosmochimica Acta 94, 95-108.

Johnson, R.L., Schmidt-Rohr, K., 2014. Quantitative solid-state ^{13}C NMR with signal enhancement by multiple cross polarization. Journal of Magnetic Resonance 239, 44-49.

Jørgensen, L., Stedmon, C.A., Kragh, T., Markager, S., Middelboe, M., Søndergaard, M., 2011. Global trends in the fluorescence characteristics and distribution of marine dissolved organic matter. Marine Chemistry 126, 139-148.

Kaiser, E., Simpson, A.J., Dria, K.J., Sulzberger, B., Hatcher, P.G., 2003. Solid-state and multidimensional solution-state NMR of solid phase extracted and ultrafiltered riverine dissolved organic matter. Environmental Science & Technology 37, 2929-2935.

Kaiser, N.K., Quinn, J.P., Blakney, G.T., Hendrickson, C.L., Marshall, A.G., 2011. A novel 9.4 Tesla FTICR mass spectrometer with improved sensitivity, mass resolution, and mass range. Journal of the American Society for Mass Spectrometry 22, 1343-1351.

Kellerman, A.M., Dittmar, T., Kothawala, D.N., Tranvik, L.J., 2014. Chemodiversity of dissolved organic matter in lakes driven by climate and hydrology. Nature Communications 5, 3804.

Kendrick, E., 1963. A mass scale based on CH_2 = 14.0000 for high resolution mass spectrometry of organic compounds. Analytical Chemistry 35, 2146-2154.

Kim, S., Kaplan, L.A., Hatcher, P.G., 2006. Biodegradable dissolved organic matter in a temperate and a tropical stream determined from ultra-high resolution mass spectrometry. Limnology and Oceanography 51, 1054-1063.

Kim, S., Kramer, R.W., Hatcher, P.G., 2003a. Graphical method for analysis of ultrahigh-resolution broadband mass spectra of natural organic matter, the van Krevelen diagram. Analytical Chemistry 75, 5336-5344.

Kim, S., Simpson, A.J., Kujawinski, E.B., Freitas, M.A., Hatcher, P.G., 2003b. High resolution electrospray ionization mass spectrometry and 2D solution NMR for the analysis of DOM extracted by C-18 solid phase disk. Organic Geochemistry 34, 1325-1335.

Koch, B., Dittmar, T., 2006. From mass to structure: an aromaticity index for high - resolution mass data of natural organic matter. Rapid Communications in Mass Spectrometry 20, 926-932.

Koch, B.P., Ludwichowski, K.-U., Kattner, G., Dittmar, T., Witt, M., 2008. Advanced characterization of marine dissolved organic matter by combining reversed-phase liquid chromatography and FT-ICR-MS. Marine Chemistry 111, 233-241.

Koehler, B., von Wachenfeldt, E., Kothawala, D., Tranvik, L.J., 2012. Reactivity continuum of dissolved organic carbon decomposition in lake water. Journal of Geophysical Research: Biogeosciences 117, G01024.

Köhler, S.J., Kothawala, D., Futter, M.N., Liungman, O., Tranvik, L., 2013. In-lake processes offset increased terrestrial inputs of dissolved organic carbon and color to lakes. PloS one 8, e70598.

Koprivnjak, J.F., Pfromm, P.H., Ingall, E., Vetter, T.A., Schmitt-Kopplin, P., Hertkorn, N., Frommberger, M., Knicker, H., Perdue, E.M., 2009. Chemical and spectroscopic characterization of marine dissolved organic matter isolated using coupled reverse osmosis-electrodialysis. Geochimica et Cosmochimica Acta 73, 4215-4231.

Kothawala, D.N., Stedmon, C.A., Müller, R.A., Weyhenmeyer, G.A., Köhler, S.J., Tranvik, L.J., 2014. Controls of dissolved organic matter quality: evidence from a large - scale boreal lake survey. Global Change Biology 20, 1101-1114.

Kritzberg, E., Cole, J.J., Pace, M.L., Granéli, W., Bade, D.L., 2004. Autochthonous versus allochthonous carbon sources of bacteria: Results from whole-lake C-13 addition experiments. Limnology and Oceanography 49, 588-596.

Kujawinski, E.B., Del Vecchio, R., Blough, N.V., Klein, G.C., Marshall, A.G., 2004. Probing molecular-level transformations of dissolved organic matter: insights on photochemical degradation and protozoan modification of DOM from electrospray ionization Fourier transform ion cyclotron resonance mass spectrometry. Marine Chemistry 92, 23-37.

Kujawinski, E.B., Longnecker, K., Blough, N.V., Del Vecchio, R., Finlay, L., Kitner, J.B., Giovannoni, S.J., 2009. Identification of possible source markers in marine dissolved organic matter using ultrahigh resolution mass spectrometry. Geochimica et Cosmochimica Acta 73, 4384-4399.

LaBaugh, J.W., Rosenberry, D.O., Winter, T.C., 1995. Groundwater contribution to the water and chemical budgets of Williams Lake, Minnesota, 1980-1991. Canadian Journal of Fisheries and Aquatic Sciences 52, 754-767.

Lam, B., Baer, A., Alaee, M., Lefebvre, B., Moser, A., Williams, A., Simpson, A.J., 2007. Major structural components in freshwater dissolved organic matter. Environmental Science & Technology 41, 8240-8247.

Lam, B., Simpson, A.J., 2008. Direct 1H NMR spectroscopy of dissolved organic matter in natural waters. Analyst 133, 263-269.

Ledford Jr, E.B., Rempel, D.L., Gross, M., 1984. Space charge effects in Fourier transform mass spectrometry. II. Mass calibration. Analytical Chemistry 56, 2744-2748.

Leenheer, J., Wilson, M., Malcolm, R., 1987. Presence and potential significance of aromatic-ketone groups in aquatic humic substances. Organic Geochemistry 11, 273-280.

Leenheer, J.A., 1994. Chemistry of Dissolved Organic Matter in Rivers, Lakes, and Reservoirs. In: Baker, L.A. (Ed.), Environmental Chemistry of Lakes and Reservoirs, pp. 195-221.

Leenheer, J.A., 2009. Systematic Approaches to Comprehensive Analyses of Natural Organic Matter. Annals of Environmental Science 3, 1-130.

Leenheer, J.A., Nanny, M.A., McIntyre, C., 2003. Terpenoids as major precursors of dissolved organic matter in landfill leachates, surface water, and groundwater. Environmental Science & Technology 37, 2323-2331.

Leenheer, J.A., Noyes, T.I., Rostad, C.E., Davisson, M.L., 2004. Characterization and origin of polar dissolved organic matter from the Great Salt Lake. Biogeochemistry 69, 125-141.

Leenheer, J.A., Rostad, C.E., 2004. Tannins and terpenoids as major precursors of Suwannee River fulvic acid, U.S. Geological Survey Scientific Investigations Report 2004-5276, p. 16p.

Leenheer, J.A., Wershaw, R.L., Reddy, M.M., 1995. Strong-acid, carboxyl-group structures in fulvic acid from the Suwannee River, Georgia. 2. Major structures. Environmental Science & Technology 29, 399-405.

Liu, Z.F., Sleighter, R.L., Zhong, J.Y., Hatcher, P.G., 2011. The chemical changes of DOM from black waters to coastal marine waters by HPLC combined with ultrahigh resolution mass spectrometry. Estuarine, Coastal and Shelf Science 92, 205-216.

Lobbes, J.M., Fitznar, H.P., Kattner, G., 2000. Biogeochemical characteristics of dissolved and particulate organic matter in Russian rivers entering the Arctic Ocean. Geochimica et Cosmochimica Acta 64, 2973-2983.

Loh, A.N., Bauer, J.E., Druffel, E.R.M., 2004. Variable ageing and storage of dissolved organic components in the open ocean. Nature 430, 877-881.

Malcolm, R.L., 1990. The uniqueness of humic substances in each of soil, stream and marine environments. Analytica Chimica Acta 232, 19-30.

Mann, P., Davydova, A., Zimov, N., Spencer, R., Davydov, S., Bulygina, E., Zimov, S., Holmes, R., 2012. Controls on the composition and lability of dissolved organic matter in

Siberia's Kolyma River basin. Journal of Geophysical Research: Biogeosciences 117, G01028.

Mannino, A., Harvey, H.R., 2000. Terrigenous dissolved organic matter along an estuarine gradient and its flux to the coastal ocean. Organic Geochemistry 31, 1611-1625.

Mao, J., Chen, N., Cao, X., 2011. Characterization of humic substances by advanced solid state NMR spectroscopy: Demonstration of a systematic approach. Organic Geochemistry 42, 891-902.

Mao, J., Fang, X., Lan, Y., Schimmelmann, A., Mastalerz, M., Xu, L., Schmidt-Rohr, K., 2010. Chemical and nanometer-scale structure of kerogen and its change during thermal maturation investigated by advanced solid-state ^{13}C NMR spectroscopy. Geochimica et Cosmochimica Acta 74, 2110-2127.

Mao, J.D., Hu, W.G., Schmidt-Rohr, K., Davies, G., Ghabbour, E.A., Xing, B.S., 2000. Quantitative characterization of humic substances by solid-state carbon-13 nuclear magnetic resonance. Soil Science Society of America Journal 64, 873-884.

Mao, J.D., Johnson, R.L., Lehmann, J., Olk, D.C., Neves, E.G., Thompson, M.L., Schmidt-Rohr, K., 2012a. Abundant and stable char residues in soils: Implications for soil fertility and carbon sequestration. Environmental Science & Technology 46, 9571-9576.

Mao, J.D., Kong, X.Q., Schmidt-Rohr, K., Pignatello, J.J., Perdue, E.M., 2012b. Advanced solid-state NMR characterization of marine dissolved organic matter isolated using the coupled reverse osmosis/electrodialysis method. Environmental Science & Technology 46, 5806-5814.

Mao, J.D., Schmidt-Rohr, K., 2004a. Accurate quantification of aromaticity and nonprotonated aromatic carbon fraction in natural organic matter by ^{13}C solid-state nuclear magnetic resonance. Environmental Science and Technology 38, 2680-2684.

Mao, J.D., Schmidt-Rohr, K., 2004b. Separation of aromatic-carbon ^{13}C NMR signals from di-oxygenated alkyl bands by a chemical-shift-anisotropy filter. Solid State Nuclear Magnetic Resonance 26, 36-45.

Mao, J.D., Schmidt-Rohr, K., 2005. Methylene spectral editing in solid-state C-13 NMR by three-spin coherence selection. Journal of Magnetic Resonance 176, 1-6.

Mao, J.D., Schmidt-Rohr, K., 2006. Absence of mobile carbohydrate domains in dry humic substances proven by NMR, and implications for organic-contaminant sorption models. Environmental Science and Technology 40, 1751-1756.

Marshall, A.G., Hendrickson, C.L., Jackson, G.S., 1998. Fourier transform ion cyclotron resonance mass spectrometry: a primer. Mass Spectrometry Reviews 17, 1-35.

McCallister, S., Bauer, J.E., Cherrier, J.E., Ducklow, H.W., 2004. Assessing sources and ages of organic matter supporting river and estuarine bacterial production: A multiple-isotope ($\Delta^{14}C$, $\delta^{13}C$, and $\delta^{15}N$) approach. Limnology and Oceanography 49, 1687.

McCallister, S.L., Bauer, J.E., Ducklow, H.W., Canuel, E.A., 2006. Sources of estuarine dissolved and particulate organic matter: A multi-tracer approach. Organic Geochemistry 37, 454-468.

McCaul, M.V., Sutton, D., Simpson, A.J., Spence, A., McNally, D.J., Moran, B.W., Goel, A., O'Connor, B., Hart, K., Kelleher, B.P., 2011. Composition of dissolved organic matter within a lacustrine environment. Environmental Chemistry 8, 146-154.

McGuire, A.D., Anderson, L.G., Christensen, T.R., Dallimore, S., Guo, L., Hayes, D.J., Heimann, M., Lorenson, T.D., Macdonald, R.W., Roulet, N., 2009. Sensitivity of the carbon cycle in the Arctic to climate change. Ecological Monographs 79, 523-555.

McIntyre, C., McRae, C., Batts, B.D., Piccolo, A., 2005. Structural characterisation of groundwater hydrophobic acids isolated from the Tomago Sand Beds, Australia. Organic Geochemistry 36, 385-397.

McKnight, D., Hood, E., Klapper, L., 2003. Trace organic moieties of dissolved organic material in natural waters. In: Findlay, S.E., Sinsabaugh, R.L. (Eds.), Aquatic Ecosystems: Interactivity of Dissolved Organic Matter. Academic Press, San Diego, pp. 71-96.

McKnight, D.M., Aiken, G.R., 1998. Sources and age of aquatic humus. In: Hessen, D.O., Tranvik, L.J. (Eds.), Aquatic Humic Substances. Springer-Verlag, New York, pp. 9-39.

McKnight, D.M., Aiken, G.R., Smith, R.L., 1991. Aquatic fulvic acids in microbially based ecosystems: results from two desert lakes in Antarctica. Limnology and Oceanography 36, 998-1006.

McKnight, D.M., Boyer, E.W., Westerhoff, P.K., Doran, P.T., Kulbe, T., Andersen, D.T., 2001. Spectrofluorometric characterization of dissolved organic matter for indication of precursor organic material and aromaticity. Limnology and Oceanography 46, 38-48.

McKnight, D.M., Harnish, R., Wershaw, R.L., Baron, J.S., Schiff, S., 1997. Chemical characteristics of particulate, colloidal, and dissolved organic material in Loch Vale Watershed, Rocky Mountain National Park. Biogeochemistry 36, 99-124.

McNichol, A.P., Aluwihare, L.I., 2007. The power of radiocarbon in biogeochemical studies of the marine carbon cycle: insights from studies of dissolved and particulate organic carbon (DOC and POC). Chemical Reviews 107, 443-466.

Meili, M., 1992. Sources, concentrations and characteristics of organic matter in softwater lakes and streams of the Swedish forest region. Dissolved Organic Matter in Lacustrine Ecosystems. Springer, pp. 23-41.

Meyers-Schulte, K.J., Hedges, J.I., 1986. Molecular evidence for a terrestrial component of organic matter dissolved in ocean water. Nature 321, 61-63.

Minor, E.C., Swenson, M.M., Mattson, B.M., Oyler, A.R., 2014. Structural characterization of dissolved organic matter: a review of current techniques for isolation and analysis. Environmental Science: Processes & Impacts 16, 2064-2079.

Mitchell, P.J., Simpson, A.J., Simpson, M.J., 2013. Dissolved organic matter. eMagRes, 503-516.

Mopper, K., Stubbins, A., Ritchie, J.D., Bialk, H.M., Hatcher, P.G., 2007. Advanced instrumental approaches for characterization of marine dissolved organic matter: extraction techniques, mass spectrometry, and nuclear magnetic resonance spectroscopy. Chemical Reviews 107, 419-442.

Moran, M.A., Pomeroy, L.R., Sheppard, E.S., Atkinson, L.P., Hodson, R.E., 1991. Distribution of terrestrially derived dissolved organic matter on the southeastern U.S. continental shelf. Limnology and Oceanography 36, 1134-1149.

Mulholland, P.J., Elwood, J.W., 1982. The role of lake and reservoir sediments as sinks in the perturbed global carbon cycle. Tellus 34, 490-499.

Murphy, E.M., 1987. Carbon-14 Measurements and Characterization of Dissolved Organic Carbon in Ground Water. University of Arizona, Arizona, USA

Murphy, K.R., Butler, K.D., Spencer, R.G., Stedmon, C.A., Boehme, J.R., Aiken, G.R., 2010. Measurement of dissolved organic matter fluorescence in aquatic environments: an interlaboratory comparison. Environmental Science & Technology 44, 9405-9412.

Neff, J.C., Finlay, J.C., Zimov, S.A., Davydov, S.P., Carrasco, J.J., Schuur, E.A.G., Davydova, A.I., 2006. Seasonal changes in the age and structure of dissolved organic carbon in Siberian rivers and streams. Geophysical Research Letters 33, L23401.

O'Donnell, J.A., Aiken, G.R., Walvoord, M.A., Butler, K.D., 2012. Dissolved organic matter composition of winter flow in the Yukon River basin: implications of permafrost thaw and increased groundwater discharge. Global Biogeochemical Cycles 26, GB0E06.

Obernosterer, I., Benner, R., 2004. Competition between biological and photochemical processes in the mineralization of dissolved organic carbon. Limnology and Oceanography 49, 117-124.

Ogawa, H., Amagai, Y., Koike, I., Kaiser, K., Benner, R., 2001. Production of refractory dissolved organic matter by bacteria. Science 292, 917-920.

Opsahl, S., Benner, R., 1997. Distribution and cycling of terrigenous dissolved organic matter in the ocean. Nature 386, 480-482.

Opsahl, S., Benner, R., 1998. Photochemical reactivity of dissolved lignin in river and ocean waters. Limnology and Oceanography 43, 1297-1304.

Opsahl, S., Benner, R., Amon, R.M.W., 1999. Major flux of terrigenous dissolved organic matter through the Arctic Ocean. Limnology and Oceanography 44, 2017-2023.

Opsahl, S.P., Zepp, R.G., 2001. Photochemically-induced alteration of stable carbon isotope ratios ($\delta^{13}C$) in terrigenous dissolved organic carbon. Geophysical Research Letters 28, 2417-2420.

Osburn, C., Morris, D., Thorn, K., Moeller, R., 2001. Chemical and optical changes in freshwater dissolved organic matter exposed to solar radiation. Biogeochemistry 54, 251-278.

Osburn, C.L., Morris, D.P., 2003. Photochemistry of chromophoric dissolved organic matter in natural waters. In: Helbling, E.W., Zagarese, H. (Eds.), UV Effects in Aquatic Organisms and Ecosystems. The Royal Society of Chemistry, pp. 185-218.

Osburn, C.L., Retamal, L., Vincent, W.F., 2009. Photoreactivity of chromophoric dissolved organic matter transported by the Mackenzie River to the Beaufort Sea. Marine Chemistry 115, 10-20.

Panagiotopoulos, C., Repeta, D.J., Johnson, C.G., 2007. Characterization of methyl sugars, 3-deoxysugars and methyl deoxysugars in marine high molecular weight dissolved organic matter. Organic Geochemistry 38, 884-896.

Perdue, E., 1984. Analytical constraints on the structural features of humic substances. Geochimica et Cosmochimica Acta 48, 1435-1442.

Perdue, E.M., Ritchie, J.D., 2003. 5.10 - Dissolved organic matter in freshwaters. In: Turekian, H.D.H.K. (Ed.), Treatise on Geochemistry. Pergamon, Oxford, pp. 273-318.

Poulin, M.B., Lowary, T.L., 2010. Methods to study the biosynthesis of bacterial furanosides. Methods in Enzymology 478, 389-411.

Quan, T.M., Repeta, D.J., 2007. Periodate oxidation of marine high molecular weight dissolved organic matter: Evidence for a major contribution from 6-deoxy- and methyl sugars. Marine Chemistry 105, 183-193.

Raymond, P.A., Bauer, J.E., 2001a. Riverine export of aged terrestrial organic matter to the North Atlantic Ocean. Nature 409, 497-500.

Raymond, P.A., Bauer, J.E., 2001b. Use of ^{14}C and ^{13}C natural abundances for evaluating riverine, estuarine, and coastal DOC and POC sources and cycling: a review and synthesis. Organic Geochemistry 32, 469-485.

Raymond, P.A., McClelland, J.W., Holmes, R.M., Zhulidov, A.V., Mull, K., Peterson, B.J., Striegl, R.G., Aiken, G.R., Gurtovaya, T.Y., 2007. Flux and age of dissolved organic carbon exported to the Arctic Ocean: a carbon isotopic study of the five largest arctic rivers. Global Biogeochemical Cycles 21, GB4011.

Repeta, D.J., Quan, T.M., Aluwihare, L.I., Accardi, A.M., 2002. Chemical characterization of high molecular weight dissolved organic matter in fresh and marine waters. Geochimica et Cosmochimica Acta 66, 955-962.

Roulet, N., Moore, T.R., 2006. Environmental chemistry: Browning the waters. Nature 444, 283-284.

Sanderman, J., Kramer, M.G., 2013. Differential production yet chemical similarity of dissolved organic matter across a chronosequence with contrasting nutrient availability in Hawaii. Biogeochemistry 113, 259-269.

Sannigrahi, P., Ingall, E.D., Benner, R., 2005. Cycling of dissolved and particulate organic matter at station Aloha: insights from C-13 NMR spectroscopy coupled with elemental, isotopic and molecular analyses. Deep-Sea Research Part I: Oceanographic Research Papers 52, 1429-1444.

Savory, J.J., Kaiser, N.K., McKenna, A.M., Xian, F., Blakney, G.T., Rodgers, R.P., Hendrickson, C.L., Marshall, A.G., 2011. Parts-per-billion Fourier transform ion cyclotron resonance mass measurement accuracy with a "walking" calibration equation. Analytical Chemistry 83, 1732-1736.

Schmidt-Rohr, K., Mao, J.D., 2002. Efficient CH-group selection and identification in C-13 solid-state NMR by dipolar DEPT and H-1 chemical-shift filtering. Journal of the American Chemical Society 124, 13938-13948.

Schmidt-Rohr, K., Spiess, H.W., 1994. Multidimensional Solid-State NMR and Polymers. Elsevier.

Schuur, E.A., Bockheim, J., Canadell, J.G., Euskirchen, E., Field, C.B., Goryachkin, S.V., Hagemann, S., Kuhry, P., Lafleur, P.M., Lee, H., 2008. Vulnerability of permafrost carbon to climate change: implications for the global carbon cycle. Bioscience 58, 701-714.

Schwede-Thomas, S.B., Chin, Y.P., Dria, K.J., Hatcher, P., Kaiser, E., Sulzberger, B., 2005. Characterizing the properties of dissolved organic matter isolated by XAD and C-18 solid phase extraction and ultrafiltration. Aquatic Sciences 67, 61-71.

Shank, G.C., Evans, A., 2011. Distribution and photoreactivity of chromophoric dissolved organic matter in northern Gulf of Mexico shelf waters. Continental Shelf Research 31, 1128-1139.

Simpson, A.J., 2002. Determining the molecular weight, aggregation, structures and interactions of natural organic matter using diffusion ordered spectroscopy. Magnetic Resonance in Chemistry 40, S72-S82.

Sleighter, R.L., Hatcher, P.G., 2007. The application of electrospray ionization coupled to ultrahigh resolution mass spectrometry for the molecular characterization of natural organic matter. Journal of Mass Spectrometry 42, 559-574.

Sleighter, R.L., Hatcher, P.G., 2008. Molecular characterization of dissolved organic matter (DOM) along a river to ocean transect of the lower Chesapeake Bay by ultrahigh

resolution electrospray ionization Fourier transform ion cyclotron resonance mass spectrometry. Marine Chemistry 110, 140-152.

Sleighter, R.L., McKee, G.A., Hatcher, P.G., 2009. Direct Fourier transform mass spectral analysis of natural waters with low dissolved organic matter. Organic Geochemistry 40, 119-125.

Sobek, S., Söderbäck, B., Karlsson, S., Andersson, E., Brunberg, A.K., 2006. A carbon budget of a small humic lake: an example of the importance of lakes for organic matter cycling in boreal catchments. AMBIO: A Journal of the Human Environment 35, 469-475.

Spencer, R.G.M., Aiken, G.R., Butler, K.D., Dornblaser, M.M., Striegl, R.G., Hernes, P.J., 2009a. Utilizing chromophoric dissolved organic matter measurements to derive export and reactivity of dissolved organic carbon exported to the Arctic Ocean: A case study of the Yukon River, Alaska. Geophysical Research Letters 36, L06401.

Spencer, R.G.M., Aiken, G.R., Dyda, R.Y., Butler, K.D., Bergamaschi, B.A., Hernes, P.J., 2010. Comparison of XAD with other dissolved lignin isolation techniques and a compilation of analytical improvements for the analysis of lignin in aquatic settings. Organic Geochemistry 41, 445-453.

Spencer, R.G.M., Aiken, G.R., Wickland, K.P., Striegl, R.G., Hernes, P.J., 2008. Seasonal and spatial variability in dissolved organic matter quantity and composition from the Yukon River basin, Alaska. Global Biogeochemical Cycles 22, GB4002.

Spencer, R.G.M., Stubbins, A., Hernes, P.J., Baker, A., Mopper, K., Aufdenkampe, A.K., Dyda, R.Y., Mwamba, V.L., Mangangu, A.M., Wabakanghanzi, J.N., Six, J., 2009b.

Photochemical degradation of dissolved organic matter and dissolved lignin phenols from the Congo River. Journal of Geophysical Research: Biogeosciences 114, G03010.

Stedmon, C.A., Bro, R., 2008. Characterizing dissolved organic matter fluorescence with parallel factor analysis: a tutorial. Limnology and Oceanography: Methods 6, 572-579.

Stedmon, C.A., Markager, S., 2005. Resolving the variability in dissolved organic matter fluorescence in a temperate estuary and its catchment using PARAFAC analysis. Limnology and Oceanography 50, 686-697.

Stedmon, C.A., Thomas, D.N., Granskog, M., Kaartokallio, H., Papadimitriou, S., Kuosa, H., 2007. Characteristics of dissolved organic matter in Baltic coastal sea ice: allochthonous or autochthonous origins? Environmental Science & Technology 41, 7273-7279.

Stenson, A.C., Landing, W.M., Marshall, A.G., Cooper, W.T., 2002. Ionization and fragmentation of humic substances in electrospray ionization Fourier transform-ion cyclotron resonance mass spectrometry. Analytical Chemistry 74, 4397-4409.

Stenson, A.C., Marshall, A.G., Cooper, W.T., 2003. Exact masses and chemical formulas of individual Suwannee River fulvic acids from ultrahigh resolution electrospray ionization Fourier transform ion cyclotron resonance mass spectra. Analytical Chemistry 75, 1275-1284.

Stets, E.G., Striegl, R.G., Aiken, G.R., Rosenberry, D.O., Winter, T.C., 2009. Hydrologic support of carbon dioxide flux revealed by whole - lake carbon budgets. Journal of Geophysical Research: Biogeosciences 114, G01008.

Strain, S., Armitage, I., 1985. Selective detection of 3-deoxymannooctulosonic acid in intact lipopolysaccharides by spin-echo ^{13}C NMR. Journal of Biological Chemistry 260, 12974-12977.

Striegl, R.G., Aiken, G.R., Dornblaser, M.M., Raymond, P.A., Wickland, K.P., 2005. A decrease in discharge-normalized DOC export by the Yukon River during summer through autumn. Geophysical Research Letters 32, L21413.

Striegl, R.G., Dornblaser, M.M., Aiken, G.R., Wickland, K.P., Raymond, P.A., 2007. Carbon export and cycling by the Yukon, Tanana, and Porcupine rivers, Alaska, 2001-2005. Water Resources Research 43, W02411.

Strome, D., Miller, M., 1978. Photolytic changes in dissolved humic substances, Proceedings: 20 th Congress, Internationale Vereinigung fur Theoretische und Angewandte Limnologie.

Stubbins, A., Spencer, R.G.M., Chen, H.M., Hatcher, P.G., Mopper, K., Hernes, P.J., Mwamba, V.L., Mangangu, A.M., Wabakanghanzi, J.N., Six, J., 2010. Illuminated darkness: Molecular signatures of Congo River dissolved organic matter and its photochemical alteration as revealed by ultrahigh precision mass spectrometry. Limnology and Oceanography 55, 1467-1477.

Stuermer, D.H., Payne, J.R., 1976. Investigation of seawater and terrestrial humic substances with carbon-13 and proton nuclear magnetic resonance. Geochimica et Cosmochimica Acta 40, 1109-1114.

Stuiver, M., Polach, H.A., 1977. Discussion: reporting of ^{14}C data. Radiocarbon 19, 355-363.

Sulzberger, B., Durisch-Kaiser, E., 2009. Chemical characterization of dissolved organic matter (DOM): a prerequisite for understanding UV-induced changes of DOM absorption properties and bioavailability. Aquatic Sciences 71, 104-126.

Tarnocai, C., Canadell, J., Schuur, E., Kuhry, P., Mazhitova, G., Zimov, S., 2009. Soil organic carbon pools in the northern circumpolar permafrost region. Global Biogeochemical Cycles 23, GB2023.

Templier, J., Derenne, S., Croue, J.P., Largeau, C., 2005. Comparative study of two fractions of riverine dissolved organic matter using various analytical pyrolytic methods and a C-13 CP/MAS NMR approach. Organic Geochemistry 36, 1418-1442.

These, A., Reemtsma, T., 2003. Limitations of electrospray ionization of fulvic and humic acids as visible from size exclusion chromatography with organic carbon and mass spectrometric detection. Analytical Chemistry 75, 6275-6281.

Thorn, K.A., Cox, L.G., 2009. N-15 NMR spectra of naturally abundant nitrogen in soil and aquatic natural organic matter samples of the International Humic Substances Society. Organic Geochemistry 40, 484-499.

Thurman, E.M., 1985. Humic substances in groundwater. In: Aiken, G.R., McKnight, D.M., Wershaw, R.L., MacCarthy, P. (Eds.), Humic substances in soil, sediment, and water: geochemistry, isolation and characterization. John Wiley & Sons, New York, pp. 87-103.

Tranvik, L.J., Downing, J.A., Cotner, J.B., Loiselle, S.A., Striegl, R.G., Ballatore, T.J., Dillon, P., Finlay, K., Fortino, K., Knoll, L.B., 2009. Lakes and reservoirs as regulators of carbon cycling and climate. Limnology and Oceanography 54, 2298-2314.

Tremblay, L.B., Dittmar, T., Marshall, A.G., Cooper, W.J., Cooper, W.T., 2007. Molecular characterization of dissolved organic matter in a North Brazilian mangrove porewater and mangrove-fringed estuaries by ultrahigh resolution Fourier transform-ion cyclotron resonance mass spectrometry and excitation/emission spectroscopy. Marine Chemistry 105, 15-29.

Vahatalo, A.V., Wetzel, R.G., 2008. Long-term photochemical and microbial decomposition of wetland-derived dissolved organic matter with alteration of C-13 : C-12 mass ratio. Limnology and Oceanography 53, 1387-1392.

van Krevelen, D.W., 1950. Graphical-statistical method for the study of structure and reaction processes of coal. Fuel 29, 269-284.

Vetter, T.A., Perdue, E.M., Ingall, E., Koprivnjak, J.F., Pfromm, P.H., 2007. Combining reverse osmosis and electrodialysis for more complete recovery of dissolved organic matter from seawater. Separation and Purification Technology 56, 383-387.

Vogel, J.S., Southon, J.R., Nelson, D.E., 1987. Catalyst and binder effects in the use of filamentous graphite for AMS. Nuclear Instruments and Methods in Physics Research Section B 29, 50-56.

von Wachenfeldt, E., Bastviken, D., Tranvik, L.J., 2009. Microbially induced flocculation of allochthonous dissolved organic carbon in lakes. Limnology and Oceanography 54, 1811-1818.

von Wachenfeldt, E., Sobek, S., Bastviken, D., Tranvik, L.J., 2008. Linking allochthonous dissolved organic matter and boreal lake sediment carbon sequestration: the role of light-mediated flocculation. Limnology and Oceanography 53, 2416.

Weishaar, J.L., Aiken, G.R., Bergamaschi, B.A., Fram, M.S., Fujii, R., Mopper, K., 2003. Evaluation of specific ultraviolet absorbance as an indicator of the chemical composition and reactivity of dissolved organic carbon. Environmental Science & Technology 37, 4702-4708.

Wickland, K., Neff, J., Aiken, G., 2007. Dissolved organic carbon in Alaskan boreal forest: sources, chemical characteristics, and biodegradability. Ecosystems 10, 1323-1340.

Wickland, K.P., Aiken, G.R., Butler, K., Dornblaser, M.M., Spencer, R.G.M., Striegl, R.G., 2012. Biodegradability of dissolved organic carbon in the Yukon River and its tributaries: Seasonality and importance of inorganic nitrogen. Global Biogeochemical Cycles 26, GB0E03.

Wilkinson, G.M., Pace, M.L., Cole, J.J., 2013. Terrestrial dominance of organic matter in north temperate lakes. Global Biogeochemical Cycles 27, 1-9.

Wilson, M.A., Hatcher, P.G., 1988. Detection of tannins in modern and fossil barks and in plant residues by high-resolution solid-state ^{13}C nuclear magnetic resonance. Organic Geochemistry 12, 539-546.

Wilson, M.A., Pugmire, R.J., Grant, D.M., 1983. Nuclear magnetic resonance spectroscopy of soils and related materials. Relaxation of ^{13}C nuclei in cross polarization nuclear magnetic resonance experiments. Organic Geochemistry 5, 121-129.

Winter, T.C., Rosenberry, D.O., 1997. Physiographic and geologic characteristics of the Shingobee River headwaters area. Interdisciplinary Research Initiative: Hydrological and Biogeochemical Research in the Shingobee River Headwaters Area, North-Central Minnesota: US Geological Survey, Water Resources Investigations Research, 96-4215.

Woods, G.C., Simpson, M.I., Kelleher, B.P., McCaul, M., Kingery, W.L., Simpson, A.J., 2010. Online high-performance size exclusion chromatography-nuclear magnetic resonance for the characterization of dissolved organic matter. Environmental Science & Technology 44, 624-630.

Woods, G.C., Simpson, M.J., Pautler, B.G., Lamoureux, S.F., Lafrenière, M.J., Simpson, A.J., 2011. Evidence for the enhanced lability of dissolved organic matter following

permafrost slope disturbance in the Canadian High Arctic. Geochimica et Cosmochimica Acta 75, 7226-7241.

Woods, G.C., Simpson, M.J., Simpson, A.J., 2012. Oxidized sterols as a significant component of dissolved organic matter: Evidence from 2D HPLC in combination with 2D and 3D NMR spectroscopy. Water Research 46, 3398-3408.

Wu, X.L., Zilm, K.W., 1993. Complete Spectral Editing in CPMAS NMR. Journal of Magnetic Resonance Series A 102, 205-213.

Xian, F., Hendrickson, C.L., Blakney, G.T., Beu, S.C., Marshall, A.G., 2010. Automated broadband phase correction of Fourier transform ion cyclotron resonance mass spectra. Analytical Chemistry 82, 8807-8812.

Yamashita, Y., Tanoue, E., 2008. Production of bio-refractory fluorescent dissolved organic matter in the ocean interior. Nature Geoscience 1, 579-582.

Zhang, Y., van Dijk, M.A., Liu, M., Zhu, G., Qin, B., 2009. The contribution of phytoplankton degradation to chromophoric dissolved organic matter (CDOM) in eutrophic shallow lakes: field and experimental evidence. Water Research 43, 4685-4697.

Zigah, P.K., Minor, E.C., Abdulla, H.A., Werne, J.P., Hatcher, P.G., 2014. An investigation of size-fractionated organic matter from Lake Superior and a tributary stream using radiocarbon, stable isotopes and NMR. Geochimica et Cosmochimica Acta 127, 264-284.

Zigah, P.K., Minor, E.C., Werne, J.P., 2012. Radiocarbon and stable-isotope geochemistry of organic and inorganic carbon in Lake Superior. Global Biogeochemical Cycles 26, GB1023.

VITA

Xiaoyan Cao
Department of Chemistry and Biochemistry
Old Dominion University
Norfolk, VA 23529
Email: xcaox001@odu.edu

Education:

Ph.D. in Chemistry, Old Dominion University, Norfolk, VA, USA, December 2014.
B.S. in Agricultural Resources and Environment, Nanjing Agricultural University, Nanjing, Jiangsu, China, June 2008.

Selected Publications:

Cao, X., Lattao, C., Pignatello, J.J., Mao, J., Schmidt-Rohr, K., 2014. Sorption selectivity in natural organic matter probed with fully deuterium-exchanged and carbonyl-^{13}C-labeled benzophenone and ^{1}H–^{13}C NMR spectroscopy. Environmental Science & Technology 48, 8645-8652.

Cao, X., Ro, K.S., Libra, J.A., Kammann, C.I., Lima, I., Berge, N., Li, L., Li, Y., Chen, N., Yang, J., 2013. Effects of biomass types and carbonization conditions on the chemical characteristics of hydrochars. Journal of Agricultural and Food Chemistry 61, 9401-9411.

Cao, X., Yang, J., Mao, J., 2013. Characterization of kerogen using solid-state nuclear magnetic resonance spectroscopy: a review. International Journal of Coal Geology 108, 83-90.

Cao, X., Birdwell, J.E., Chappell, M.A., Li, Y., Pignatello, J.J., Mao, J., 2013. Characterization of oil shale, isolated kerogen, and postpyrolysis residues using advanced ^{13}C solid-state nuclear magnetic resonance spectroscopy. AAPG Bulletin 97, 421-436.

Cao, X., Chappell, M.A., Schimmelmann, A., Mastalerz, M., Li, Y., Hu, W., Mao, J., 2013. Chemical structure changes in kerogen from bituminous coal in response to dike intrusions as investigated by advanced solid-state ^{13}C NMR spectroscopy. International Journal of Coal Geology 108, 53-64.

Cao, X., Pignatello, J.J., Li, Y., Lattao, C., Chappell, M.A., Chen, N., Miller, L.F., Mao, J., 2012. Characterization of wood chars produced at different temperatures using advanced solid-state ^{13}C NMR spectroscopic techniques. Energy & Fuels 26, 5983-5991.

Cao, X., Mastalerz, M., Chappell, M.A., Miller, L.F., Li, Y., Mao, J., 2011. Chemical structures of coal lithotypes before and after CO_2 adsorption as investigated by advanced solid-state ^{13}C nuclear magnetic resonance spectroscopy. International Journal of Coal Geology 88, 67-74.

Cao, X., Olk, D.C., Chappell, M., Cambardella, C.A., Miller, L.F., Mao, J., 2011. Solid-state NMR analysis of soil organic matter fractions from integrated physical–chemical extraction. Soil Science Society of America Journal 75, 1374-1384.

Cao, X., Ro, K.S., Chappell, M., Li, Y., Mao, J., 2010. Chemical structures of swine-manure chars produced under different carbonization conditions investigated by advanced solid-state ^{13}C nuclear magnetic resonance (NMR) spectroscopy. Energy & Fuels 25, 388-397.